Title
Data-Driven Approaches to Evaluating Traffic-Related Air Pollution Exposure and Health Impacts in California, USA

Author
Liu, Jonathan Zhong

Publication Date
2023

Peer reviewed|Thesis/dissertation

UNIVERSITY OF CALIFORNIA

Los Angeles

Data-Driven Approaches to Evaluating Traffic-Related Air Pollution Exposure and Health Impacts in California, USA

A dissertation submitted in partial satisfaction

of the requirements for the degree

Doctor of Philosophy in Environmental Health Sciences

by

Jonathan Liu

2023

ABSTRACT OF THE DISSERTATION

Data-Driven Approaches to Evaluating Traffic-Related Air Pollution Exposure and Health Impacts in California, USA

by

Jonathan Liu
Doctor of Philosophy in Environmental Health Sciences
University of California, Los Angeles, 2023
Professor Michael Leo B. Jerrett, Co-Chair
Professor Yifang Zhu, Co-Chair

Automobile traffic has been a longstanding source of air pollution in human communities. The target of major regulations in the past few decades, the transportation sector has gone through significant changes, ranging from shifts in vehicle fleet composition to natural and artificial disruptions to traffic patterns. Both an essential form of transportation as well as a major source of air pollution, traffic, to this day, remains a human necessity and a public health challenge. As such, measuring and modeling the temporal and spatial distribution of traffic related air pollution (TRAP) is a critical necessity for exposure scientists, epidemiologists, and other public health professionals.

In this dissertation, we investigate methods to measure TRAP in response to recent trends and disruptions in traffic patterns and composition, with a particular focus on California State. To this end, we employ novel combinations of big data, including regulatory air quality data in addition to traffic, land-use, and internet-of-things network data. It is divide into five chapters: an introduction (chapter 1), three chapters of original research (chapters

2-4), and a discussion of the conclusions of the work (chapter 5).

Chapter 2 evaluates the near-road air quality impacts of traffic disruptions associated with the COVID-19 pandemic. Following global activity stoppages associated with stay-at-home measures, studies reported improved air quality in several cities and countries around the world. While widely observed, many studies could not properly attribute the decline of traffic in this chapter evaluates the relationship between traffic volume as reported by the California Department of Transportation and near-road NO and NO_2 emissions at seven EPA monitoring sites in California state: four in Northern California and three in Southern California.

Chapter 3 models the spatial distribution of non-tailpipe emissions-related $PM_{2.5}$ chemical species and oxidative potential in Southern California. Combining gold-standard filter samples, land-use data, and a novel internet-of-things low-cost sensor network dataset in a spatial regression (Co-Kriging with External Drift) model, we create a set of exposure surfaces for exposures that serve as tracers of TRAP. Results indicate that compared to typical modelling techniques, namely land-use regressions, the addition of low-cost sensor data improves model accuracy and precision.

Chapter 4 evaluates the associations between exposures modeled in Chapter 3 and the ischemic placental disease (IPD) in a prospectively-followed pregnancy cohort of 178 women. Air quality regulation have resulted in declines in tailpipe emissions in recent years. As stated earlier, TRAP is also generated from non-tailpipe sources, including brake and tire wear. Concerned that brake and tire wear particles contain metals and other organic compounds that could harm fetal health, this study uses a logistic regression model to estimate exposure outcome associations. Compared to conventional exposures, namely $PM_{2.5}$ and black carbon, we find stronger associations between IPD and exposures more specific to brake and tire wear, such as barium, as well as oxidative potential markers.

At the time of filing, Chapter 2 has been published in *Environmental Science and Technology Letters*, Chapter 3 has been published in *Environment International*, and Chapter 4

is currently in preparation for submission to an academic journal.

The dissertation of Jonathan Liu is approved.

Beate R. Ritz

Sudipto Banerjee

Yifang Zhu, Committee Co-Chair

Michael Leo B. Jerrett, Committee Co-Chair

University of California, Los Angeles

2023

To my family and friends
who have shown me a world
marvelous beyond imagination

TABLE OF CONTENTS

LIST OF FIGURES

LIST OF TABLES

ACKNOWLEDGMENTS

A heartfelt thanks to my PhD co-advisors, Dr. Michael Jerrett, and Dr. Yifang Zhu. I have been very lucky to have received guidance from two brilliant scientists who both passed on to me a wealth of knowledge from both of their areas of expertise. Dr. Jerrett's has taught me the ins and outs of GIS and spatial analysis as applied to Environmental Health Sciences, and Dr. Zhu has taught me invaluable knowledge regarding aerosol dynamics and exposure sampling. They have both treated me with care, respect, and trust here at UCLA, and I am indebted to their kindness and mentorship.

I would also like to thank my doctoral committee members, Dr. Sudipto Banerjee and Dr. Beate Ritz. Dr. Banerjee has given me key guidance throughout my scientific journey and has provided essential statistical feedback for many of my projects. Dr. Ritz, as a seasoned environmental epidemiologist, has taught me the intricacies of doing epidemiology research, both in the classroom and my own academic work.

My research would not have been possible without several academic collaborations between my colleagues and myself. I would like to give my warmest thanks to my classmates and colleagues in the labs of Dr. Jerrett and Dr. Zhu, who welcomed me in the moment I entered UCLA; I moved to Los Angeles alone and confused, and thanks to you all I have had the time of my life here. Thank you to Dr. Farzan Oroumiyeh for being my first collaborator. Thank you to Dr. Jonah Lipsitt for your technical help, advice, and support. Thank you Qi Meng for the close and supportive collaboration throughout these years.

I dedicate this thesis to the memory of my maternal grandparents, Guan Ying and Zheng Yongxi, who passed away during my application process – thank you for guiding me in ways I never thought possible. To my mother and father, my greatest teachers, you have taught me that questions are worth asking, and that there will always be so, so much more to learn. To Moli Liu, you are a role model and constant source of support; to be your brother is my life's highest honor. To the rest of my family, thank you for your unconditional love and

support.

To my friends, old and new, thank you for being a source of energy, growth, and support. I wouldn't be who I am without you, and I'm so happy that one way or another, we have all entered each others' lives.

VITA

2016	B.A. (Public Health Studies), Phi Beta Kappa, Johns Hopkins University
2017	M.H.S. (Environmental Health Sciences), Johns Hopkins Bloomberg School of Public Health
2019–2023	Graduate Research Assistant, UCLA School of Public Health
2022–2023	Teaching Assistant, UCLA School of Public Health
2022	Research Intern, Microsoft Research

PUBLICATIONS AND PRESENTATIONS

- **Liu J**, Lipsitt J, Jerrett M, Zhu Y. 2020. Decreases in Near-Road NO and NO 2 Concentrations during the COVID-19 Pandemic in California. Environmental Science Technology Letters

- **Liu J**, Banerjee S, Oroumiyeh F, Shen J, del Rosario I, Lipsitt J, et al. 2022. Cokriging with a low-cost sensor network to estimate spatial variation of brake and tire-wear metals and oxidative stress potential in Southern California. Environment International 168:107481

- Kramer AL, **Liu J**, Li L, Connolly R, Barbato M, Zhu Y. 2023. Environmental justice analysis of wildfire-related PM2.5 exposure using low-cost sensors in California. Science of The Total Environment 856:159218 [co-first author]

- Lipsitt J, Chan-Golston AM, **Liu J**, Su J, Zhu Y, Jerrett M. 2021. Spatial analysis of COVID-19 and traffic-related air pollution in Los Angeles. Environ Int 153:106531

- Connolly RE, Yu Q, Wang Z, Chen Y-H, **Liu J**, Collier-Oxandale A, et al. 2022. Long-Term Evaluation of a Low-Cost Air Sensor Network for Monitoring Indoor and Outdoor Air Quality at the Community Scale. Science of The Total Environment 807:

- Oroumiyeh F, Jerrett M, Del Rosario I, Lipsitt J, **Liu J**, Paulson SE, et al. 2022. Elemental composition of fine and coarse particles across the greater Los Angeles area: Spatial variation and contributing sources. Environmental Pollution 292:118356

- Shen J, Taghvaee S, La C, Oroumiyeh F, **Liu J**, Jerrett M, et al. 2022. Aerosol Oxidative Potential in the Greater Los Angeles Area: Source Apportionment and Associations with Socioeconomic Position. Environmental Science and Technology 56:17795–17804

- Janzen C, Lei MYY, Lee BR, Vangala S, DelRosario I, Meng Q, Ritz B, **Liu J**, et al., 2022. A Description of the Imaging Innovations for Placental Assessment in Response to Environmental Pollution study (PARENTs). American Journal of Perinatology 0

- **Liu J**, Oroumiyeh F, Shen J, Del Rosario I, Lipsitt J, Paulson S, Ritz B, Su J, Weichenthal S, Lakey P, Zhu Y, Jerrett M, Statistical Analysis and Geospatial Exposure Model of Air Pollution Derived from Brake and Tire Wear. Poster Presentation. American Association for Aerosol Research 39th Annual Conference. October 2020 [Winner, Student Poster Presentation]

- **Liu J**, Banerjee S, Oroumiyeh F, Shen J, Del Rosario I, Lipsitt J, Paulson S, Ritz B, Su J, Weichenthal S, Lakey P, Zhu Y, Jerrett M, Cokriging with a Low-cost Air Sensor Network to Estimate Spatial Variation of Brake and Tire-wear Related Heavy Metals and Reactive Oxygen Species in Southern California. Poster Presentation. American Association for Aerosol Research 39th Annual Conference. October 2021

- Kramer A, **Liu J.**, Li L, Connolly R, Barbato M, Zhu Y, Using Low-Cost Air Sensors to Assess Community Level PM Exposure from California Wildfires. University of California, Los Angeles. Poster Presentation. American Association for Aerosol Research 39th Annual Conference. October 2021

CHAPTER 1

Introduction

1.1 Background

The internal combustion engine is one the most consequential products of the Industrial Revolution. One of the most visible applications of the internal combustion engine is the existence of the automobile, the dominant form of personal transportation around the world. Since its initial proliferation in the early 20th century, the automobile has had profound impacts on human society. Modern day road networks, built to accommodate vast volumes of automobile traffic, form the circulatory system of human society, transporting goods and services across space. In the US, these networks expanded greatly expanded during amidst the post-WWII boom. The era was characterized by the proliferation of the personal automobile, suburbanization, highway construction, and closure of some public transportation systems. Consequently, during the mid-20th century, heavy air pollution plagued not only the US, but much of the rest of the Western world, which led to increase awareness and public action over air quality and gave rise to modern day clean air policy [1]. In the US, the Clean Air Act of 1963 gave the Environmental Protection Agency (EPA) two functions critical for addressing air pollution: setting automobile emission standards and establishing ambient air monitoring infrastructure [2]. Armed with the proper authorities, the EPA successfully reduced tailpipe emissions throughout the following decades [3].

Using the Clean Air Act, the EPA established a national ambient air monitoring network, finalizing nationally consistent operations and quality assurance procedures in 1980

[4]. In the decades following, exponential growth in the information technology sector led to transformations in environmental monitoring. Notably, since the 2010s, air quality data has been made available to laypersons using what are commonly known as low-cost sensors. At the expense of data quality and consistency, low-cost sensors are cheaper than regulatory equipment by multiple orders of magnitude. Recent devices are internet-connected and with a critical mass of devices, can form their own air quality network. Prior studies have hailed low-cost sensors as having changed the paradigm of air monitoring, complementing existing regulatory monitoring systems and scientific practices with a novel, often crowdsourced dataset [5]. At the same time, advances in fields such as environmental health, epidemiology, and physiology have deepened our understanding of the relationship between air pollution and human health. Recent air quality studies have focused on source-specific individual and groups of constituents of fine particulate matter (aerodynamic diameter < 2.5 μm, $PM_{2.5}$), such as traffic-related air pollution (TRAP). Amidst reductions in tailpipe emissions over since the Clean Air Act, there is renewed focus on non-tailpipe emissions, which contain metals and organics that are potentially more relevant to human health [6].

1.2 Traffic-Related Air Pollution Exposure and Health Effects

Despite improved access to transportation, widespread automobile use is also associated with an decline in air quality and adverse public health consequences. Automobiles emit particulates and gaseous pollutants via both tailpipe and non-tailpipe pathways. Tailpipe emissions form as a result of incomplete combustion of fuel, and includes compounds such as organic compounds and nitrous oxides (NO, NO_2, and other NO_x compounds), the latter of which interacting with O_3 and UV light to produce smog [7, 8]. NO_2 is a commonly-used tracer of tailpipe emissions [6]. As a source of free radicals, it has been shown to inflict changes in the respiratory system via oxidative stress [9], with prolonged exposure having been linked to adverse health outcomes [10].

Non-tailpipe emissions include road dust resuspension and the emission of brake and tire wear [6]. The latter are generated during automobile operations as brakes and tires wear down over time. Braking action releases particulate matter in both the fine and ultrafine (diameter < 0.1 μm) size fractions via friction and nucleation, respectively [6]. Laboratory and field studies have identified several metals associated with non-tailpipe emissions, including organics and metals such as Ti, Cu, Fe, and Ba, and Zn [6]. Some of these components, such as Cu and Fe, induce oxidative stress in Fenton reactions [11].

1.2.1 Exposure Assessment

1.2.1.1 Traffic and Natural Experiments

Studies around air pollution, traffic-related or otherwise, often feature natural experiment study designs, observational studies in which the researcher has little to no control over experimental conditions. Early natural in the non-traffic air quality sector focused on point sources, where researchers would evaluate pollution levels before and after the opening or closure of factories or other industrial sites [12]. More recent studies focusing on traffic-related pollution have studies traffic disruptions. Disruptions include large sporting events such as the Olympics in Beijing in 2008 [13, 14] and Atlanta in 1996 [12, 15–17], as well as more localized events including scheduled major highway closures in West Los Angeles [18]. These observational studies have been able to measure large changes in traffic, but additional downstream air quality improvements and reductions in adverse respiratory and cardiovascular health outcomes [14].

1.2.1.2 Measuring Exposure

In the field, measuring TRAP specifically and separately from other air pollutants is technically infeasible. Therefore, assessing TRAP exposure typically involves the use of specific tracers, which are chemicals or pollutants that have been found to be relatively specific to

traffic, and whose measurements correlate with and are representative of the complex mixture of TRAP. Common tracers include $PM_{2.5}$ or its individual chemical components, black carbon for diesel emissions, and gases such as NO_2, NO, NO_x, CO, and benzene among others [19]. NO_2 is the most common forms following the emissions of NO, a byproduct of fuel combustion, react with oxygen and UV light in the atmosphere [20].

A potential issue with using NO_2 and other tailpipe emissions-related gases as tracers is the recent and significant decline in tailpipe emissions due to clean air regulations driving improvements in fuel efficiency [21]. Clean air regulations, notably, currently do not address brake and tire wear. Consequently, as vehicle fleets improve in efficiency and electrify, NO_2 emissions from the transportation sector will continue to fall. Non-tailpipe emissions such as brake and tire wear, under the absence of similar regulations, may experience changes corresponding with trends in vehicle weight and regenerative braking that trend differently with NO_2 decreases [6]. Consequently, the continued use of tailpipe tracers of TRAP may eventually misrepresent the magnitude of TRAP from non-tailpipe sources, leading to exposure misclassification in human health studies.

There are a number of ways to measure exposure to TRAP. A review by Khan et al. (2018) identified several measurement and modeling approaches currently employed in the field [22]. These techniques range from direct ground-level or satellite measurement, to deterministic and stochastic modeling techniques. Ground-level measurements, encompass a wide range of instruments and techniques. In the US, the EPA and local air quality agencies operate a nation-wide monitoring network using stationary, high-cost federal reference measurements. Other exposure assessment techniques include the use of actively and passively filter samplers, which use pumps or diffusion, respectively, to collect particulates and gases on physical media, which can be then analyzed in a laboratory to obtain information such as chemical composition [23]. Recent developments in wireless networking and sensor technology have led to the proliferation of low-cost sensors, a growing subject of interest in the field of environmental health sciences [5]. These sensors use a combination of optical

sensors and amperometric sensors to report real-time data on particulate and gas concentrations, which encompass exposures relevant to TRAP such as $PM_{2.5}$, NO_2, and CO [24, 25]. Remote sensing techniques employ an array of Earth-orbiting satellites which measure the aerosol optical depth of a given geographic area, which reflects the degree of electromagnetic extinction at a given wavelength [26]. Many of the pollutants measured by these satellites are relevant to TRAP emissions, such as NO_2.

Each method of measuring exposure is accompanied with a set advantages and disadvantages. For example, methods with robust accuracy, such as filter samples or federal reference measurements at regulatory samples, are capital and labor intensive, requiring a combination of adequate land, maintenance, and knowledge to properly operate. Low-cost sensors are cheaper to produce and install, but numerous studies have raised concerns regarding data accuracy, sensor degradation, and long-term sustainability of projects [27]. Similarly, remote sensing data covers a wide geographic scope and relatively high resolutions, but require expensive equipment, do not necessarily reflect the ground truth of air quality, and are affected by local meteorological factors such as cloud cover [22].

1.2.1.3 Exposure Modeling

When estimating exposures across a geographic domain, measurement techniques all face limitations in spatial resolution; they only provide information on air pollution exposures at the exact point of sample collection. To interpolate exposures in locations not directly monitored, scientists employ exposure models. These models employ tools such as large datasets and geographic information systems (GIS) to explain or serve as proxy for information from both direct measurements using outside variables. More rudimentary forms of TRAP exposure assessment include the use of simple use of GIS variables, such as intersection density or distance to major roads. Other methods instead estimate TRAP concentrations in areas otherwise difficult, impractical, or impossible to monitor with modeling. Models can be divided into deterministic models – which estimate exposure concentrations using dispersion model-

ing and a series of model validation steps – as well as stochastic models, which by contrast uses the empirical statistical relationships between exposures of interest and other related factors [22]. In the measurement of TRAP, stochastic models, which are featured in the following dissertation, include but are not limited to regressions such as land use regressions (LUR) and spatial regressions such as inverse distance weighting and kriging [22].

Approaches like LUR models, also known as regression mapping, use combinations of GIS variables to explain air pollution monitoring data collected at a limited set of points in a geographic domain [28]. Common variables used in LUR modelling include traffic (distance to road, road length, traffic density), land use (urban, green space, commercial use), and physical geography [28]. Specific independent variable candidates in LUR models are generated by drawing areal buffers of variable radii (usually in between 50-1000 meters) and calculating summary statistics of land use variables (mean, sum) within each areal unit. After finalizing the list of variable candidates, models are trained and variables are selected based on cross-validation accuracy. LUR models are most often multiple linear regressions, but can also be non-parametric regressions, which include generalized additive models [29] and decision trees such as random forest [30]. After proper training, the model is then applied a study area where information on independent variables is known across the entire geographic domain. In recent years, researchers have improved upon traditional multiple linear regression LUR models, integrating information from deterministic models [31] or accounting for spatially autocorrelation using geospatial regressions such as kriging or co-kriging [32].

Different methods in pollution modeling come with their own set of advantages and limitations, particularly as they relate to causality, exposure (mis)classification, and resolution limits. Nonetheless, models remain an important toolkit in health studies, environmental policy-making, and exposure research. The selection of appropriate measurement methods, external variables, and modeling techniques is critical to properly answering scientific and public health problems of interest. As we continue to witness improvements in wireless

connectivity, and environmental sensing technology, big data and the ability to better understand environment-health relationships will grow. Similarly, the study of TRAP continues to evolve alongside methods of data fusion in exposure sciences and public health.

Typically, geospatial models of air pollution are designed to be used in the interest of public health and environmental epidemiology studies. After models have been built, they typically are used in tandem with health data, including administrative records and cohorts, to better understand associations between environmental exposure and human disease [33, 34]. These health data typically contain geographical information. Depending on study design and data source, geographic information varies in precision. Some studies use highly precise location ascertainment, such as individual addresses or GPS-tracked real-time location. Others, due to data privacy concerns or limitations in data access, use more coarse information, such as resident ZIP code. Using geography to bridge human health and environmental data, spatial epidemiologists determine and draw inference from associations between environmental exposure and health outcomes.

1.2.2 Health Effects

Human health concerns drive the interest in regulating and reducing air pollution levels. The primary hypothesized mechanisms through which air pollution affects human health is by way of oxidative stress, autonomic function disregulation, and translocation into the circulatory system [35]. Oxidative stress is a disruption to the redox (reduction-oxidation) signaling reactions resulting from an elevated concentration of oxidants, such as free radicals, over antioxidants [36]. Chemical constituents of TRAP PM are high in oxidative potential, and include metals such as copper and iron from non-exhaust emissions [37]. After inhalation, these particulates and the chemical constituents present on their surfaces may undergo Fenton reactions to generate hydroxyl radicals, which lead induce lipid, protein, and DNA damage [37].

Traffic is unique compared to other sources of air pollution in its periodicity, close proxim-

ity to a large portion of the human population, and constituents which include both tailpipe and non-tailpipe sources. The relationship between all-source $PM_{2.5}$ and health effects is well studied [38], and recent studies have shifted focus to source-specific health effects. An extensive review found a number of adverse health outcomes associated with exposure to TRAP, including circulatory mortality, all-cause mortality, ischemic heart disease events, diabetes, childhood asthma onset, acute lower respiratory infections, term low birth weight, and small for gestational age, among other outcomes [7].

1.3 Research Setting

Chapters 2, **3**, and **4** report findings from research conducted in the State of California. **Chapter 2** focuses on seven EPA near-road monitoring sites in major population centers: four in Northern California and three in Southern California. We collected data from heavily-trafficked roadways, with Northern California sites experiencing a typical weekday daily average of 100,000 passenger vehicles per day and 5,000 heavy duty vehicles per day. Southern California sites similarly report between a weekday daily average of 75,000-100,000 passenger vehicles and 7,500 heavy duty vehicles. **Chapters 3** and **4** focus specifically on Southern California in an area consisting primarily of Los Angeles County, but also parts of Ventura, Orange, Riverside, and San Bernardino counties. The area is home to an ethnically diverse population of over 10 million.

1.4 Summary of Aims

In the context of the evolving profile of air pollution and increasingly available "big data" in exposure sciences, the goal of this dissertation to use novel data fusion techniques to model the changes, distribution, and health effects of TRAP. The three following chapters each detail a relevant research study. In **Chapter 2**, we combine three sources of government

data: air quality data from the EPA AQS monitoring network, traffic data from the California Department of Transportation Performance Measurement System (PeMS), and weather data consolidated by the University of Utah's MesoWest service. Using these three datasets, **Chapter 2** aims to quantify reductions in near-road NO and NO_2 emissions attributable to declines in traffic following stay-at-home orders in California. **Chapter 3** aims to assess the role of low-cost sensors in modeling the spatial distribution of metals and oxidative potential associated with non-tailpipe emissions. Using a combination of fieldwork and laboratory measurements, land-use and traffic data, and crowdsourced low-cost $PM_{2.5}$ sensor network data, we compare two modeling methods: LUR and co-kriging with external drift, which consists of a LUR model combined with additional data from the low-cost sensor network. Finally, **Chapter 4** aims to quantify relationship between non-tailpipe emissions-related exposures and adverse birth outcomes, we apply the exposure models generated in **Chapter 3** to a pregnancy cohort. The results presented in **Chapters 2-4** highlight the use of novel data sources and combinations to deepen our understanding of TRAP and inform how clean air policy can better address public health issues.

CHAPTER 2

Decreases in near-road NO and NO_2 concentrations during the COVID-19 pandemic in California

2.1 Abstract

The COVID-19 pandemic and resulting shelter-in-place measures led to widespread adoption of remote work policies and temporary business closures or operation curtailments, disrupting typical commuting patterns. This chapter investigates how these sudden shifts in traffic patterns affected near-road NO and NO_2 concentrations in California. We used (1) near-road air pollution data from the U.S. Environmental Protection Agency's (EPA) AirNow database, (2) passenger and heavy-duty traffic data from the Caltrans Performance Monitoring System (PeMS), and (3) weather data from MesoWest between January 1st to April 30th during the years 2017-2020 to model NO and NO_2 concentrations as functions of highway traffic and meteorology. We then simulated NO and NO_2 under business-as-usual traffic conditions and compared modeled data to observed values. Weekday passenger traffic significantly declined in Northern and Southern California by 29% and 24%, respectively. As a result, Northern and Southern California near-road locations experienced statistically significant declines in NO by 35% and 32% and NO_2 by 15 and 29%, respectively, compared to modeled estimates. As a natural experiment, our findings demonstrate that reduced vehicle activity significantly improved air quality, contributing to the body of evidence linking shelter-in-place and cleaner air.

2.2 Introduction

In late 2019, the first outbreak of COVID-19, was detected in Wuhan, Hubei Province, China. The Chinese response included a lockdown of several cities and widespread social distancing measures. In California, the first confirmed cases were detected in late January 2020, with confirmed community spread soon thereafter. In March, many workplaces instituted remote work and government bodies issued regulations starting with a statewide emergency declaration on March 4th, 2020. Local jurisdictions followed by banning public gatherings and the state declared a shelter-in-place order on March 19, 2020 [39].

As the COVID-19 pandemic spread, human activity halted under shelter-in-place measures. Many studies in China [40–54], India [55–62], Europe [63–65], South America [66–68], Central Asia [69], and the United States [58, 70–73] have used satellite and stationary monitoring to demonstrate decreases in regional PM2.5 and NO_2 levels during shelter-in-place periods. While satellite data are widely available across the world, this approach has a few limitations. The target of many of these studies, NO_2, is a harmful secondary pollutant regulated by the Clean Air Act and common tracer of vehicle activity [74]. In California, only 62% of net NO_x emissions, the sum of NO and NO_2 emissions, come from mobile sources, with the rest coming from cropland, fuel combustion, and miscellaneous sources [75]. Consequently, without quantifying changes in traffic, regional studies can only implicitly link shelter-in-place to cleaner air. On the other hand, NO has not been linked to adverse health effects, but is a more specific tracer of vehicle activity, directly generated by fuel combustion [20]. Once emitted, however, NO quickly oxidizes into NO_2, making it very responsive to sudden changes in highway traffic but difficult to measure outside of near-road monitoring networks [18]. As a result, regional studies that do not measure traffic are limited in their ability to form causal conclusions between shelter-in-place and air pollution. We attempt to address this knowledge gap by focusing on traffic data and NO/NO_2 data from the U.S. Environmental Protection Agency's (EPA) near-road network, which explicitly measures mobile

source air pollutants.

In California, the COVID-19 pandemic prompted a decline in economic activity and an unprecedented shift to remote work for many jobs, likely reducing the need for daily vehicle commuting and truck cargo traffic. Because (1) mobile sources contribute to over half of all NOx emissions in California [75], (2) about 70% of gasoline and 80% of diesel traffic is on the highway system [76], and (3) NO is a tracer of vehicle traffic and precursor to other air pollutants, changes in regional air pollution levels likely stem from changes in highway traffic and subsequent reductions in near-road NO concentrations. This chapter aims to relate pandemic-related traffic changes to near-road NO and NO_2 concentrations, accounting for potential seasonal and meteorological confounders as well as separate the relative contributions of passenger versus truck traffic.

2.3 Materials and Methods

2.3.1 Data Source

This chapter draws data from January 1st to April 30th, matching previous COVID-19 studies [77–79], for the years 2017 through 2020:

1. Air quality data are sourced from AirNow, a database that reports hourly pollution and includes EPA's near-road network [80]. California has 13 EPA near-road pollution monitoring sites, of which 7 had complete air pollution and traffic data available. Northern California had four sites, while Southern California had three, each targeting a different highway. Table 2.2 summarizes the name, county, and target road of each site and Figures 2.1, 2.2, and 2.3 show the locations of each site. The most commonly available pollutants are NO and NO_2 concentrations (ppb), while other pollutants such as black carbon, $PM_{2.5}$, CO, and ozone are inconsistently reported. Fewer than half of the sites report meteorology data, which we used to validate more thorough

meteorology data obtained from MesoWest.

2. California traffic data are sourced from the Caltrans Performance Measurement System (PeMS), which reports traffic across all major metropolitan areas of the State of California [81].

    - In order to systematically retrieve data from PeMS, we created two web scrapers: one to identify traffic loop detectors within a certain geographic distance of a pre-specified location, and another to download hourly light- and heavy-duty traffic traffic from a set of loop detectors in a pre-specified time range.
    - Using the above tool, we first downloaded daily traffic data from all traffic monitors within a 0.1-, 0.25-, and 1.0-mile radius of each near-road site. We then found that the 0.25-mile is the closest distance that provide sufficient traffic data to allow us to calculate average traffic per site. Each vehicle detection system separately reports daily total passenger vehicles and trucks per day, defined by vehicle height, and percent observed – an indicator of completeness – for both measurements. For each traffic monitor, we downloaded the daily total number of passenger vehicles and trucks during our study period, selecting data that were 50% or more observed over the entire day.

3. Weather data are sourced from MesoWest, a weather database run by the University of Utah [82]. For each near-road site, we downloaded temporally aligned data from the closest weather station, located between 2 and 11 miles away. Weather data included temperature, air pressure, relative humidity, wind speed, and type of precipitation reported at five-minute intervals.

We calculated daily statistics for AirNow data and MesoWest weather data to match PeMS traffic data, which reports daily total flow. We calculated daily averages for NO and NO_2 concentrations, traffic data, wind speed, relative humidity, and atmospheric pressure.

We calculated daily minimum for air temperature, based on findings from a previous study [83]. We coded precipitation as a dichotomous variable (1 for any precipitation, 0 for none). In our final dataset, our data points were identifiable by their date (month, day, year) and location.

2.3.2 Data Analysis and Model Development

We began with exploratory data analysis, including univariate plots, summary statistics, and correlation analysis. To account for non-linear relationships, we applied generalized additive models (GAM), often used in air pollution research [54, 84, 85]. We generated our models with a forward selection process, beginning with traffic variables and individually adding meteorology covariates. We kept variables if they substantially improved model fit and accuracy as determined by AIC and adjusted R^2. For each variable, we chose either a linear or a smoothing component by calculating the estimated degrees of freedom (EDF) and statistical significance of the GAM smoother as well as by plotting the variable in question against dependent variables across each location. During this process, we considered a variable with an EDF greater than or equal to 2 non-linear. Due to spatial and temporal variations in vehicle fleet composition, we assumed emissions per vehicle differed at each location-year combination [86]. Additionally, because Northern and Southern California have different climates, we divided our sites accordingly and included a region variable which interacts multiplicatively with our meteorology variables [87]. The dependent variables are daily average NO (ppb) and NO_2 (ppb). We selected the following independent variables: year and location, region, passenger traffic and truck traffic by year and location (vehicles per day), daily average wind speed (miles per hour) by region, precipitation by region (1 if any precipitation, 0 if none), daily average relative humidity (%) by region, daily average atmospheric pressure (pascals) by region, and daily minimum temperature (degrees Celsius) by region.

Exploratory analysis revealed that traffic related linearly to NO and NO_2 at all sites

except Long Beach and Ontario Etiwanda (EDF > 1). For those two sites, we predicted NO and NO_2 concentrations with a model that treats traffic non-parametrically (Eq. 2.1), with other sites using a linear term with traffic (Eq. 2.2). Our models are as follows:

$$E(Y_d) = \alpha + yr_L + R + \beta(Z_{1,R}) + s(Z_{2,R}) + s(T_{yr,L}) \tag{2.1}$$

$$E(Y_d) = \alpha + yr_L + R + \beta(Z_{1,R}) + s(Z_{2,R}) + \beta(T_{yr,L}) \tag{2.2}$$

where, Y_d is NO or NO_2 concentration on a given day d; α is a constant; β refers to a regression coefficient; R is a dummy variable denoting region; yr_L is a dummy variable denoting yearly differences at each location L; $Z_{1,R}$ is a set of meteorology variables found to have a linear relationship with the outcome at region R; $Z_{2,R}$ refers to the remaining meteorology variables; $T_{yr,L}$ refers to the effect of traffic variables at each location L during a given year yr; and s is the smoothing nonparametric spline function.

2.3.3 Model Validation

We used the K-fold cross-validation method with 10 folds to assess our models. We randomly assigned the data into 80% training, 20% testing and calculated the adjusted R^2, repeating the procedure 10 times to derive a mean R^2 of our CV results. Our mean adjusted R^2 values for NO were 0.66 with linear terms for traffic and 0.68 with a nonparametric smoother. For NO_2, our adjusted R^2 values were 0.78 with linear terms for traffic and 0.81 with a nonparametric smoother. This suggests a strong fit for both dependent variables that matches the performance of prior studies [84], though we did find that our models slightly underestimated mobile source emissions.

2.3.4 Simulating Traffic and NO and NO_2

We simulated a business-as-usual scenario by assuming that without the COVID-19 pandemic, passenger and truck traffic would experience identical weekly patterns as those in the months of January and February 2020 and those in March and April from 2017-2019. Traffic levels were similar between the two sets, but the inter-year variation between the same months was greater than the inter-month variation within the same year at most sites (see Table 2.3). This led us to simulate passenger and truck traffic using data from January and February 2020, which represents a more accurate estimate, as a business-as-usual scenario. Days between March 1st and April 30th, matching previous studies [77–79], were assigned a passenger and truck flow a value equivalent to the weekday average of each day during the first two months of the year. For example, Mondays were traffic measurements equivalent to the average Monday traffic in January and February. We calculated the change in traffic with the following equation:

$$\Delta_T = \frac{T_s - T_o}{T_s} * 100 \tag{2.3}$$

Where the percent change in traffic Δ_T is the difference between simulated (T_s) and observed (T_o), normalized over simulated traffic and multiplied by 100. Based on simulated business-as-usual traffic values, we used our GAMs (Eq. 2.1 and 2.2) to predict NO and NO_2 during the months of March and April under two scenarios. Scenario A predicts NO and NO_2 with business-as-usual simulated passenger and truck traffic. Scenario B predicts with business-as-usual simulated passenger traffic and observed truck traffic data. The difference between the two scenarios illustrates the relative contribution of the decline in passenger vehicles to the overall reduction of NO and NO_2. We then used Welch two-sample t-tests to assess the statistical significance of the differences between the observed and predicted traffic, NO, and NO_2 measurements on weekdays and weekends. In Table 2.1, significant differences as indicated by the Welch's t-test, are marked with an asterisk. We used the

following equation to calculate percent change in the gas G:

$$\Delta_G = \frac{G_s - G_o}{G_s} * 100 \tag{2.4}$$

We used R version 3.6.3 [88] to conduct data retrieval, analysis, and visualization in this chapter.

2.4 Results and Discussion

2.4.1 Changes in Vehicle Flow

Figure 2.4 depicts passenger vehicle and truck traffic in Northern and Southern California between March 1st and April 30th. Figures 2.4a and 2.4b depict a substantial decline in passenger traffic beginning in early March, reflecting the massive shift to remote work. Figures 2.4c and 2.4b show that truck flow, a possible indicator of commercial activity, decreased in Northern, but not Southern California. Table 2.1 quantifies the above observations by location and splits the data into weekday and weekend. We find percent declines in traffic during both weekdays and weekends. The former likely indicates declines in commuting and the latter likely indicates declines in non-commuting activity, such as recreational activities and travelling. Passenger traffic in declined in Northern and Southern California, by 29% and 24% on weekdays and 42% and 37% on weekends, respectively. Weekday truck flow decreased by between 13% and 37% in Northern California locations and between 2% and 7% in Southern California locations with varying degrees of statistical significance, marked by an asterisk, suggesting that during the weekdays, flow of goods did not change as much as in the North. Similarly, on weekends, we noticed a 44% decline in truck traffic in Northern California, compared to 21% in Southern California, which was not statistically significant.

2.4.2 Changes in NO and NO_2 concentrations

Figure 2.5 depicts 14-day rolling averages of NO and NO_2 levels in Northern and Southern California. The black solid line represents observed data, while the yellow dashed line depicts predicted NO and NO_2 under Scenario A, which simulates business-as-usual truck and passenger vehicle traffic. The blue dashed line represents predicted NO and NO_2 concentrations under Scenario B, simulating business-as-usual passenger traffic only. We find that a greater share of NO and NO_2 reductions is attributable to passenger traffic decline in Southern California, shown by a smaller gap between blue and yellow lines, due to smaller, insignificant changes in the region's truck flow.

As shown in Table 2.1, NO concentrations fell by 35% and 60% in weekdays and weekends, respectively in Northern California, and 32% and 20% in weekdays and weekends, respectively, in Southern California. Our results agree with previous COVID-19 related studies that have reported NO_2 emission reductions in California [78, 79, 89]. Outside of California, studies around the world have also found a consistent decline in NO_2. While traffic reductions of this scale are historically unprecedented, other smaller scale natural experiments that disrupt automobile traffic, such as a major highway closure [18], major sporting events [90–92], and odd-even license plate traffic policies [93] have found similar declines in direction and magnitude in air pollution following declines in traffic. Our results confirm and reinforce the relationship between traffic and mobile source pollution.

Our analysis has a few limitations. We ended our study period on April 30th to focus on the most stringent shelter in place period and match previous studies. As a result, we could not observe how scattered opening up of California localities affected traffic and air quality which warrants further studies. Regarding our data sources and methodology, a cutoff of 50% observed traffic may lead to an excess of algorithmically generated data which ignore immediate pandemic-related traffic impacts. As a result, we may be overestimating traffic flow and underestimating NO and NO_2 reductions. Another limitation is related to

uncertainty of traffic and pollution estimates. While we did not quantity these uncertainties, we found that traffic changed very little during January and February 2020 (mean coefficient of variation: 11%). Due to the low coefficient of variation, large effect size, and statistical significance of the results, we do not expect such uncertainties would alter our conclusions. Lastly, another source of bias may arise from weather data. Fewer than half of the EPA near-road sites in California reported meteorology data, necessitating the use of a different data source. Nevertheless, meteorology reported by near-road sites were very highly correlated with MesoWest data, with correlation coefficients between sources of temperature, relative humidity, and wind speed data at 0.97, 0.95, and 0.75, respectively. In addition, the data fit well based on adjusted R^2 values, suggesting a robust model.

In summary, we estimated the meteorology-adjusted decline in NO and NO_2 concentrations attributable to quantified changes in near-road traffic following shelter-in-place in California. We found that the contribution of passenger vs. truck traffic declines to changes in NO and NO_2 differs between Northern and Southern California. We report one of the first studies that quantifies the effect of directly measured traffic on NO and NO_2 reduction, the former a significant precursor to the latter as well as other mobile source-derived pollutants including ozone, PM2.5, and smog. This chapter shows a directly measured link between reduced traffic and reduced NO and NO_2 emissions, strengthening the evidence base between COVID-19, shelter-in-place, and cleaner air.

2.5 Figures and Tables

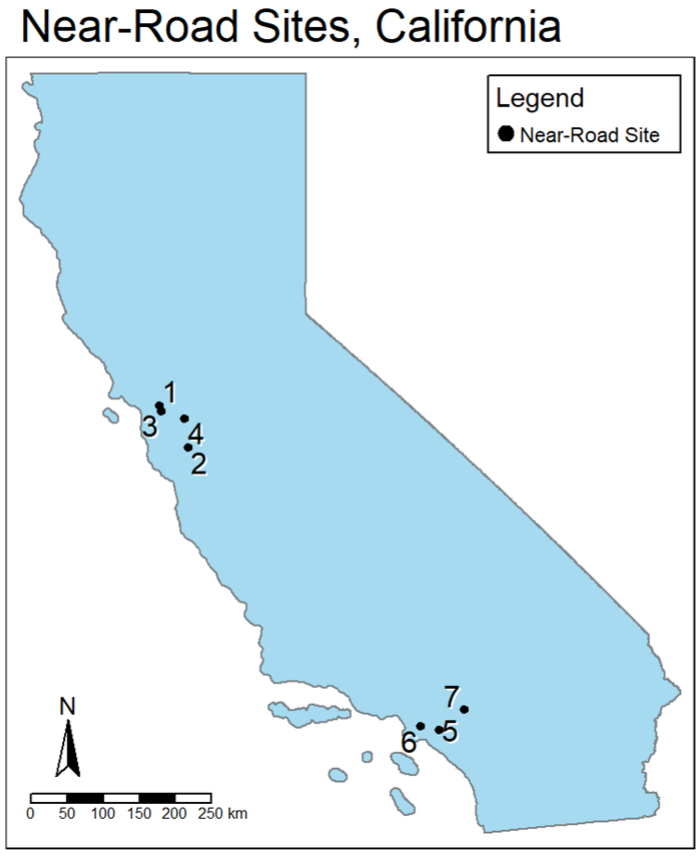

Figure 2.1: Map of near-road monitoring sites in California. Numbers refer to, from 1 to 7: Berkeley Aquatic Park, Knox Avenue, Laney College, Owens Court, Anaheim Route 5 Near Road, Long Beach Route 710 Near Road, and Ontario Etiwanda Near Road.

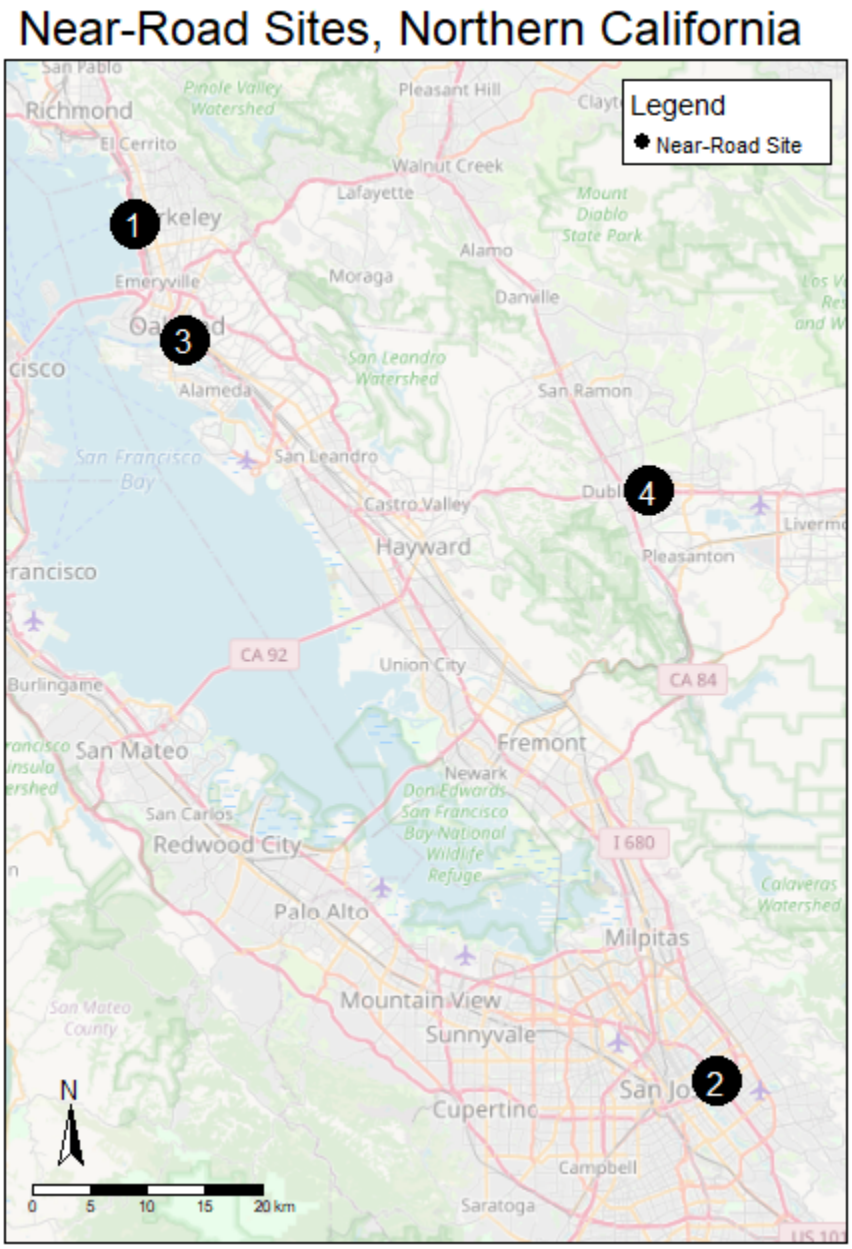

Figure 2.2: Map of near-road monitoring sites in Northern California. Numbers refer to, from 1 to 4: Berkeley Aquatic Park, Knox Avenue, Laney College, and Owens Court.

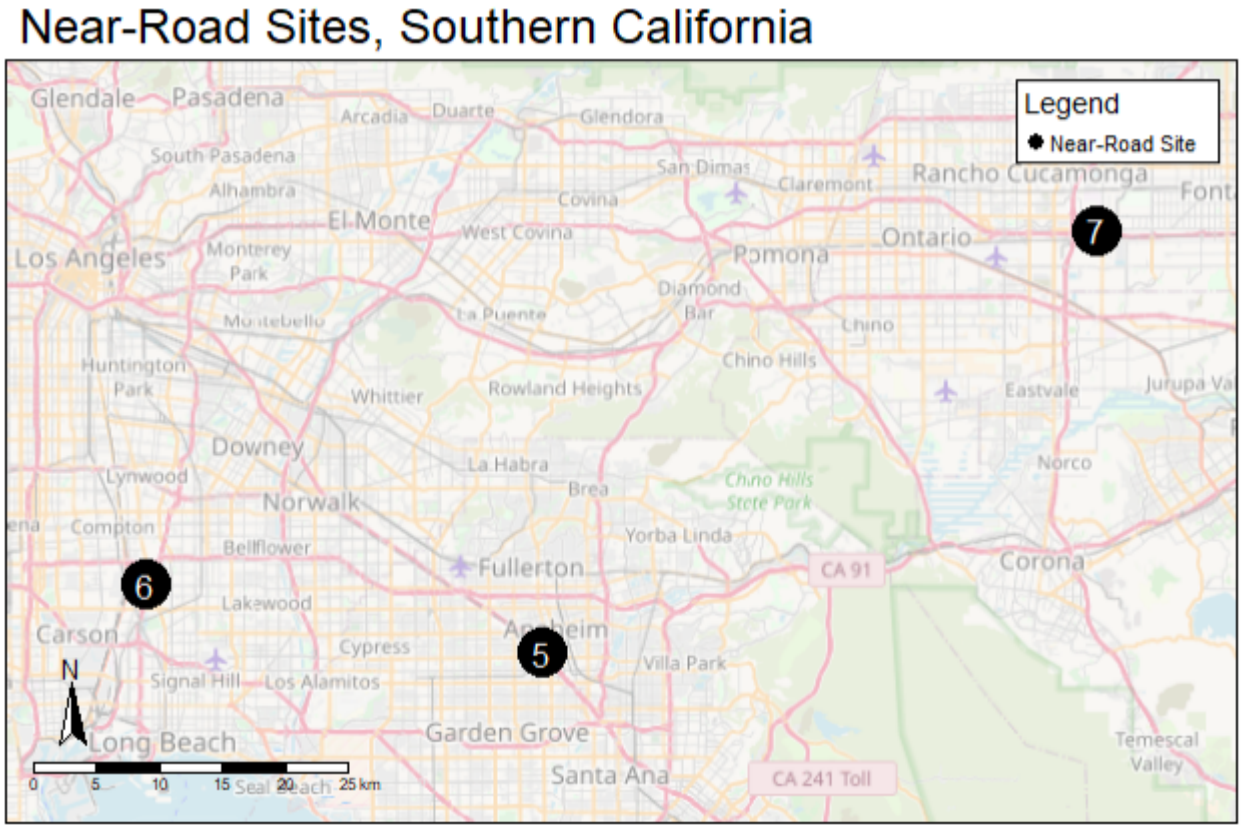

Figure 2.3: Map of near-road monitoring sites in Southern California. Numbers refer to, from 5 to 7: Anaheim Route 5 Near Road, Long Beach Route 710 Near Road, and Ontario Etiwanda Near Road.

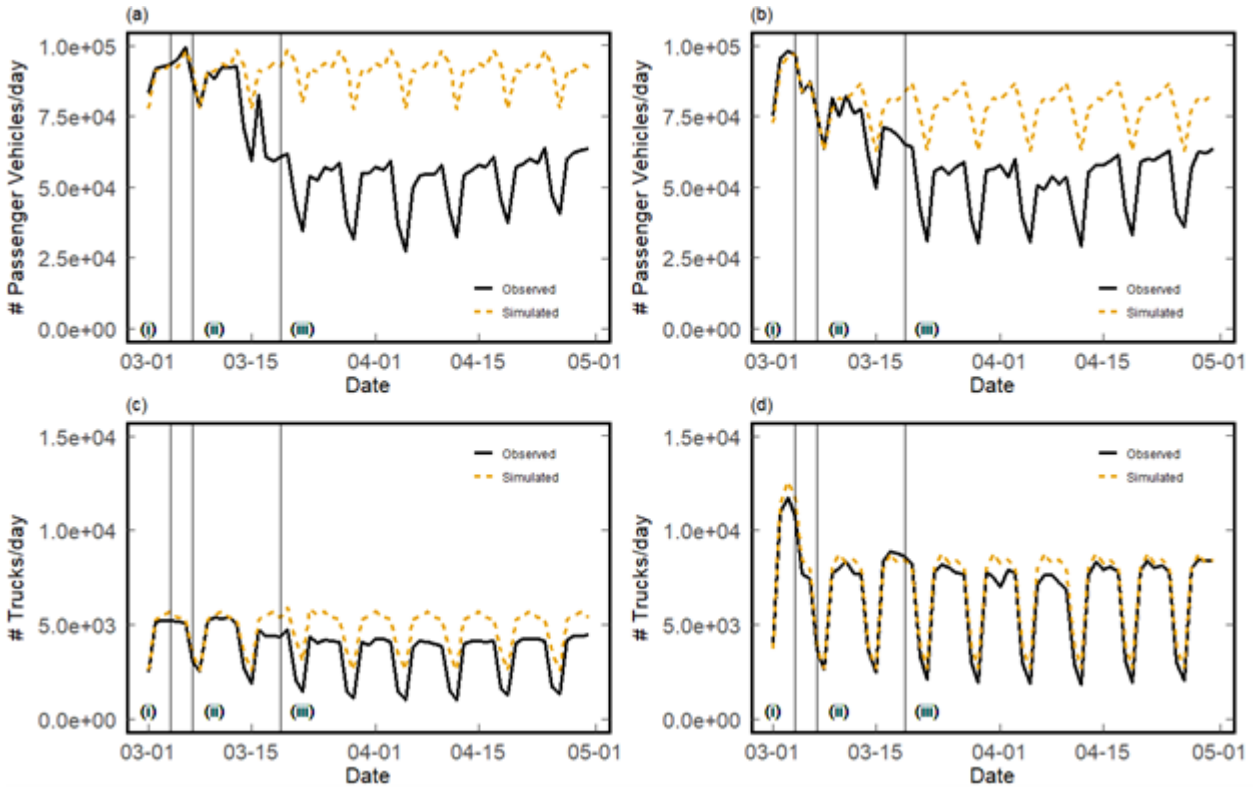

Figure 2.4: Observed (black solid line) vs. Business-as-Usual (yellow dotted line) traffic flow in California from March 1st to April 30th, 2020. (a) Northern California Passenger Vehicle Traffic, (b) Southern California Passenger Vehicle Traffic, (c) Northern California Truck Traffic, and (d) Southern California Truck Traffic. The three vertical lines represent, from left to right (i) March 3rd, when California declares a state of emergency, (ii) March 7th, when the city of San Francisco banned large group gatherings, and (iii) when California declares a statewide shelter-in-place order.

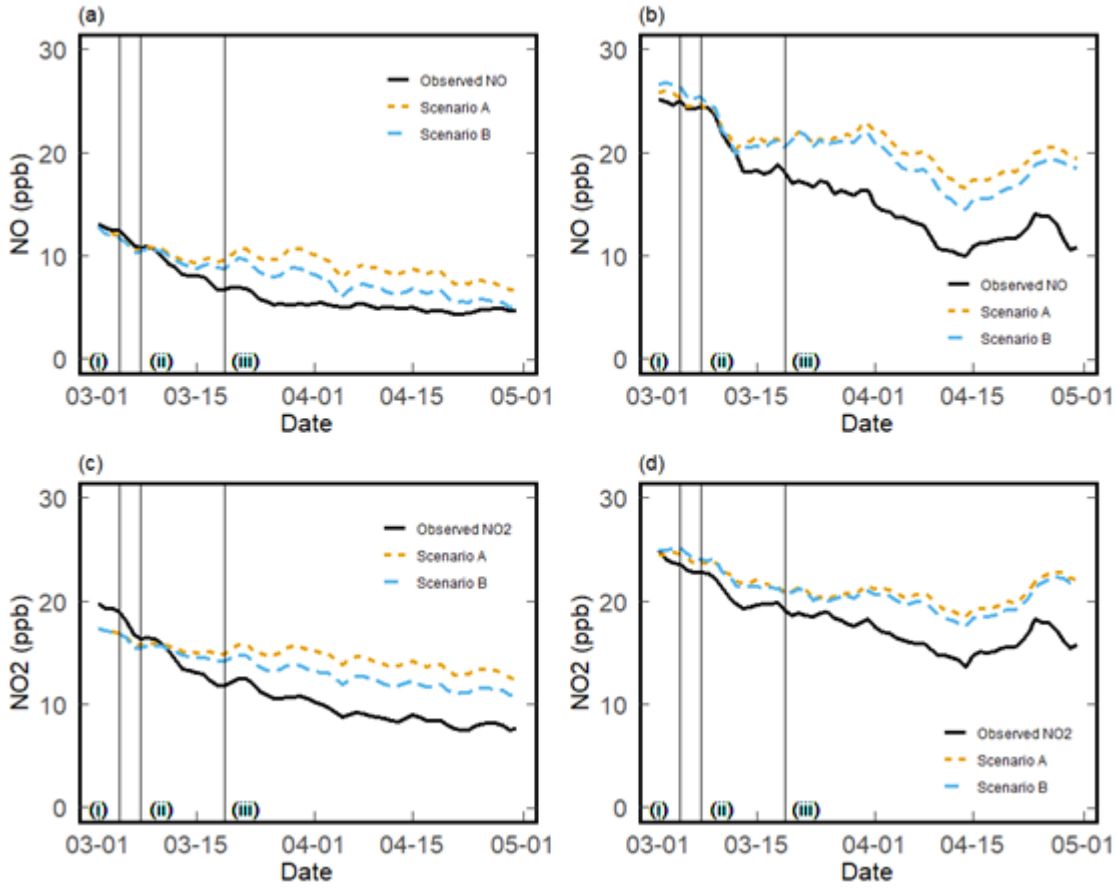

Figure 2.5: Two-week rolling averages of observed near-roadway NO and NO_2 concentrations versus simulated scenarios in California: (a) Northern California NO, (b) Southern California NO, (c) Northern California NO_2, and (d) Southern California NO_2. The black solid line is observed data. The yellow dotted line depicts predicted NO and NO_2 concentrations under Scenario A, simulated business-as-usual passenger flow and truck flow. The blue dashed line depicts predicted NO and NO_2 concentrations under Scenario B, simulated business-as-usual passenger and observed truck flow. The three vertical lines represent, from left to right (i) March 3rd, when California declares a state of emergency, (ii) March 7th, when the city of San Francisco banned large group gatherings, and (iii) when California declares a statewide shelter-in-place order.

Table 2.1: Percent reductions in vehicle flow and NO emissions between observed measurements and simulated business-as-usual from March 1, 2020 to April 30, 2020. Data are separated by site and overall region as well as into weekdays and weekends. Standard deviations of percentage reductions are in parenthesis.

	% Passenger Flow Reduction (SD)		% Truck Flow Reduction (SD)		% NO concentration reduction (SD)		% NO2 concentration reduction (SD)	
Region/Site	Weekday (N = 44)	Weekend (N = 17)	Weekday (N = 44)	Weekend (N = 17)	Weekday (N = 44)	Weekend (N = 17)	Weekday (N = 44)	Weekend (N = 17)
Northern California	29 (17)*	42 (23)*	23 (14)*	44 (20)*	35 (5.1)*	60 (2)*	29 (7.3)*	44 (0.87)*
Berkeley Aquatic Park	23 (15)*	38 (23)*	13 (10)*	34 (21)*	26 (4.6)*	22 (13)*	19 (4.2)*	26 (0.96)*
Knox Avenue	31 (19)*	42 (23)*	37 (16)*	53 (20)*	44 (6.2)*	43 (20)*	39 (9.6)*	54 (1.4)*
Laney College	29 (14)*	40 (25)*	22 (5.4)*	43 (9.4)*	42 (8.5)*	33 (21)*	31 (6.8)*	45 (0.85)*
Owens Court	34 (19)*	47 (25)*	20 (12)*	48 (24)*	30 (10)*	25 (23)*	26 (9.4)*	49 (1.1)*
Southern California	24 (15)*	37 (20)*	4 (9.3)	21 (15)	32 (9.3)*	20 (6.8)*	15 (5.8)*	31 (3.6)*
Anaheim Route 5 Near Road	31 (18)*	41 (21)*	3 (13)	16 (14)*	-11 (9.2)*	-15 (20)	21 (5.3)*	45 (0.99)*
Long Beach Route 710 Near Road	22 (12)*	37 (19)*	7 (6.1)*	34 (12)*	47 (8.5)*	40 (16)*	15 (6.4)*	29 (1.5)*
Ontario Etiwanda Near Road	19 (11)*	34 (20)*	2 (6.7)	13 (11)*	28 (13)*	19 (17)*	10 (10)*	22 (9.2)*

Table 2.2: List of near-road monitoring sites in study, location (county), and target highway. Unshaded sites are were classified as in Northern California, while sites shaded in green were classified as in Southern California.

Local Site Name	County	Target Road
Berkeley Aquatic Park	Alameda	I-80
Knox Avenue	Santa Clara	US 101
Laney College	Alameda	I-880
Owens Court	Alameda	I-580
Anaheim Route 5 Near Road	Orange	I-5
Long Beach Route 710 Near Road	Los Angeles	I-710
Ontario Etiwanda Near Road	San Bernardino	I-10

Table 2.3: Mean standard deviation of passenger and truck flow for (a) within-month traffic between 2017-2019 and (b) within-year traffic between January and April within the same year for the years 2017-2019. Unshaded sites were classified as in Northern California, while sites shaded in green were classified as in Southern California.

	(a) Mean SD Flow, Within Months		(b) Mean SD Flow, Within Year	
Local Site Name	Passenger	Truck Flow	Passenger	Truck Flow
Berkeley Aquatic Park	9433	1816	6973	1758
Knox Avenue	4923	423	7096	156
Laney College	8402	1328	8788	1380
Owens Court	10866	1250	10146	1220
Anaheim Route 5 Near Road	5726	396	5410	393
Long Beach Route 710 Near Road	14694	4586	13307	4517
Ontario Etiwanda Near Road	8431	2290	8265	1974

CHAPTER 3

Co-kriging with a low-cost sensor network to estimate spatial variation of brake and tire-wear metals and oxidative stress potential in Southern California

3.1 Abstract

Due to regulations and technological advancements reducing tailpipe emissions, an increasing proportion of emissions arise from brake and tire wear particulate matter (PM). PM from these non-tailpipe sources contains heavy metals capable of generating oxidative stress in the lung. Although important, these particles remain understudied because the high cost of actively collecting filter samples. Improvements in electrical engineering, internet connectivity, and an increased public concern over air pollution have led to a proliferation of dense low-cost air sensor networks such as the PurpleAir monitors, which primarily measure unspeciated $PM_{2.5}$. In this study, we model the concentrations of Ba, Zn, black carbon, reactive oxygen species concentration in the epithelial lining fluid, dithiothreitol (DTT) loss, and OH formation. We use a co-kriging approach, incorporating data from the PurpleAir network as a secondary predictor variable and a LUR model as an external drift. For most pollutant species, co-kriging models produced more accurate predictions than an LUR model, which did not incorporate data from the PurpleAir monitors. This finding suggests that low-cost sensors can enhance predictions of pollutants that are costly to measure extensively in the field.

3.2 Introduction

Exposure to $PM_{2.5}$ and $PM_{2.5\text{-}10}$ has been associated with a wide array of adverse human health effects [38]. The composition of PM, as a complex, multisource pollutant, varies depending on factors such as season, geography, and time of day [94–96]. Traffic is an important source of ambient $PM_{2.5}$ and is a dominant contributor to metals found in PM [8, 97]. Recent vehicle emissions regulations have decreased average tailpipe emissions, but not those from brake and tire wear [3]. As a result, the relative importance of non-exhaust vehicle emissions, namely those from brake and tire wear as well as road wear, has increased in recent years [98, 99]. This trend is expected to continue particularly as the sale of electric vehicles continues to grow [6].

Brake and tire wear particles are generated due to friction and abrasion caused by braking and normal driving conditions. Studies have found that brake and tire wear particles exist in both the fine and coarse ranges, with diameters rangng from 1-10 μm. Sharp spikes in temperature associated with braking action also generate ultrafine particles, provided that temperatures achieve a critical temperature ($140°C < T < 240°C$) [6]. Prior studies on roadways and in the laboratory have identified specific metals that can serve as tracers with varying specificity for identifying non-exhaust emissions, including Ba, Cu, and Sb for brake wear particles and Zn for tire wear particles [100–104]. These metals, in addition to serving as tracers for brake and tire wear, are themselves highly reactive. In surrogate lung fluid, heavy metals such as Cu cause oxidative stress when reacting with H_2O_2 to form OH radicals in a process known as the Fention reaction [105]. The presence of ultrafine particulates emitted by brake wear that contain highly reactive heavy metals may have human health implications, as ultrafine particles when inhaled travel deeper in the lung and can enter the bloodstream. Knowledge concerning the spatial distribution of such elements, however, remains limited.

LUR is a well-established technique used for exposure assessment of intraurban air pollution, where regression models include land use, traffic, physical geography, and business

density as predictors of measured air pollution concentrations [28, 106, 107]. Model derived coefficients can then be applied to generate an interpolated exposure surface for an entire study area.

LUR has been used extensively to study of traffic-related pollutants including unspeciated particulate matter and NO_2 [28], but relatively few studies have applied such methods to particulate matter constituents. In an early study, de Hoogh et al. (2013) [108] analyzed spatial data from 400 sampling locations in 20 study areas across Europe and constructed LUR models for each site and each metal. They found that traffic-related variables, including traffic intensity and road length were often associated with metals identified as brake and tire tracers, such as Cu and Zn. Zhang et al. (2015) [109] collected PM_1 data at 54 samplinglocations (25 in the summer, 29 in winter) in Calgary, Alberta and found that auto- and traffic-related variables contributed strongly to the predictions of monitored Ba, Zn, Cu, and Sb. Ito et al. (2016) [110] sampled at 99 locations in New York City and used speciated particle data to produce LUR models, identifying Cu, Fe, and Ti as markers of near-road pollution. Weichenthal et al. (2018) [111] used LUR to model Cu, Fe, and generated a reactive oxygen species (ROS) concentration in lung fluid based on these two metals using 67 sites at which they monitored in two seasons and found strong associations between road and traffic-related variables such as distance to and length of highways, length of major roads, and traffic counts and all three of their dependent variables, while also finding strong correlations between Cu, Ba, and Fe.

Other studies expanded on the traditional LUR approach by altering either the statistical methodology or including additional predictors in their LUR model. Brokamp et al. (2017) [30] collected $PM_{2.5}$ samples at 24 sites in Cincinnati, Ohio, and modeled metal concentrations using both linear land use regression models and machine learning-based random forest regression models. Their approach resulted in better fit compared to previous models. For metals associated with brake and tire wear, including Cu and Zn, they found that traffic or road variables such as length of road and truck traffic were significant predictors. Tripathy

et al. (2019) [31] continued with a linear regression approach but integrated a Gaussian atmospheric dispersion model into their predictions, also finding improved model fit compared to only using land-use variables.

A general barrier of measuring speciated $PM_{2.5}$ elements is the time and labor involved in the sample collection and analysis. Collection of air samples on filters followed by inductively coupled mass spectrometry analysis is the current gold standard, offering precise information on multiple metal constituents and isotopes. Collecting many samples simultaneously can be very challenging due to equipment and labor demands. As a result, assimilating other forms of data to assist with interpolation has clear advantages.

A potential solution to this problem involves using low-cost air sensor networks, such as PurpleAir [112]. Low-cost air sensor networks have grown following improvements in wireless connectivity technology and electrical engineering and have received increased attention from government regulatory agencies, such as the U.S. Environmental Protection Agency and the California Air Quality Management District [5, 113]. The PurpleAir device consists of two Plantower PMS5003 laser particle (channels A and B), which use light scattering of a laser to count suspended particulates in the air at various sizes and provides the mass concentration of $PM_{1.0}$, $PM_{2.5}$, and PM_{10} [112]. Devices also include wireless internet connectivity, and with the consent of the user, uploads time series data to the PurpleAir website, which provides data free of charge. PurpleAir sensors are not reference grade, although they correlate well with federal reference monitors [114]. In addition, these low-cost sensors do not measure speciated $PM_{2.5}$ constituents. The network, however, is far denser in major metropolitan areas compared to regulatory monitors and monitors deployed in academic studies, and information is collected and stored in real-time.

In this chapter we leverage the PurpleAir network to enhance the prediction of metal species and indicators of oxidative stress. We implemented geostatistical modeling employing the co-kriging method to predict a target, gold standard variable (i.e., filter-based particle samples) based on auxiliary measures from more widely distributed PurpleAir sensors. While

widely used in mining and petroleum engineering, co-krigi has previously seen limited, but effective use in air pollution studies [115]. With a focus on brake and tire wear derived particles, this chapter is the first to model speciated $PM_{2.5}$ integrating information from a low-cost air sensor network.

3.3 Methods

3.3.1 Site selection, $PM_{2.5}$ speciation data

A related publication details the site selection and sampling methods of this chapter, and thus are described only briefly here [103]. Our study targeted the greater Los Angeles area, a geographically diverse and heavily populated region of 11.4 million people. The region is characterized as a Mediterranean climate, and is mild to hot year-round, with mean temperatures ranging from 15-17°C in the winter to 21-23°C in the summer. Average rainfall varies seasonally, with average ranfall at between 29-92 mm in the winter and 0-2.3 mm in the summer. We conducted two sampling campaigns, one in summer 2019 and the other in winter 2020. In each campaign, monitors simultaneously collected two-week samples at 46 different locations in the Greater Los Angeles region, with four sites serving as repeat locations. Our site selection methods, detailed in a prior report, involved a Multi-Criteria Decision Analysis, combining variables hypothesized a priori to be associated with brake and tire wear such as traffic intensity, road slope variance, and intersection density, as well as expert understanding of local geographies and PurpleAir densities to improve co-kriging [116]. The chapter analyzes data on ambient fine and coarse PM samples using Harvard cascade impactors (CI) and personal environmental monitors (PEM).

In addition to chemical analyses described by Oroumiyeh et al. (2022) [103], PEM samples were analyzed for black carbon and oxidative stress activity at UCLA with absorption at 880 and 370 nm, using an optical transmissometer (Magee Scientific). Oxidative stress potential was measured with two assays: OH radical formation and dithiothreitol (DTT) loss. We

measured OH formation by incubating samples in surrogate lung fluid containing an OH probe disodium terephthalate, and monitoring formation the reaction product of OH and terephthalate, which is highly fluorescent [117]. DTT loss was measured by incubating filters in phosphate buffer containing DTT, as detailed in Cho et al., (2005) [118].

Prior to deployment, a preliminary list of metals hypothesized to serve as specific tracers for different sources (brake wear, tire wear, tailpipe emissions, and dust and soil) based on a prior literature search. To finalize a list of potential dependent outcomes, we calculated Spearman correlations between hypothesized tracers and selected Ba (brake wear), Zn (tire wear), DTT loss, OH formation, and black carbon, and a calculated ROS formation based on the kinetic multilayer model for surface and bulk chemistry in the epithelial lining fluid (KM-SUB-ELF ROS) [119], as well as unspeciated $PM_{2.5}$. KM-SUB-ELF ROS uses concentrations of Cu and Fe, metals both associated with brake and tire wear, to calculate the rate of production of ROS in the epithelial lining fluid. Except for gravimetric $PM_{2.5}$ and KM-SUB-ELF ROS, we generated predictive surfaces for all metals and oxidative stress markers based on both volume-normalized and mass-normalized concentrations.

3.3.2 Land-use data

We downloaded land-use data from the following sources: (i) raster data on impervious surfaces, tree canopy, and green space data from the 2016 National Land Cover Database (NLCD) [120]; (ii) 2018 annual average daily traffic data from the federal highway administration [121]; (iii) road network and rail network information from the U.S. Census Bureau [122]; and (iv) businesses likely to emit metals, such as auto repair shops and metal processing units, from the ESRI business analyst [123] .

NLCD data came in three raster files, each at a resolution of 30 by 30 meters: impervious percent, tree canopy percent, and a dataset which classified each pixel into type of land use [120]. Following a previous study, we created green space by grouping the following variables together: open water, ice/snow, developed/open space, developed/low intensity, decidu-

ous forest, evergreen forest, mixed forest, dwarf scrub, shrub/scrub, grassland/herbaceous, sedge/herbaceous, pasture/hay, and cultivated crops [124]. We classified the following as non-green space: medium intensity land cover, high intensity land cover, and barren land (rock/sand/clay) (Table 3.1)

Information on all businesses in the study area were downloaded from the ESRI business analyst. We selected businesses that potentially emit heavy metals and those related to brake and tire wear such as auto shops and brake and tire manufacturers based on North American Industry Classification System code. Subsections for codes selected are available in Table 3.2.

3.3.3 Buffering and zonal statistics

We assigned land-use data to our sampling sites using nested circular buffers [125, 126]. Around each monitoring site, we constructed circle-shaped areal units of 100-, 200-, 300-, 400-, 500-, 750-, and 1000-meter radii. For each circle, we calculate either the average value for land use for NLCD and traffic data or the density for intersection and businesses data. The complete list of potential variables as well as well as their sources are found in Table 3.3.

3.3.4 Land-use regression model building and validation

In line with other studies, we approach our data assuming a linear relationship between independent and dependent variables [109]. We began by plotting histograms and univariate plots to investigate the distribution of dependent and independent variables. If a histogram revealed the distribution of a variable to be skewed, or if univariate plots showed a non-linear relationship between independent and dependent variable, we log transformed our variables. To reduce collinearity between variables of the same class but different buffer radii, for each class of variable, we selected the buffer distance with the highest univariate correlation with

the outcome of interest. After generating variables for each point, we used a method previously used to predict $PM_{2.5}$ concentrations in the United States, selecting variables using a deletion-substitution-addition (DSA) algorithm [127]. The DSA algorithm selected variables based on prediction accuracy with a L2 loss cross-validation function [128]. After the DSA algorithm chose the optimal set of predictors of sizes 1-10 variables, we conducted another round of K-fold cross-validation with five folds to select an optimal number of variables in the final model based on the mean square predictor error.

To adjust for seasonality, we included a dummy variable indicating the sampling season (0 = summer, 1 = winter). In our final prediction surfaces, we calculated the average of the summer and winter surfaces by dividing the season coefficient by two and adding the resultant term to the remainder of the model.

3.3.5 PurpleAir data

Within the study area, we downloaded hourly-averaged PurpleAir data temporally aligned with both study periods from the PurpleAir website. PurpleAir sensors contain two sensors, which separately report $PM_{2.5}$ measurements through two channels, A and B. We restricted our sample to outdoor sensors. Downloaded data contained date and time of measurement, estimated particle matter mass concentration at 1, 2.5, and 10 microns reported by the two sensors in each device labeled channels A and B, temperature in $^{\circ}F$, and relative humidity. Initial data quality assurance and quality control (QA/QC) steps included excluding sensors if they:

- Had a missing data rate of 10% or higher
- Did not report temperature

Next, we verified that our sensors were outdoor by creating time series temperature plots. If sensors reported a very low range of temperature, we assumed that they were mislabeled

indoor sensors and subsequently deleted the sensor.

After obtaining a final list of PurpleAir sensors, we conducted further QA/QC per Plantower's factory standards [129]. Data points were removed if they did not meet the following criteria:

- $PM_{2.5}$ mass concentrations above 500 $\mu g/m^3$
- For observations below 100 $\mu g/m^3$, remove rows if the difference between $PM_{2.5}$ measurements reported in channels A and B exceeds 10 $\mu g/m^3$
- For observations greater than 100 $\mu g/m^3$, remove rows if the difference between $PM_{2.5}$ measurements reported in channels A and B exceeds 10%

Finally, we also removed a limited number of rows with extreme temperature and relative humidity values (RH% $\leq$ 0 or RH% $\geq$ 100; temperature $\leq$ -200°F (-129°C) or temperature $\geq$ 1000°F (537 °C)). Once cleaned, for each sensor, we obtained a final measurement by averaging measurements from the A and B sensors.

We selected PurpleAir estimated $PM_{2.5}$ concentrations as our auxiliary variable in our co-kriging model, as it exhibited the highest univariate correlations with our speciated $PM_{2.5}$ data. Locations of both filter samplers and PurpleAir sensors are plotted on Figure 3.1. Our final dataset used data from 50 filter samplers across two seasons and 294 PurpleAir sensors.

3.3.6 Co-kriging with external drift

Co-kriging [130, 131] refers to predicting the value of an outcome of interest at a spatial location exploiting information from (i) direct measurements of the primary variable; and (ii) measurements of other variables, sometimes referred to as auxiliary variables or co-variables, with which the outcome is assumed to be statistically dependent. The key advantage of co-kriging over ordinary kriging is that we incorporate the dependence between the primary variable and the auxiliary variable as well as the spatial dependence exhibited by all the

variables. The external drift refers to a set of linear predictors, in this case our LUR models. By incorporating spatial dependencies between our measurements and PurpleAir estimates, we can model using spatial relationships unaccounted for with standard LUR models.

Co-kriging with external drift (CED) uses a multivariate spatial regression model

$$y_i(s) = x_i^\top(s)\beta + w_i(s) + \epsilon_i(s) \ , \quad i = 1, 2, \ldots, q \ , \tag{3.1}$$

where $y_i(s)$ is the i-th outcome at location s, $x_i(s)$ is the external drift, a $p \times 1$ vector of land-use covariates or predictors corresponding to the i-th outcome at location s, $w_i(s)$ is a zero-centered spatial process capturing spatial dependence and $\epsilon_i(s)$ is a white-noise process independent of $w_i(s)$ capturing micro-scale variation arising from measurement errors or other fine resolution dependencies.

To avoid singularity issues, for co-located points in both speciated metals and PurpleAir data, we shifted longitude and latitude coordinates by a random distance between 0 and 5 meters. For each exposure (outcome variable), we estimated $w_i(s)$, the spatial process, as a covariogram modeling the cross-covariance between the exposure and auxiliary variable as a function of distance. After fitting initial theoretical covariograms, we evaluated the performance by simultaneously conducting 1000 iterations of 10-fold cross-validation for both the original LUR model as well as the CED model. We then used two-sample t-tests to compare the mean and standard deviation of the 1000 subsequent mean square errors generated and made manual adjustments to the cross co-variogram parameters. We repeated this process with the goal of minimizing both the mean and standard deviation of the MSE as much as possible.

We implemented co-kriging using the `gstat` library [132] in the `R` statistical computing environment to implement co-kriging. Locations of the filter samplers and PurpleAir monitors used in the study are mapped in Figure 3.1.

3.3.7 Generating exposure surfaces

After completing LUR model building, we created raster surfaces for predictor variables using the focal statistics function in ArcMap 10.8 (ESRI, Redlands, CA). In our convex hull, we used R 3.6.3 [88] to generate a 30-meter by 30-meter grid of our study area, extract independent variable values at each point in the grid, and predict with both the LUR and CED models. We avoided predicting exposures in the Angeles National Forest, a national forest with a very few permanent inhabitants not represented in our study sample.

3.4 Results and Discussion

3.4.1 Summary statistics

We built land use regression and co-kriging models for six different components/measures in the $PM_{2.5}$ size fraction: Ba, Zn, OH formation, DTT loss, black carbon, and KM-SUB-ELF ROS. Table 3.4 summarizes both the volume-normalized concentration and mass-normalized (or equivalent) measurement for each model outcome, when available.

Our summary statistics are mostly in-line with findings from previous studies. Our mean gravimetric $PM_{2.5}$ concentration of 9.4 $\mu g/m^3$ was slightly lower, but overall comparable to the 2019 Los Angeles County average of 12.7 $\mu g/m^3$, likely because our 2- week sampling periods in two seasons only covered four of the 52 weeks. Zn measurements are similar to the lower end of measurements reported by de Hoogh et al. (2013) [108], Brokamp et al. (2017) [30], and Kuang et al. (2020) [133] but are much lower than those reported by Tripathy et al. (2019) [31], despite all of these studies having taken place in either European or American metropolitan areas, including some in Los Angeles. Zn is a product of some industrial processes such as steel production, as well as being a component of tires, which may cause the differences in measurements, both spatially and temporally. A reason might be that Zn emissions, while a product with car tire wear, is a multisource pollutant also

associated with the lubrication oil and steel production [30, 31, 133].

For black carbon, our average concentration of 0.41 $\mu g/m^3$ was lower compared to a different study that sampled in the same region, who reported an average concentration of 0.59 $\mu g/m^3$ [134]. The discrepancy in black carbon levels is likely due differences in sampling strategy; Jones et al. (2020) [134] focused on clustering monitoring sites around major freeways in the Los Angeles area, whereas we sampled in both high- and low-traffic areas. Additionally, we collected a single 14-day sample which included sampling during the day and night, with the latter having reduced levels of traffic. Jones et al. (2020) [134] instead measured for shorter periods during the daytime, albeit outside of rush hour traffic. Regarding DTT loss, our average loss rate of 61.9 pmol/min/μg is comparable, but on the higher end of findings published by [135], who analyzed $PM_{2.5}$ samples from the San Joaquin Valley in California, US and found DTT loss rates between 17 and 70 pmol/min/μg [135]. DTT was also studied by Yang et al. (2015) [136]. Compared to our mean volume-normalized mean DTT loss rate of 550 pmol/min/m^3, they measured generally higher rates of DTT loss, ranging from 700 to 2000 pmol/min/μg. Ba is less commonly reported, however, while $PM_{2.5}$, Zn and many other elements measured in our study are much lower than measured in a multi-site air quality campaign in Los Angeles in 1987, Ba concentrations (in ng/m^3) fall in the same range (17 ng/m^3 in our study vs. 13-32 ng/m^3) as the measurements made in 1987. Two earlier studies have reported OH formation in simulated lung fluid from ambient particles, for particles collected at one site during summer in Los Angeles and the other in Beijing and Wangdu in Northern China respectively [137, 138]. Our mass-normalized average value of 0.55 pM/min/μg is reasonably close to the earlier Los Angeles value (0.32 pM/min/μg, Kuang et al. 2017 [137]) and falls in the range of values observed in China (0.22 – 1.13 pM/min/μg). Finally, we found higher levels of ROS generation estimated by KM-SUB-ELF ROS (100 nmol/L), compared to Weichenthal et al. (2018) [111], who sampled during the summer and winter seasons in Toronto, Canada and reported an annual average ROS concentration of 52 nmol/L, possibly due to generally lower particulate concentrations

in Toronto.

We calculated univariate Spearman correlation coefficients between our six outcome variables, summarized in Figure 3.2. Observing changes in correlation coefficients between summer and winter we have divided our correlation matrix into summer (top/left) and winter (bottom/right) and added a dummy variable indicating sampling period (0 for summer, 1 for winter) to our land use regression. We find Spearman correlations are very high (ρ: 0.8-0.98) for metal concentrations or measurements based on metal concentrations (Ba, Zn, and ROS). Such high correlations between brake and tire-wear associated metal-based variables are consistent with a study of speciated PM_1 by Zhang et al. (2015) [109]. For other measurements, correlations are positive, but differ between summer and winter. DTT loss is most highly correlated with other measures in the winter sample (ρ: 0.51-0.73) and only moderately in the summer (ρ: 0.24-0.47), which are consistent with a prior study finding Spearman correlations ranging from 0.24 to 0.52 [136]. In contrast, for OH formation correlations with other measures were slightly higher during the summer (ρ: 0.53-0.71) compared to the winter (0.46-0.60).

Figure 3.3 shows the cross-validation errors for models of each model size chosen by the DSA search algorithm resulting from a 5-fold out-of-sample cross validation process. For each exposure, we chose the model with the minimum error, regardless of model size. Table 3.5 summarizes the results of variable selection while building of 11 different land use regression models for six exposures, including predictors selected, regression coefficients, and adjusted R^2. The most common predictor, which appears in all LUR models except for $PM_{2.5}$, is the dummy variable for monitoring period, indicating seasonal difference among most exposures. All models featured at least one traffic-related variable, either distance to railway, heavy duty traffic, or both. Other common predictors included the land use variables tree canopy cover percent, impervious surface percent, and number of businesses within the buffer distance. The best performing models were for volumized concentrations of Ba, black carbon, and DTT loss, with adjusted R^2 statistics of 0.60, 0.64, and 0.68, respectively.

Despite mainly relying on cross-validation error, our model R^2 values are similar to those obtained in prior literature [109, 136]. Our CV method has previously been shown to be optimized for predictive accuracy, which allows us to minimize the risk of overfitting in our modeling common among studies that choose models based on an R^2 statistic [139].

Across our 12 LUR models, the direction of effect associated with each variable remained consistent, which we interpret as a sign of internal consistency in our results. For example, a positive period variable indicates that exposure concentrations were greater in the winter compared to the summer. Negative distance to rail coefficients indicates that higher levels of exposure closer to railways. Business count coefficients, regardless of buffer distance, were uniformly positive, matching a prior study finding that auto-repair and related businesses are positively correlated with brake and tire wear metals or that they may also be destinations correlated with heavier traffic in the surrounding area (Hasheminassab et al., 2020). Similarly, the coefficient for heavy duty traffic, a variable very highly correlated with passenger traffic, was uniformly positive across our 12 models. Unexpectedly, tree canopy percentage coefficients were not only commonly selected as predictors into models, but were also uniformly positive. Although tree canopy cover may serve as a marker for green space, our study almost exclusively monitored in urban or residential areas, where it is common to plant trees alongside sidewalks near roadways. In our data, we found that log distance to road and tree canopy cover were positively correlated (Pearson $\rho = 0.34$-0.51), which may suggest that in a large, highly developed urban setting, tree canopy serves as a proxy not for density of green space, but instead proximity to the roads.

After completing LUR modeling, we assessed spatial autocorrelation by examining spatial residual maps, constructing and visually inspecting Thiessen polygons, calculating the Moran's I statistic, and modeling the semivariogram of the residuals. All four methods did not show evidence of significant spatial autocorrelation among LUR residuals.

3.4.2 Changes in cross-validation accuracy between LUR and CED

Cross covariograms between LUR residuals and PurpleAir $PM_{2.5}$ showed a degree of cross-covariance (Figures 3.4 and 3.5). We find this reflected in the results of iterated 10-fold cross validation, where after optimizing the cross covariogram parameters, a statistically significant improvement in prediction accuracy among several of our exposures (Table 3.6).

After conducting 1000 iterations of 10-fold cross validation comparing CED and LUR, we found statistically significant reductions in the mean and standard deviation of the MSE for 8 out of the 12 the study's exposures, as shown on Table 3.6. There were statistically significant changes in neither mean or standard deviation of the MSE for mass-normalized Zn concentrations and volumized DTT loss. While black carbon percentage had a small but statistically significant increase in mean MSE, standard deviation of MSE decreased, suggesting increased precision but slightly reduced accuracy. For other outcomes, we found mean reductions in MSE ranging between 2.1% and 14.1%, and reductions in MSE standard deviation between 3.1% and 36%. These results suggest that for most brake and tire wear-related outcomes, incorporating low-cost $PM_{2.5}$ measurements via co-kriging leads to improved predictive accuracy and precision. While co-kriging methods have been used in the past to improve PM_{10} based on incorporating wind speed curves, to our knowledge this chapter is the first to show that compared to conventional LUR methods, co-kriging with a low-cost air sensor network improves predictions of $PM_{2.5}$ species and markers of oxidative stress.

Modeled surfaces for selected dependent variables comparing CED and LUR are illustrated in Figure 3.6. In addition to generally lower MSE and MSE standard deviation, visual inspection reveals that CED appears to act as a smoother for the LUR model. This is particularly noticeable when mapping out the volumized exposure surfaces for of Zn, $PM_{2.5}$, and black carbon. LUR models for those pollutants shows noticeable hotspots along rail lines and major roadways, which result from the distance to rail and traffic-related predictors.

Potential explanations include the choice of modeling method and auxiliary variable. The auxiliary variable in the co-kriging model is $PM_{2.5}$, which as a multisource mixture, generally displays smoother spatial patterns than primary particles from brake and tire wear. Its inclusion as a variable in our prediction model may consequently over-smooth our exposure surfaces. Consequently, co-kriging may lead to a sacrifice in small-area signal, in exchange for more accurate and precise predictions of overall concentrations. Notably, greater degrees of smoothing occurred among among exposures that exhibited higher increases of predictive accuracy and precision, such as $PM_{2.5}$, Zn, and black carbon, compared to DTT loss, which did not experience a significant change in predictive accuracy.

Environmental features may also be responsible for differences in spatial distribution that may be captured by PurpleAir data but not in standalone LUR models. Although we did observed systematic patterns in neither LUR spatial residuals nor clustering, factors such as prevailing wind direction may have affected spatial patterns, leading to smoothing. Other hyperlocal environmental features such as the presence of street canyons may have affected local wind direction, leading to smoothing effects beyond wind direction alone. Traffic activity may also lead to continued resuspension of settled particles, which when entering the atmosphere, leading to more smoothing. Further study of these effects aimed at better understanding the factors behind smoothing include potential simulation studies, repeated campaigns with increased sample size, or alternative choices of auxiliary variables.

Our study has a few limitations. Although the number of sensors deployed matches that of some prior studies, such as Zhang et al. (2015) [109], our study area is much larger than that of prior studies, and the network of monitoring sites is not very dense, which may have led to over-smoothing of the prediction surfaces due to sparse data support. We decided to prioritize covering a larger study area over having many repeated monitoring sites, which resulted in very low temporal resolution, with repeated measurements at only four sites. Adding in the PurpleAir network improves cross-validation for most outcomes and improves the spatial resolution of our data, there may be concerns about this network and its data.

While low-cost, the PurpleAir sensor remains a relatively luxury item, and network density is consequently biased towards high-income households [140]. As a low-cost sensor maintained by consumers, despite attempts at laboratory and field calibration, PurpleAir sensors when inadequately maintained are at risk of unaccountable sensor drift and distortion of results due to environmental factors [129, 141]. Our results show significant improvements in predictive accuracy and precision, though future similar studies using well-maintained sensor networks may see greater improvements in predictive accuracy. With regards to speciated data, most of our filter samplers were placed at residences of participants of an existing birth cohort study, who were largely high SES homeowners. As a result, our model predictions in and around disadvantaged communities, which historically have higher levels of air pollution and lower levels of homeownership, likely have higher levels of uncertainty. Additionally, based on the observed improvements in our predictive models when adding in PurpleAir data, our study suggests that adding in temporally aligned data may help address a fundamental issue among LUR studies.

3.5 Conclusion

Here we presented a novel method for integrating low-cost sensor data with reference grade date to estimate surfaces of brake and tire wear across Southern California. We constructed several exposure surfaces over a large area for use in population health studies with information from filter samples, land-use data, and the PurpleAir low-cost sensor network. Our study demonstrates that as sensor networks continue to expand, the ease of data collection and high spatial resolution associated with such networks may have the potential to improve exposure modeling and subsequent air pollution epidemiology. Compared a conventional LUR, CED addresses spatial relationships between filter samples and PurpleAir sensors across the study area and may account for spatial distribution of brake and tire wear-related particles more accurately than an LUR. Our results reflect normal conditions

because the monitoring did not take place during major recent events affecting air quality, such as the California wildfires and the COVID-19 pandemic.

Despite limitations noted above, our model has identified various land use variables, such as traffic, business density, and impervious surfaces as important predictors of brake and tire wear metals and oxidative potential measures in a large study area. We report the first study to incorporate low-cost sensor data to model speciated PM2.5, as well as the largest-area study covering the Los Angeles metropolitan area. Our study results suggest that such sensor networks, particularly when further expanding, have potential for use in exposure modeling research. When dense enough, such networks have the potential to complement existing research-grade monitoring, particularly when studying pollutants or their markers that are difficult or expensive to measure, such as the constituents of PM2.5 or oxidative stress markers. Future research directions in the exposure field may include taking advantage of the real-time nature of the PurpleAir network to scale speciated $PM_{2.5}$ exposures at different time periods. Beyond exposure modeling, we plan in the future to apply exposure surfaces to health studies, including an existing pregnancy cohort and a study of adverse birth outcomes based on state records.

3.6 Figures and Tables

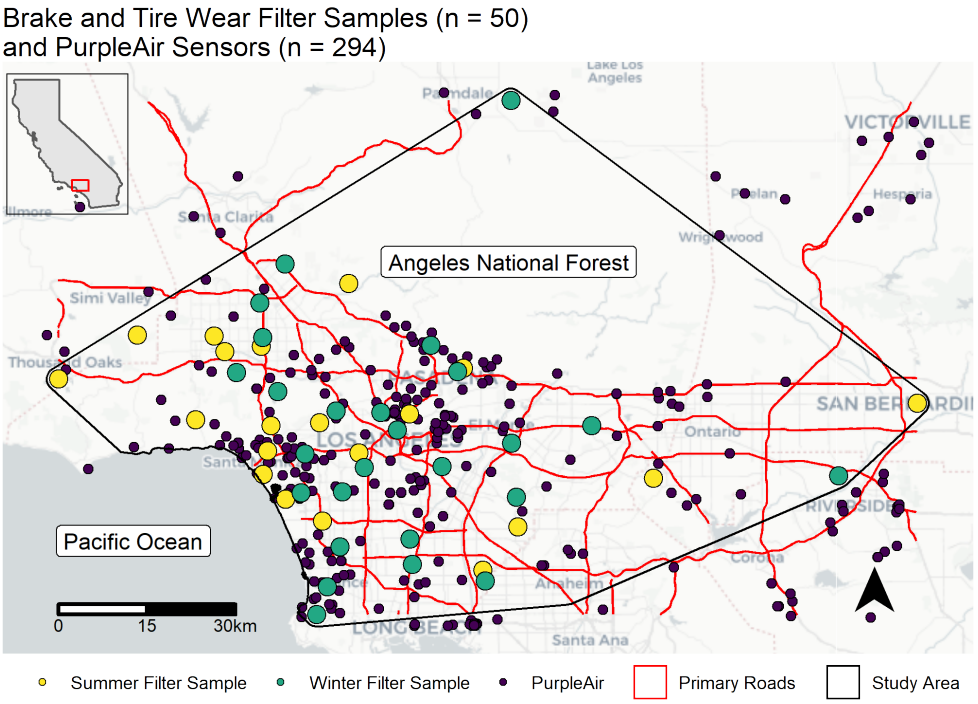

Figure 3.1: Locations of sampling locations (green and yellow) and PurpleAir sensors (purple). The study location within the state of California is illustrated on the top-left, with the study location outlined in red. The area to be interpolated, defined by the convex hull of the pump boxes is outlined in black. Primary roads in the study area's bounding box are shown in red.

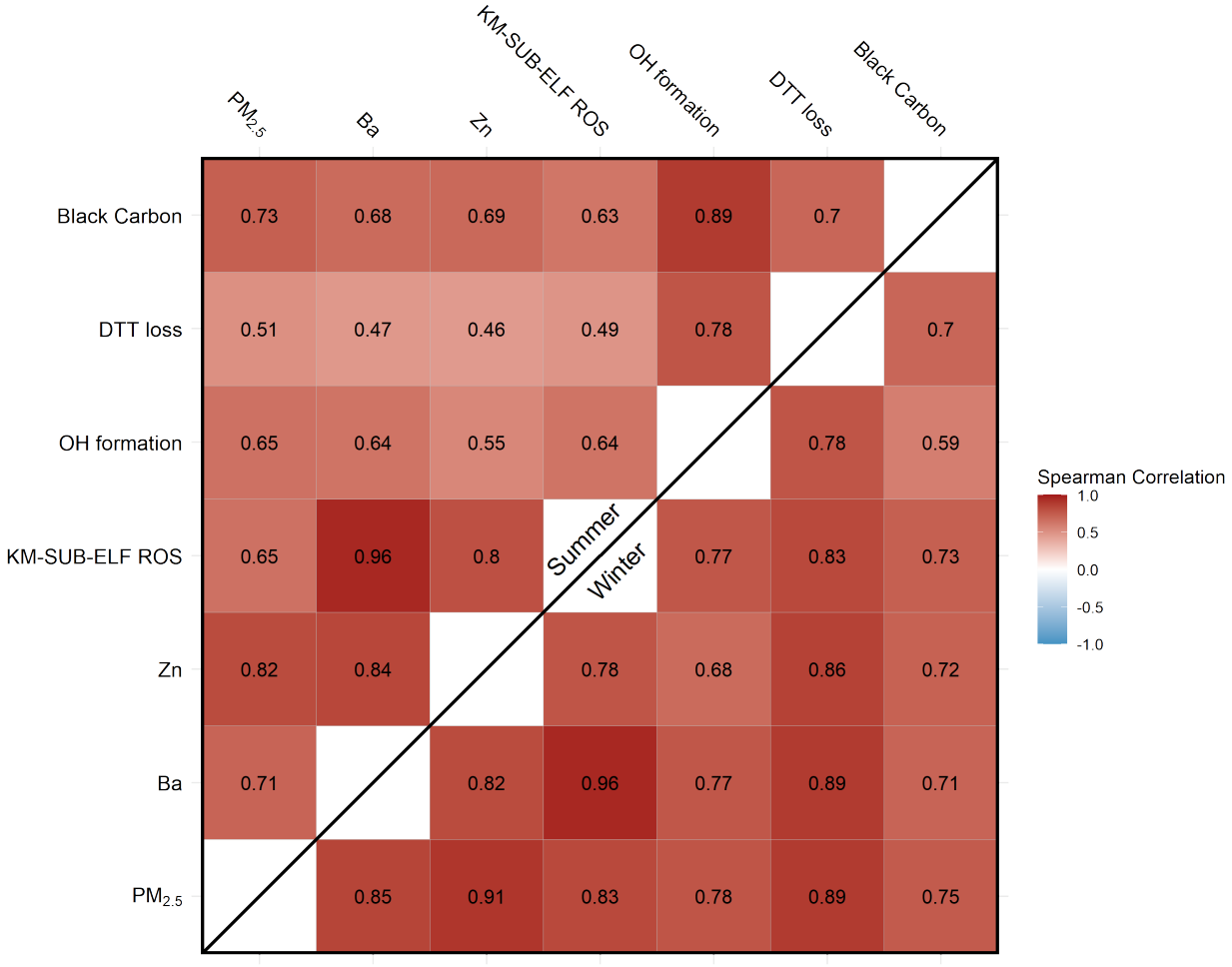

Figure 3.2: Spearman correlation matrix between volume-normalized study outcomes during the summer (top/left) and winter (bottom/right) sampling campaigns

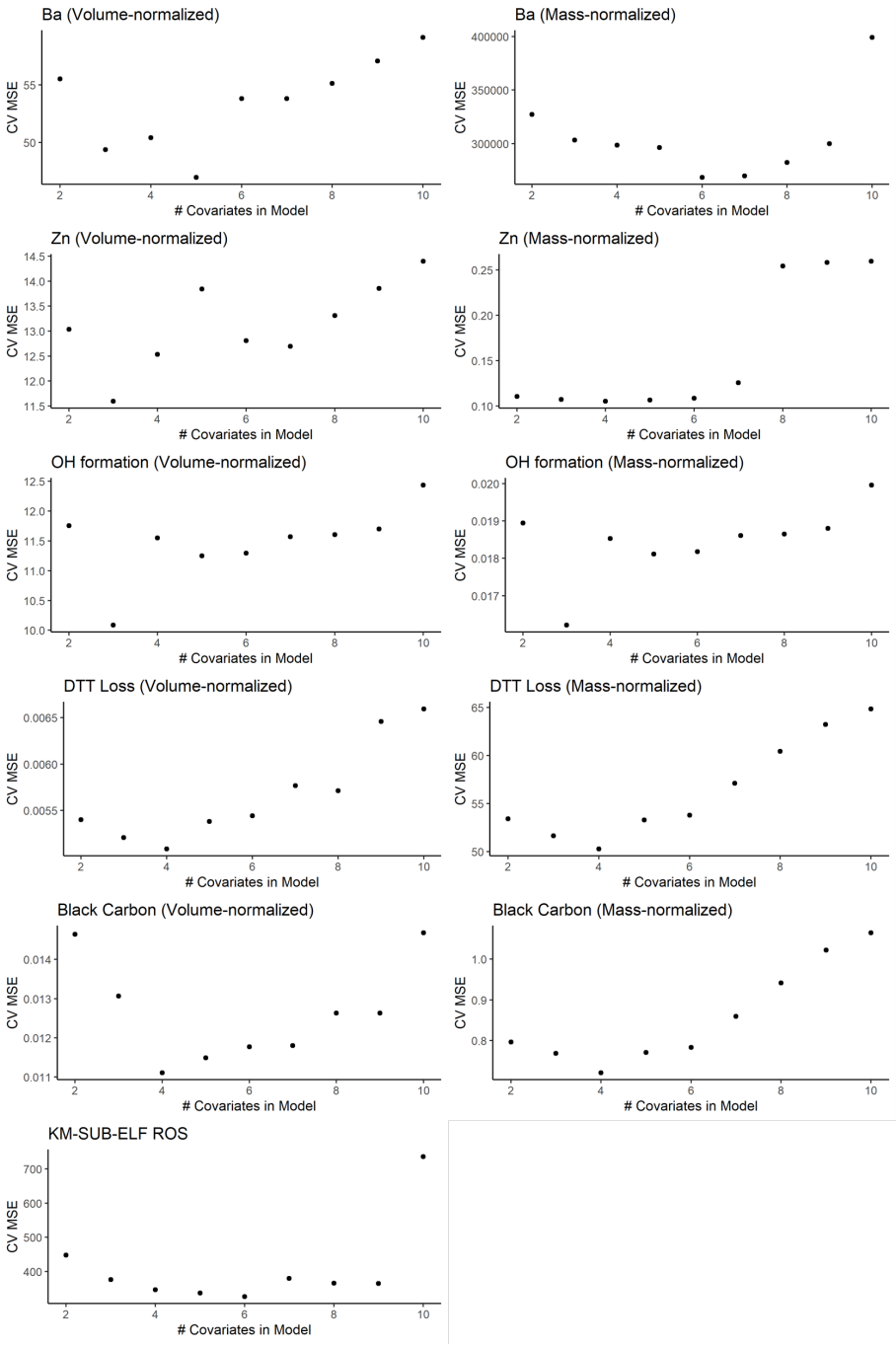

Figure 3.3: Cross validation (CV) error plots for each outcome as a function of model size.

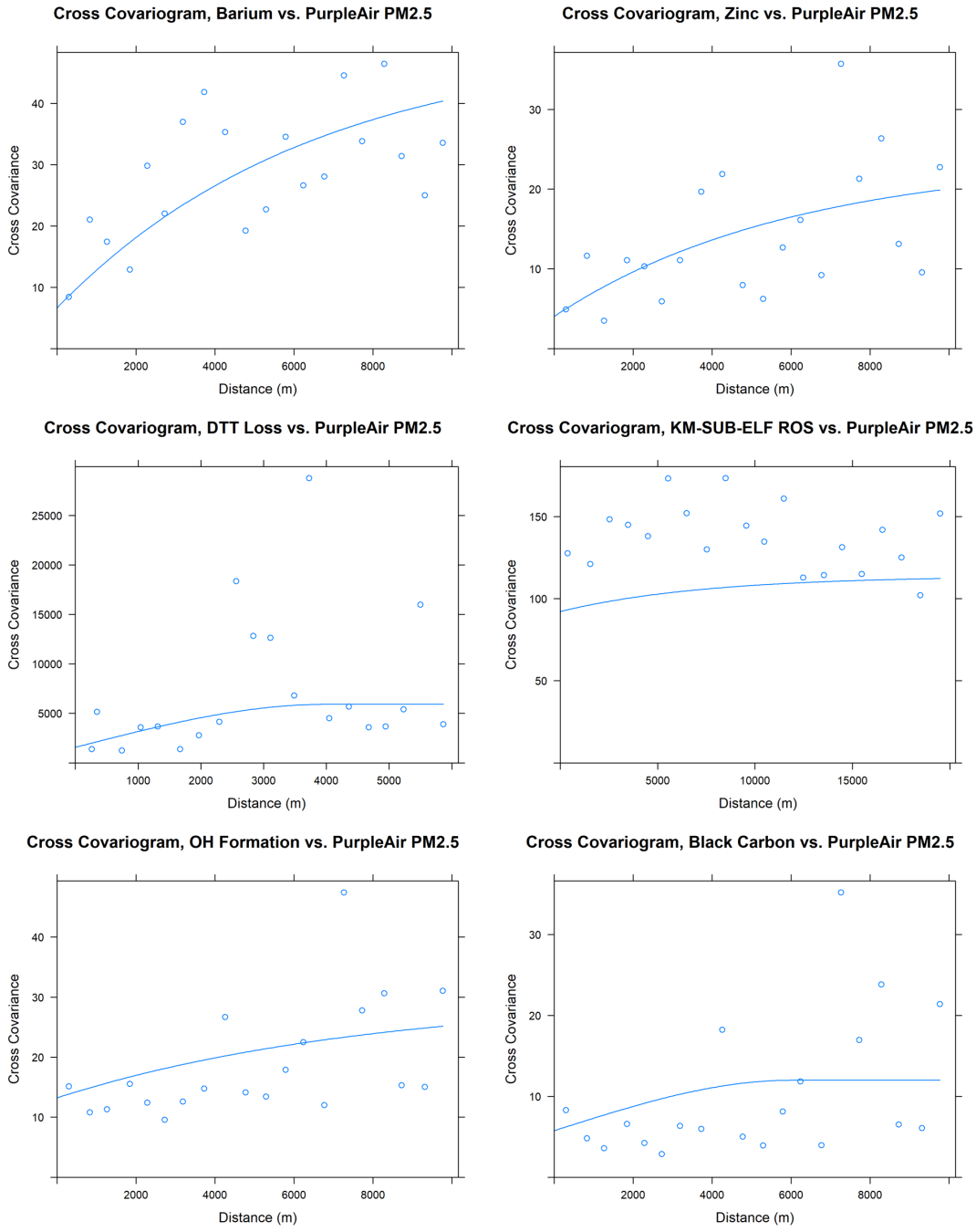

Figure 3.4: Cross covariograms between volume-normalized concentrations and PurpleAir. The theoretical (modeled) variogram is represented by the solid blue line, whereas the empirically derived variogram is represented by individual dots.

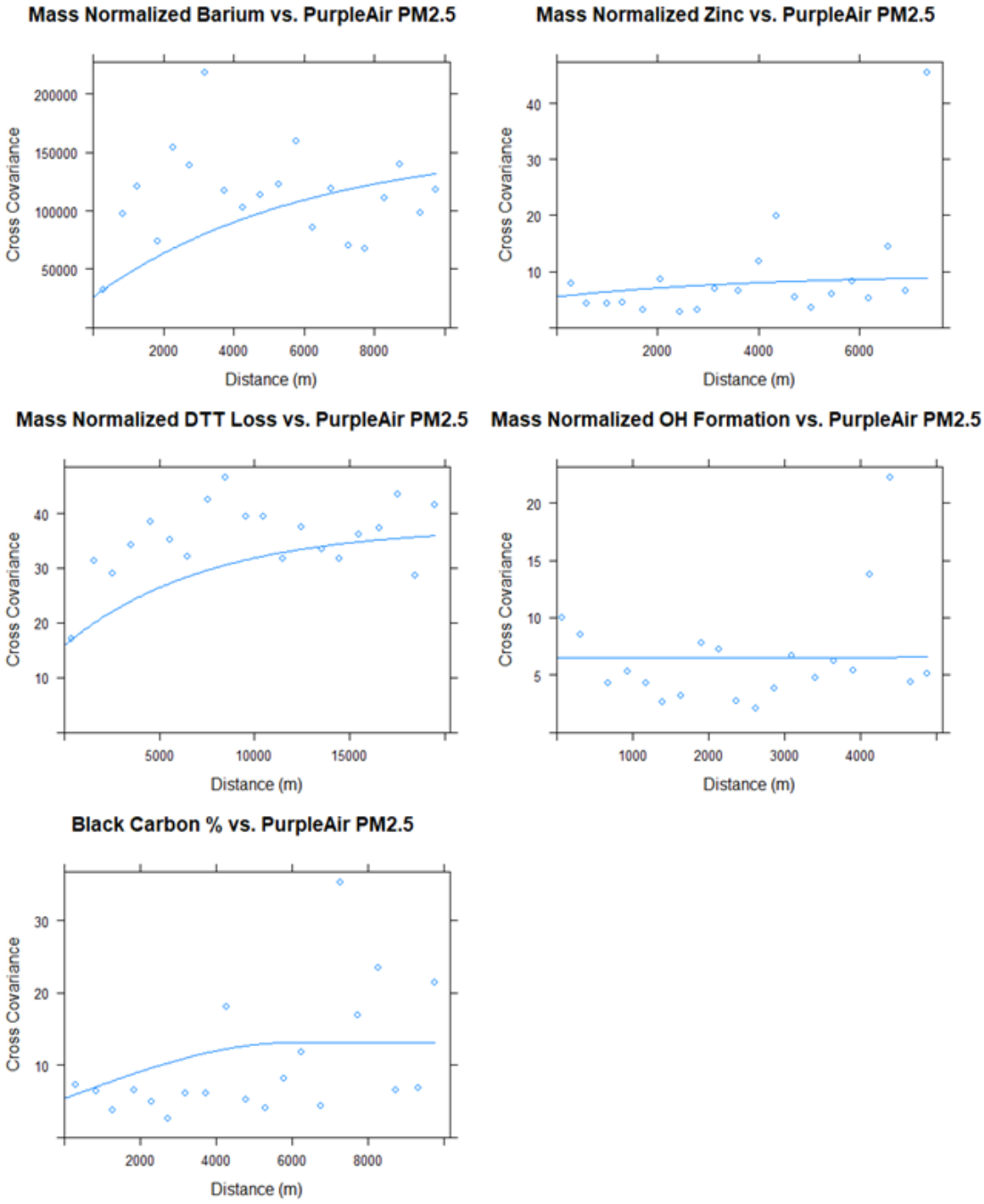

Figure 3.5: Cross covariograms between mass-normalized concentrations and PurpleAir. The theoretical (modeled) variogram is represented by the solid blue line, whereas the empirically derived variogram is represented by individual dots.

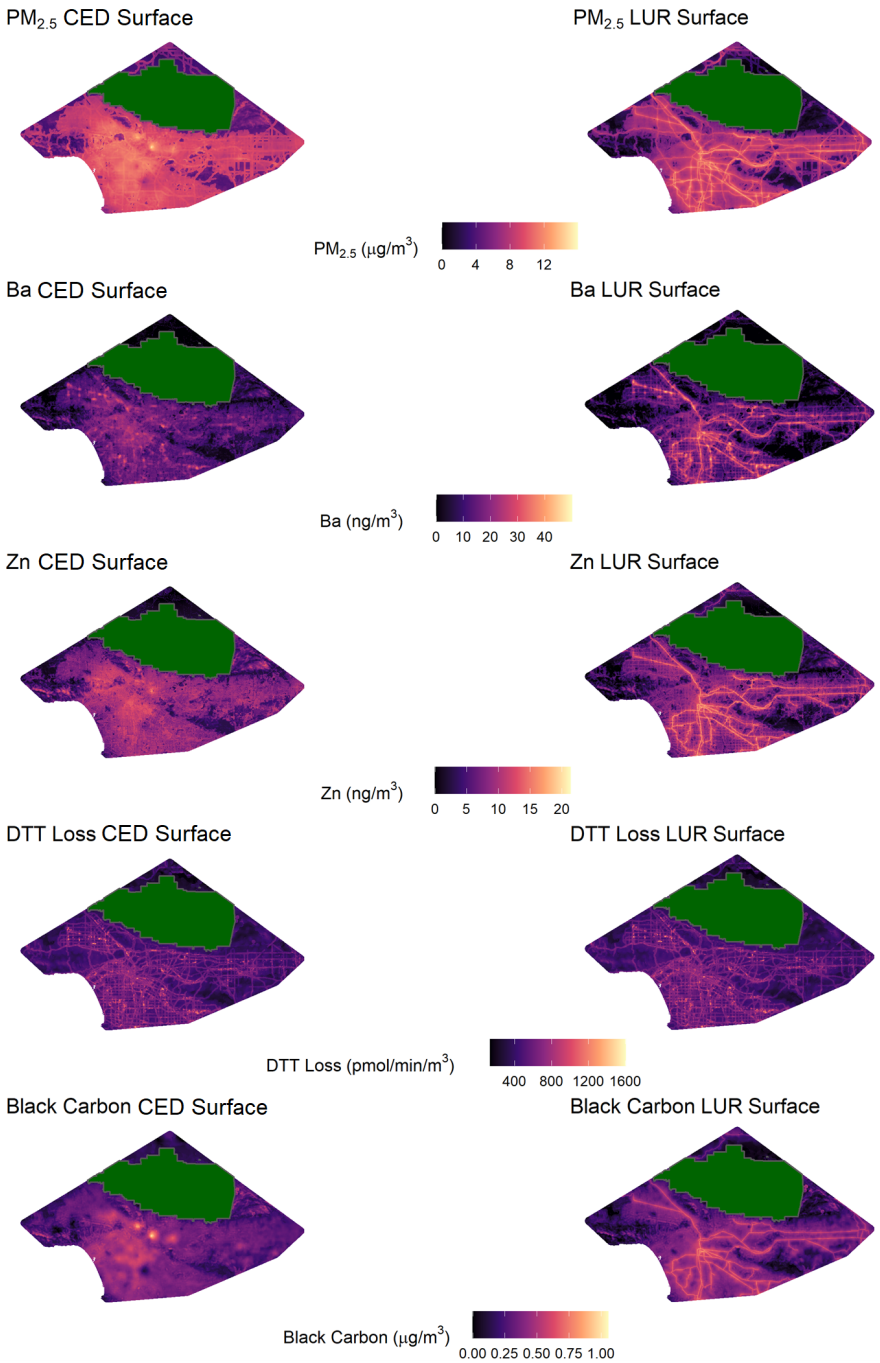

Figure 3.6: Exposure surfaces generated by CED (left) and LUR (models) for (from top to bottom) volumized estimates of $PM_{2.5}$, Ba concentration, Zn concentration, and loss rates, and black carbon, which represent brake wear, tire wear, oxidative stress potential, and combustion, respectively. The Angeles National Forest, where we do not interpolate, is shown in green.

Table 3.1: NLCD classifications

	NLCD Classification	Spatial resolution	Year
Green Space	11, 12, 21, 22, 41, 42, 43, 51, 52, 71, 72, 73, 74, 81, 82	30 x 30 meters	2016
Non-green space	23, 24, 31	30 x 30 meters	2016

Table 3.2: First three digits of NAICS codes used to identify businesses potentially associated with tire-wear related metals

NAICS 3-digit code	Classification
212	Mining (except Oil and Gas)
213	Support Activities for Mining
221	Utilities
325	Chemical Manufacturing
326	Plastics and Rubber Products Manufacturing
331	Primary Metal Manufacturing
332	Fabricated Metal Product Manufacturing
333	Machinery Manufacturing
335	Electrical Equipment, Appliance, and Component Manufacturing
336	Transportation Equipment Manufacturing
339	Miscellaneous Manufacturing
423	Merchant Wholesalers, Durable Goods
811	Repair and Maintenance

Table 3.3: List of independent variables in LUR model

Variable Category	Covariates	Data Sources
Land Use	Tree canopy (%)	2016 National Land Use Consortium Database (MRLC 2016)
	Impervious (%)	
	Green space (%)	
	Non-green space (%)	
Traffic and/or Road	Intersection density (#/m^2)	US Census Bureau (Bureau 2019)
	Slope variance (%)	
	Road length (m)	
	Annual average daily traffic (Veh/day)	Federal Highway Administration (Roff 2020)
	Annual average daily heavy-duty traffic (Veh/day)	
Distance	Distance to rail (m)	US Census Bureau
	Distance to coast (m)	
	Distance to major road (m)	
Commercial	Brake and tire-related businesses (count)	ESRI Business Analyst (ESRI, 2018)

Table 3.4: Summary statistics for dependent variables.

Outcome	Volume-Normalized Mean (SD)	Mass-Normalized Mean (SD)
$PM_{2.5}$	9.4 (2.4) µg/m^3	
Ba	17 (9.9) ng/m^3	1700 (750) ng/g
Zn	9.3 (4.6) ng/m^3	930 (320) ng/g
KM-SUB-ELF ROS	100 (26) nmol/L	
OH Formation	4.95 (2.1) pmol/min/m^3	0.56 (0.14) pmol/min/µg
DTT Loss	550 (208) pmol/min/m^3	61.9 (11.8) pmol/min/µg
Black Carbon	0.41 (0.17) µg/m^3	4.6 (1.2) %

Table 3.5: Model summaries for volume-normalized (left) and mass-normalized measurements (right). Numbers contained in parentheses next to model parameters indicates the buffer radius in the LUR model, if applicable. * indicates that the dependent variable was log-transformed.

	Volume-normalized measurement			Mass-normalized measurement		
Pollutant	Adj. R^2	Model Parameters	Coef.	Adj. R^2	Model Parameters	Coef.
$PM_{2.5}$	0.41	Log annual average daily traffic (500)	0.32	-	-	-
		Log distance to rail	-0.75			
		Log distance to major road	-0.38			
		Impervious % (1000)	0.05			
		Tree canopy % (400)	0.08			
Ba	0.60	Period	9.146	0.56	Period	725.79
		Tree canopy % (400)	0.763		Tree canopy % (750)	47.42
		Log distance to rail	-3.40		Log distance to rail	-162.9
		Impervious % (200)	0.259		Impervious % (200)	10.55
		Business count (750)	0.313		Business count (750)	25.9
					Log annual average daily heavy-duty traffic (400)	59.8
Zn	0.47	Period	3.69	0.42*	Period	6.95
		Log distance to rail	1.40		Tree canopy % (750)	0.026
		Log annual average daily traffic (300)	0.64		Log distance to rail	-0.12
					Impervious % (100)	0.0056
KM-SUB-ELF ROS	0.58	Period	81.77	-	-	-
		Tree canopy % (750)	1.57			
		Log distance to rail	-5.49			
		Impervious % (200)	0.55			
		Business count (750)	0.87			
		Log annual average daily heavy-duty traffic (400)	2.42			
OH Formation	0.56	Period	1.88	0.37	Period	0.38
		Business count (750)	0.07		Business count (750)	0.01
		Log annual average daily heavy-duty traffic (400)	0.28		Log annual average daily heavy-duty traffic (400)	0.02
		Tree canopy % (1000)	0.07			
		Impervious % (200)	0.04			
DTT Loss	0.60	Period	215.1	0.68	Period	17.49
		Business count (300)	34.1		Business count (300)	2.02
		Log annual average daily heavy-duty traffic (400)	22.1		Log annual average daily heavy-duty traffic (400)	1.04
		Tree canopy % (1000)	10.16		Tree canopy % (1000)	0.34
		Impervious % (1000)	4.26			
Black Carbon	0.64	Period	0.15	0.56	Period	1.25
		Impervious % (1000)	0.01		Impervious % (1000)	0.02
		Tree canopy % (400)	0.01		Tree canopy % (400)	0.06
		Log distance to rail	-0.06		Log distance to rail	-0.46

Table 3.6: Percent changes in mean and standard deviation of MSE after implementing CED compared to LUR for volume-normalized (left) and mass-normalized (right) measurements. Under each estimate are histograms illustrating the 10-fold cross-validation performance differences between LUR (blue) and CED (pink) modelling approaches after 1000 iterations. A darker area indicates overlap between LUR and CED results.

	Volume-normalized measurement		Mass-normalized measurement	
Pollutant	Mean MSE Change (95% CI)	Mean MSE SD Change (95% CI)	Mean MSE Change (95% CI)	Mean MSE SD Change (95% CI)
$PM_{2.5}$	-11.7% (-12.2%, -11.2%) 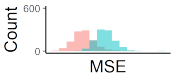	-21.8% (-22.4%, -21.3%) 	-	-
Ba	-3.1% (-3.6%, -2.6%) 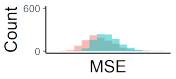	-7.9% (-8.4%, -7.4%) 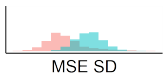	-5.7% (-6.2%, -5.2%) 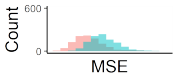	-8.8% (-9.4%, -8.2%) 
Zn	-6.9% (-7.3%, -6.4%) 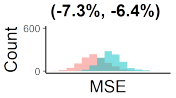	-4.9% (-5.5%, -4.3%) 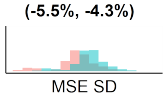	-0.1% (-0.6%, 0.4%) 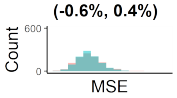	-3.5% (-4.0%, -3.0%) 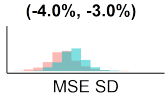
KM-SUB-ELF ROS	-14.1% (-14.6%, -13.6%) 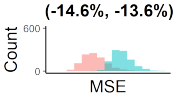	-14.3% (-14.8%, -13.7%) 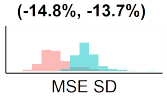	-	-
OH Formation	-6.3% (-6.7%, -5.9%) 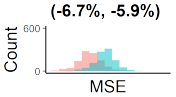	-15.8% (-16.2%, -15.3%) 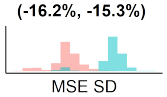	-2.1% (-2.4%, -1.8%) 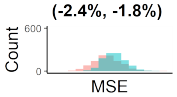	-3.1% (-3.4%, -2.9%) 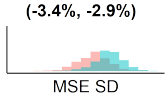
DTT Loss	0.3% (-0.2%, 0.8%) 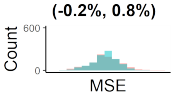	0.2% (-0.4%, 0.8%) 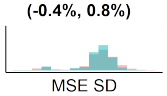	-6.1% (-6.6%, -5.5%) 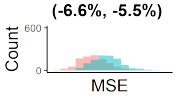	-13.8% (-14.5%, -13.2%) 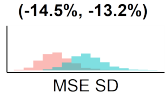
Black Carbon	-12.6% (-12.9%, -12.2%) 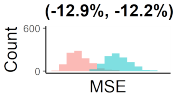	-36.0% (-36.3%, -35.7%) 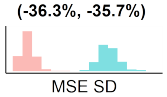	0.7% (0.3%, 1.0%) 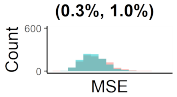	-8.1% (-8.4%, -7.9%) 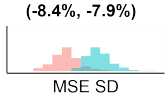

CHAPTER 4

Association of Ischemic Placental Disease in a Southern California Birth Cohort and $PM_{2.5}$ Chemical Species and Oxidative Potential Markers

4.1 Abstract

Road traffic is a significant source of particulate matter pollution, whose exposure is a significant risk factor in pregnancy-related health outcomes. The exact mechanisms behind the relationship between traffic-related air pollution (TRAP) exposure and adverse pregnancy outcomes remain unclear, partly due to a lack of detailed exposure assessment of fine $PM_{2.5}$ constituents. We aim to assess the relationship between exposure to brake and tire wear-associated metals and oxidative potential and ischemic placental disease (IPD). Data from the Placental Assessment in Response to Environmental Pollution (PARENTs) study, which was assembled from a population of women who sought specialized prenatal care at UCLA between 2016 and 2019 in Los Angeles, CA. Modeled first trimester exposures to chemical constituents and oxidative stress potential of $PM_{2.5}$, black carbon, and $PM_{2.5}$ mass concentration. Speciated measurements include tracers of brake wear (barium), tire wear (zinc), and oxidative potential markers based on metal concentrations (KM-SUB-ELF ROS) or laboratory assays (DTT loss, OH radical formation). Exposures were modeled by integrating data from filter samples, a low-cost $PM_{2.5}$ sensor network, and land-use data. IPD was defined as the presence of one or more of the following: placental abruption, hypertensive disease of pregnancy, fetal growth restriction, or small-for-gestational age. We used

logistic regression to estimate the associations between air pollution exposures and IPD, adjusting for covariates assessed through medical records and interviews. We found a positive relationship between IPD and speciated exposures. Scaled to the interquartile range, odds ratios (95% CI) were as follows: barium OR: 1.7 (1.1, 2.7), zinc OR: 1.4 (.86, 2.4), and oxidative potential markers, both modeled as well as measured through DTT loss and OH formation assays (ORs ranging from 1.1-2.0). Effect sizes for $PM_{2.5}$ and black carbon were lower than most measurements (ORs: 1.3-1.4). We observe higher effect sizes with Ba and oxidative potential markers compared to traditional measurements such as $PM_{2.5}$ mass and black carbon. Our findings suggest two key points: (i) metals associated with brake and tire wear, currently unregulated, may play a role in the relationship between TRAP and adverse pregnancy outcomes, and (ii) reducing tailpipe emissions may not be sufficient to protect pregnant women from TRAP

4.2 Introduction

Exposure to high levels of TRAP is a major risk factor for various adverse health outcomes, contributing substantially to premature mortality alongside a host of other diseases [19, 142]. TRAP itself is a multisource mixture whose PM emissions stem from both tailpipe emissions as well as non-tailpipe sources, including brake and tire wear and road dust resuspension. Southern California studies have found that TRAP contributes to 32% of all ambient $PM_{2.5}$ [8]. In recent decades, government regulation and advancements in technology have substantially reduced tailpipe emissions in California, altering the profile of particulates in TRAP [21]. Current clean air regulation in the US does not regulate non-exhaust emissions, which due to increased fleet efficiency and electrification is expected to contribute a greater share of particulates to TRAP and overall PM emissions [6]. As TRAP composition evolves with changes in vehicle trends, health studies assessing effects of air pollution will require up-to-date, informative exposure assessment [143], such as the use of metals as tracers of brake

and tire wear [103, 143, 144].

A recent review found a number of adverse pregnancy and birth outcomes associated with exposure to TRAP, including term low birth weight and small for gestational age [19]. One potential pathway through which PM affects pregnancy and birth outcomes is through oxidative stress. Oxidative stress plays an important role in the pathophysiology of the human placenta, where a balance of antioxidants and reactive oxygen species (ROS) helps regulate placental development [145]. The disruption to the balance of antioxidants and ROS has been shown to induce inflammation and subsequent morphological changes [146]. These degenerative changes in the placenta have been found associated with several pregnancy complications, including preeclampsia, fetal growth restriction, placental abruption, and gestational hypertension [145]. These disorders, while symptomatically different, have a common underlying etiology in placental ischemia, and are commonly grouped under a single term, ischemic placental disease (IPD) [147].

Prior studies have implicated oxidative stress as a primary mechanism through which PM exposure impacts human health [148]. Heightened PM exposure increases levels of oxidative stress, which have been found to correspond to inflammation leading to morphological changes in the placenta [146]. This is reflected in prior cohort studies, which have found associations between ambient $PM_{2.5}$ and outcomes including intrauterine inflammation [149], preeclampsia [150], altered lipid metabolic gene expression [151], placental DNA methylation [152], and IPD [153].

Most studies have focused on ambient $PM_{2.5}$ or other proxy variables to assess exposure to air pollution. PM is a non-specific, multisource mixture whose components vary widely based on time of year and geography [154]. One study showed that within a single city and time period, $PM_{2.5}$ samples showed measurable differences in oxidative potential [155]. A review found that chemical species may modify the association between $PM_{2.5}$ exposure and adverse health effects, and that the use of unspeciated $PM_{2.5}$ may run the risk of exposure classification [156]. This is especially salient when assessing TRAP, as brake and tire wear

are rich in metals and organic compounds that are notably capable of generating oxidative stress [6]. Consequently, there have been increasing concerns that despite reductions in tailpipe emissions, increased exposure to TRAP may continue to disrupt placental function leading to downstream adverse birth outcomes [157–160].

Here, we attempt to bridge the above mentioned knowledge gap concerning possible adverse effects of brake and tire wear-related TRAP exposures and pregnancy. We employ conventional exposure metrics, namely $PM_{2.5}$, black carbon, and novel set of exposure measures, including tracers of brake and tire wear and markers of oxidative potential. We relied on a well-documented birth cohort [161] with detailed clinical follow-up throughout pregnancy to assess associations of IPD with different measures of ambient TRAP.

4.3 Methods

4.3.1 Study population

The study cohort was established as part of the Placental Assessment in Response to Environmental Pollution (PARENTs) study. The PARENTs study enrolled a birth cohort of pregnant women who sought prenatal care and planned to deliver at UCLA hospitals between 2016 and 2019. Details regarding the cohort are summarized elsewhere [161]. Briefly, subjects were screened for eligibility early in the first trimester and subsequently followed prospectively until birth. Patient information was ascertained with both medical records and standardized questionnaires. Interviews were conducted during pregnancy, i.e. during the first trimester, early to mid-second trimester, third trimester, as well as delivery and postpartum to collect information on demographics, medical history, tobacco use, and various maternal behaviors including diet and residential and occupational exposures.

The cohort was approved by the UCLA IRB, and details are listed by ClinicalTrials.gov (NCT02786420) [162].

4.3.2 Outcome assessment

We defined the main outcome, IPD, as the noted presence of one or more of the following complications: placental abruption, hypertensive disease of pregnancy (preeclampsia or gestational hypertension), fetal growth restriction, or a newborn considered small-for-gestational age. These four diseases, while symptomatically different, are all related to a placental ischemia induced by excessive oxidative stress and are grouped under the composite outcome IPD [147].

We defined preeclampsia as blood pressure (BP) of 140/90 mmHg or higher on two occasions at least four hours apart after 20 weeks of gestation with previously normal BP, and proteinuria of >300 mg/24 hours [163]. In the absence of proteinuria, preeclampsia was defined as new-onset hypertension with new onset of thrombocytopenia, renal insufficiency, impaired liver function, pulmonary edema, cerebral or visual symptoms [163].

Gestational hypertension refers to hypertension developing after 20 weeks of gestation not associated with systemic features of preeclampsia. Chronic hypertension, on the other hand, was defined as BP 140/90 mmHg or higher that either pre-dated pregnancy or developed before 20 weeks of gestation [163].

We assessed information such as birth weight (grams), gestational age (days), and BP from participants' medical records. Small-for-gestational age was defined as a newborn birth weight less than the 10th percentile per Fenton's growth charts with a subclassification below the 3rd percentile. Small-for-gestational age was further classified by assessing percentiles of body length and head circumference [164].

4.3.3 Exposure assessment

4.3.3.1 $PM_{2.5}$ mass and elemental concentrations

We generated seven 30 by 30 meter exposure surfaces using three data sources: (i) air monitoring campaigns measurements from two campaigns we conducted in 2019-20, (ii) land-use data from public and private sources, and (iii) the PurpleAir low-cost sensor network. We previously described our data collection and modeling processes in a prior publication and in **Chapter 3** [103, 165]. In brief, we obtained $PM_{2.5}$ chemical species and oxidative potential marker data from a fieldwork campaign detailed in Oroumiyeh et al. (2022) [103]. Samplers measuring $PM_{2.5}$ during September 2019 and February 2020 were placed at government monitoring locations and individual residences, including at 17 PARENTs participants' homes. Oroumiyeh et al. (2022) describe chemical speciation analyses in detail [103, 166, 167], and Shen et al. (2023) discuss at length the assays used to measure black carbon and oxidative potential in the filter samples [155].

After obtaining speciation and oxidative potential marker data, we modeled the following:

- Ba (representing brake wear) [6]
- Zn (representing tire wear) [6]
- DTT loss (biological reductant surrogate) [118, 135, 168, 169]
- OH formation (reactive species formed in lung lining when exposed to aerosol particles) [105]
- KM-SUB-ELF ROS (an estimate of reactive oxygen species generation based on Cu and Fe concentrations) [170]
- Black carbon (combustion byproduct and diesel tailpipe tracer) [171]
- $PM_{2.5}$ mass concentration

We have detailed our exposure modeling in a prior article [165]. Briefly, for each exposure, we generated a model across the Southern California area employing universal co-kriging with each exposure as the primary variable; a land-use regression model as an external drift; and PurpleAir low-cost sensor network as an auxiliary, more spatially resolved variable. PurpleAir data covering the period between March 2019 and February 2020 for sensors in the study area were downloaded from the PurpleAir website for these purposes.

Monthly estimates of co-kriged $PM_{2.5}$, Ba, Zn, and oxidative potential were scaled using monthly average $PM_{2.5}$ measurements in the PurpleAir network. For each month, the cross-covariance between the seven exposures and PurpleAir $PM_{2.5}$ were modeled using the gstat package, which was used to predict monthly exposure estimates. We generated each subject's first trimester exposure measure by subtracting the gestational age at birth from the birth date, and adding 92 days (13 weeks). Within this date range, exposure estimates were calculated as a weighted average of the monthly exposures that were included in each woman's first trimester. For subjects who moved residences during their first trimester, the weighted average was calculated based on residence time at each address. We estimate first trimester exposures occurring prior to the incidence of IPD, making our study prospective in design.

Based on reported home addresses at enrollment and relocation dates (if applicable), we geocoded subject home locations using the Esri ArcGIS Address Locator via the Countywide Address Management System locator [172]. For addresses that failed to geocode properly, we used Google Maps via the ggmap R package [173].

4.3.4 Covariates

Using questionnaires, we collected data on covariates and potential IPD risk factors, including maternal age (years), maternal race (non-Hispanic White, Hispanic of any race, Black, Asian/Pacific Islander, or other), parity (continuous), maternal body-mass index (BMI, categorical), maternal and partner income (nominal), maternal education (categorical), and

maternal smoking status prior to and during pregnancy (never/former smoker). We assessed pregnancy complications and other medical information, such as gestational diabetes (yes/no) and fetal sex (male/female) from medical records [174]. Subjects reported maternal and partner income as belonging to one of five annual salary ranges (under $20,000, $20,000 - $40,000, $40,000 - $60,000, $60,000 - $100,000, and over $100,000). Based on reported incomes, we classified each household into low, middle, upper-middle, and high-income when applicable. Due the small sample size, we dichotomized race into non-Hispanic White and other.

We encountered missing data for some covariates. Six out of 178 subjects lacked maternal education data, five out of 178 lacked household income data, and 19 out of 178 lacked maternal smoking data prior to pregnancy. We addressed missing data using multivariate imputation using SAS [175]. Specifically, we created an imputation model based on exposure variables and complete covariates. We used the Markov Chain Monte Carlo method to assume a joint multivariate normal distributions for all variables included in the imputation model. After imputing five datasets, we randomly selected one for use in our final dataset.

4.3.5 Statistical Analysis

4.3.5.1 Summary Statistics

After assigning exposure data, we calculated the mean and interquartile range (IQR) of each exposure, stratified by IPD status. In an exploratory analysis, we calculated Pearson correlation coefficients between each exposure and checked for statistical significance ($p < 0.05$).

Prior to model fitting, we normalized exposure values by the corresponding IQR of the entire population, as has been done in previous studies that assessed air pollution and pregnancy outcomes [176–178].

4.3.5.2 Model Fitting

To assess the impact of various exposures on the risk of developing IPD, we fitted unconditional logistic regression models for each of our exposures. We generated results based on three different models: (i) a crude model, (ii) a minimally adjusted model adjusting for age, fetal sex, and race, and (iii) a fully adjusted model additionally adjusting for parity, maternal BMI, maternal smoking, gestational diabetes, maternal education, and household income. We calculated log odds ratios and corresponding 95% confidence intervals representing the change in odds of IPD per IQR increase of each exposure.

4.3.5.3 Sensitivity Analysis

Prior studies have demonstrated a relationship between diet and oxidative stress levels [179], and place of residence may affect both air quality as well as access to healthy food. In response we considered this potential effect of diet among a subset of 143 women who filed out the Diet History Questionnaire II, a food frequency questionnaire [180]. For the women who provided this information, we investigated whether adjustment for a healthy diet based on the United States Department of Agriculture 2015 Healthy Eating Index changed effect estimates.

Additional sensitivity analyses included assessing alternate methods of exposure assessment i.e. weighing exposure estimates by each month of gestation. For a small subset of subjects who moved residences during the first trimester, we investigated whether maintaining their original address, i.e. assuming they did not move, affected effect estimates. Finally, during exploratory analyses we found that four subjects lived less than two miles outside of the boundaries of the exposure surface. Instead of excluding them, we assigned these four subjects exposure surface measures closest to their addresses.

4.4 Results

We screened 841 subjects for eligibility and willingness to participate in magnetic resonance imaging (MRI) examinations during mid-pregnancy and 234 did not respond to further inquiry (Figure 4.1). There were 233 subjects who declined to enroll for reasons including time and/or travel (n = 56), lack of interest (n = 50), MRI safety concerns (n = 62) or doctor refusal (n = 7). An additional 58 women did not to provide a reason for declining participation. There were 166 women who were deemed ineligible due to late gestational age at enrolment (n = 132), twin pregnancy (n = 5), abortion or miscarriage (n = 16), discontinuation of care at UCLA (n = 12), or being too ill to continue (n = 2).

Thus, we initially enrolled 208 participants into the PARENTs study. After enrollment, we additionally excluded 30 subjects due to pregnancy complications or other illnesses resulting in MRI complications post-enrollment (n = 7); miscarriage or abortion post-enrollment (n = 5); patient withdrawal (n = 4); smoking during pregnancy (n = 1); exposure to Zika (n = 1); relocation outside the study area (n = 1); missing medical records (n = 2); or residing outside of the exposure surface boundaries (n = 9).

Baseline subject characteristics of the 47 cases and 131 non-cases are presented in Table 4.1. Compared to non-cases, cases had a slightly higher median age, BMI, and prevalence of gestational diabetes while non-cases were more often multiparous. There are also more former smokers and women missing information on smoking prior to pregnancy among cases.

Correlations between first trimester exposures are summarized in Figure 4.2. All exposures were positively correlated with each other (Pearson ρ: 0.13-0.89). Overall, the estimated average first trimester $PM_{2.5}$ exposure was 9.75 $\mu g/m^3$ with an IQR of 1.19 $\mu g/m^3$, with higher mean concentration among cases (9.85 $\mu g/m^3$) compared to non-cases (9.71 $\mu g/m^3$). We also observed higher mean exposures to Ba, Zn, and oxidative potential markers among cases than non-cases, as shown in Table 4.2.

Odds ratios and 95% confidence limits from logistic regression models shown in Figure

4.3 suggest that higher levels of every exposure modeled were positively associated with IPD, with magnitudes of the ORs ranging in size from 1.1 (DTT loss) to 2.0 (KM-SUB-ELF ROS). Adjustment for covariates suggested some bias of crude estimated effects towards the null for the brake wear and tire wear marker Ba and Zn and also for KM-SUB-ELF ROS. The adjusted estimates for Ba and KM-SUB-ELF ROS the 95% confidence intervals exclude the null value of 1. While not necessarily statistically significant, all other exposure-IPD associations were positive and exhibited the same patterns.

Sensitivity analyses did not alter our main findings. Assigning alternate locations to subjects just outside the exposure surface not change effect estimates but increased standard errors. Alternate methods of exposure assessment resulted in increases in standard error, but no qualitative changes in effect estimate.

4.5 Discussion

We believe that this is the first study to examine the contributions from brake and tire wear-related $PM_{2.5}$ components and oxidative potential of the pollutant mixtures to IPD. Effect estimate directions were consistently positive whether adjusting for a minimal or full set of risk factors and potential confounders. While we cannot rule out the possibility of residual confounding, our results suggest that common risk factors known to adversely affect pregnancy did not confound the observed exposure-outcome associations except for strengthening the associations (Figure 4.3) [147].

The positive relationships between oxidative potential markers and tracers of brake and tire wear and IPD, are consistent with physiological mechanisms that are thought to drive placental disorders. The placenta plays a key role in fetal development and is essential for the transport and provision of nutrients, water, and oxygen to the fetus [181]. An imbalance of reactive oxygen species induced by metals and organic species may lead to disruptions in placental trophoblast cell function, which has been hypothesized to play a key role in the

physiologic mechanisms behind IPD [182].

We present results that further corroborate prior work investigating the relationship between TRAP and birth outcomes. Positive associations between increased maternal $PM_{2.5}$ exposure and negative health outcomes in children have been discussed widely in the literature [183]. Many studies employed black carbon as a tailpipe exhaust marker and evidence is mixed regarding associations with adverse birth outcomes [184–187]. Studies assessing exposures specifically associated with brake and tire wear are very limited, with most studies restricted to animal experiments [188–190].

As shown in Figure 4.2, Ba and Zn were highly correlated with Cu and Fe concentrations used to calculate the KM-SUB-ELF ROS measurement. As tracers of brake and tire wear, we interpret metals Ba and Zn as proxies for the mixture of brake and tire wear particle exposures directly involved in the production of reactive oxygen species and not causal agents for IPD [105, 191]. In other words, we do not believe that reducing or replacing Ba and Zn emissions from brake and tire wear would necessarily lead to improved health outcomes. We also report the effects of various oxidative potential-related measures, which reflect the reactivity of water-soluble PM samples, and whose effect directions and magnitudes are consistent with the brake and tire wear tracers. Oxidative potential markers are positively correlated with source-specific measures in data and, thus, suggest that metals and related measures of non-tailpipe source exposures may be more effective than $PM_{2.5}$ or black carbon alone in predicting PM-related oxidative stress and adverse birth outcomes.

We estimated the strongest effects in fully adjusted models for Ba, KM-SUB-ELF ROS, and OH formation. Although both DTT loss and OH formation assays measure oxidative potential, OH formation was more strongly correlated with the metals. This could be due to the DTT assay's relative insensitivity to Fe [135, 192]. Fe and Cu play an important role in OH radical formation via Fenton reactions that occur in the human body [105, 117, 193]. Fe is a major component of brake wear and catalyzes the production of ROS; it is a component of the KM-SUB-ELF ROS model and highly correlates with Ba and Zn (Figure 4.2) [6, 170].

Other research came to similar conclusions; a prior study assessing the relationship between oxidative potential markers and census tract-level health outcomes suggested that compared to $PM_{2.5}$ mass, the OH formation assays may be better at predicting PM-related adverse health consequences [155].

Prior studies have identified TRAP as a specific source of oxidative potential associated with adverse health effects [171, 194]. In our study, we found that Ba and Zn both are strongly correlated with OH radical formation and are more strongly associated with IPD compared to $PM_{2.5}$ and black carbon. Increases in fuel efficiency and automobile electrification will likely increase the total share of PM from brake and tire wear components [6, 195]. Consequently, health studies targeting TRAP with conventional metrics may underestimate exposure-outcome associations. Similarly, our findings suggest that future changes in fleet composition and reduction in tailpipe exhaust alone may not improve pregnancy outcomes.

4.6 Strengths and Limitations

Strengths include novel and robust exposure and outcome assessments. The relationship between air pollution and IPD is understudied, with only one previous study assessing IPD and distance to roads, which may have resulted in misclassification [153]. Our exposures include measurements which are more source-specific than conventional metrics compared to solely using $PM_{2.5}$ mass concentration. Furthermore, around one-third of filter samples used in our exposure model were sampled at PARENTs subjects' homes, likely reducing exposure misclassification. Our close clinical follow-up enabled a detailed IPD outcome assessment, including criteria previously used by Wesselink et al. [153] plus gestational hypertension, and fetal growth restriction. Consequently, we believe that the risk of outcome misclassification is very low.

This study has limitations regarding sample size and temporal alignment. With a small sample size of 178, our effect estimates exhibit consistent directions but have high uncer-

tainty. As stated elsewhere [161], we designed the PARENTs cohort to study placenta-related adverse outcomes in pregnancy, i.e. a high-risk population of pregnant women with a high prevalence of IPD. This likely allowed us to detect strong exposure-outcome associations despite limitations. Notably, our cohort does not represent the general population of pregnant women: they were older, more educated and of higher socio-economic status and sought specialized care at UCLA hospitals. Thus, on one hand, our subjects were at higher risk of pregnancy complications, on the other, higher SES, education, and levels of medical care may have protected them from some pregnancy complications [196]. Finally, our exposure models were based on data collected 2-3 years after pregnancy. The main sources of our exposures, traffic and heavy industry, remained consistent during the time between recruitment and the air monitoring and sampling campaigns. Additionally, our sampling campaigns were not affected by the COVID-19 pandemic or wildfires in Southern California, such that spatial trends in pollution likely remained similar to those during time of the pregnancies, minimizing the impact of temporal misalignment.

4.7 Conclusion

For this Los Angeles birth cohort, we found consistent associations between IPD and oxidative potential markers for $PM_{2.5}$ and metals associated with brake and tire wear emissions. Compared to black carbon, and $PM_{2.5}$, Ba, KM-SUB-ELF ROS, and OH formation generated stronger effect estimates sizes that were stable or even increased after adjusting for important variables widely considered to be risk factors for IPD.

Our results indicate that the association between TRAP and these adverse pregnancy outcomes is at least partially attributable to brake and tire wear-related particulate matter and the toxicity of fine particulate matter. Clean air policy has successfully reduced tailpipe emissions but currently does not target brake and tire wear. Our results suggest that protecting public health may necessitate an expansion of vehicle emissions regulations that also

address brake and tire wear PM exposures.

4.8 Figures and Tables

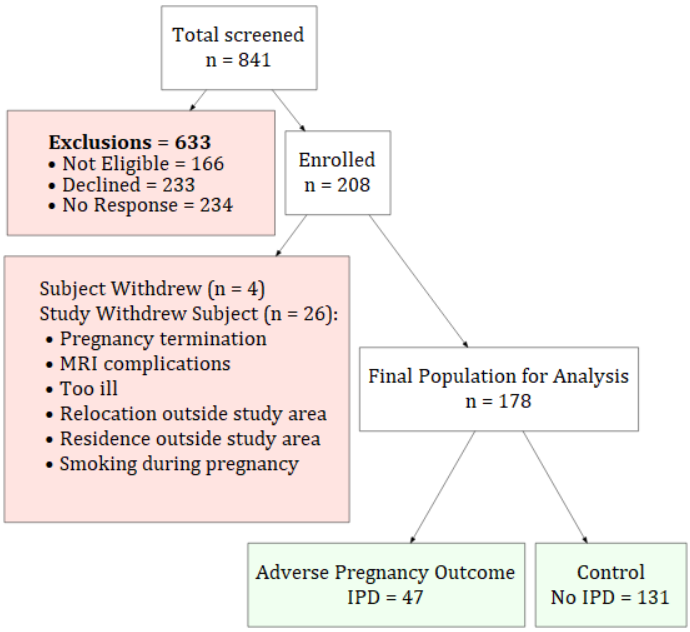

Figure 4.1: Recruitment flowchart in study population

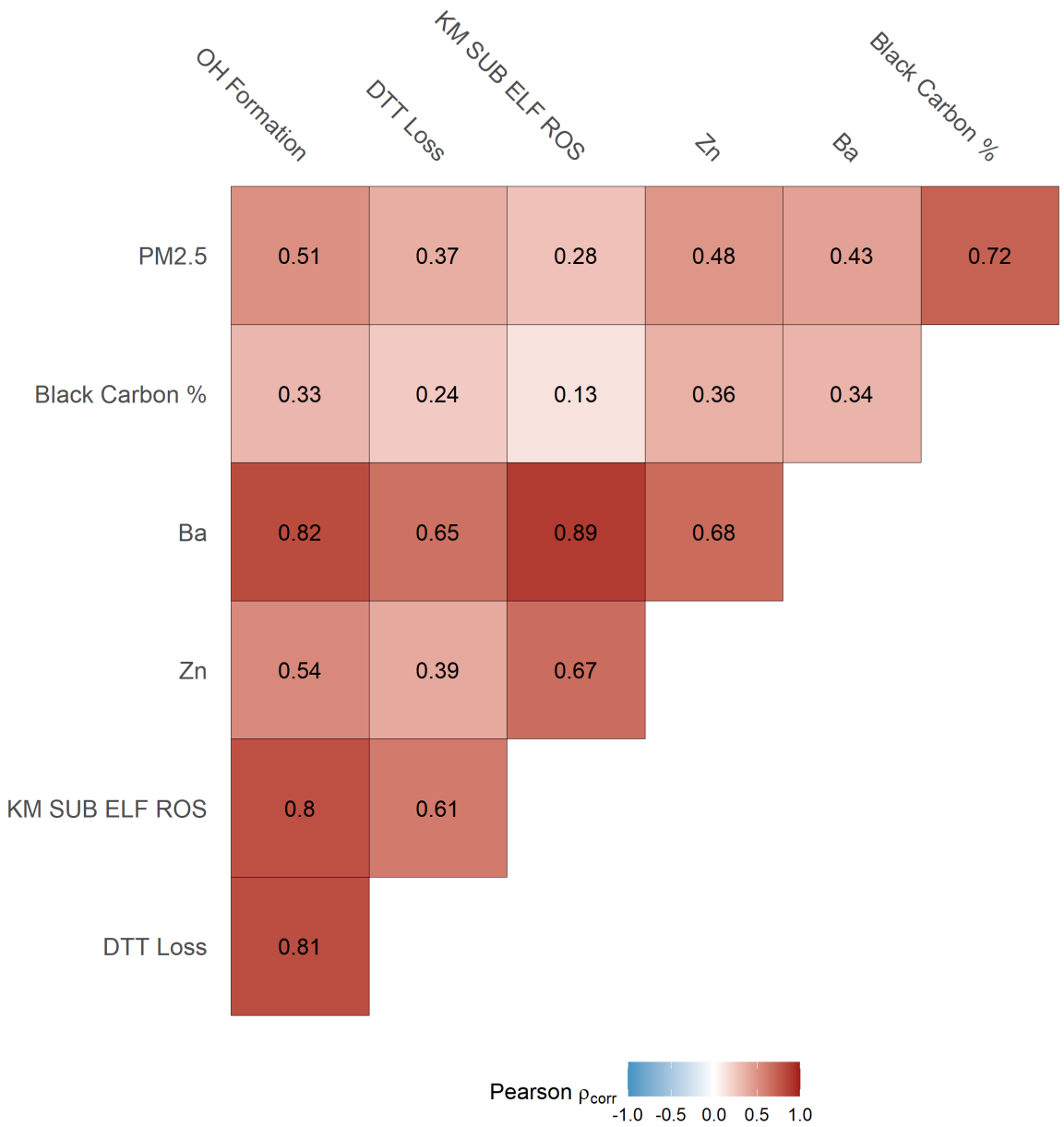

Figure 4.2: Pearson correlations between estimated exposures in the PARENTs cohort.

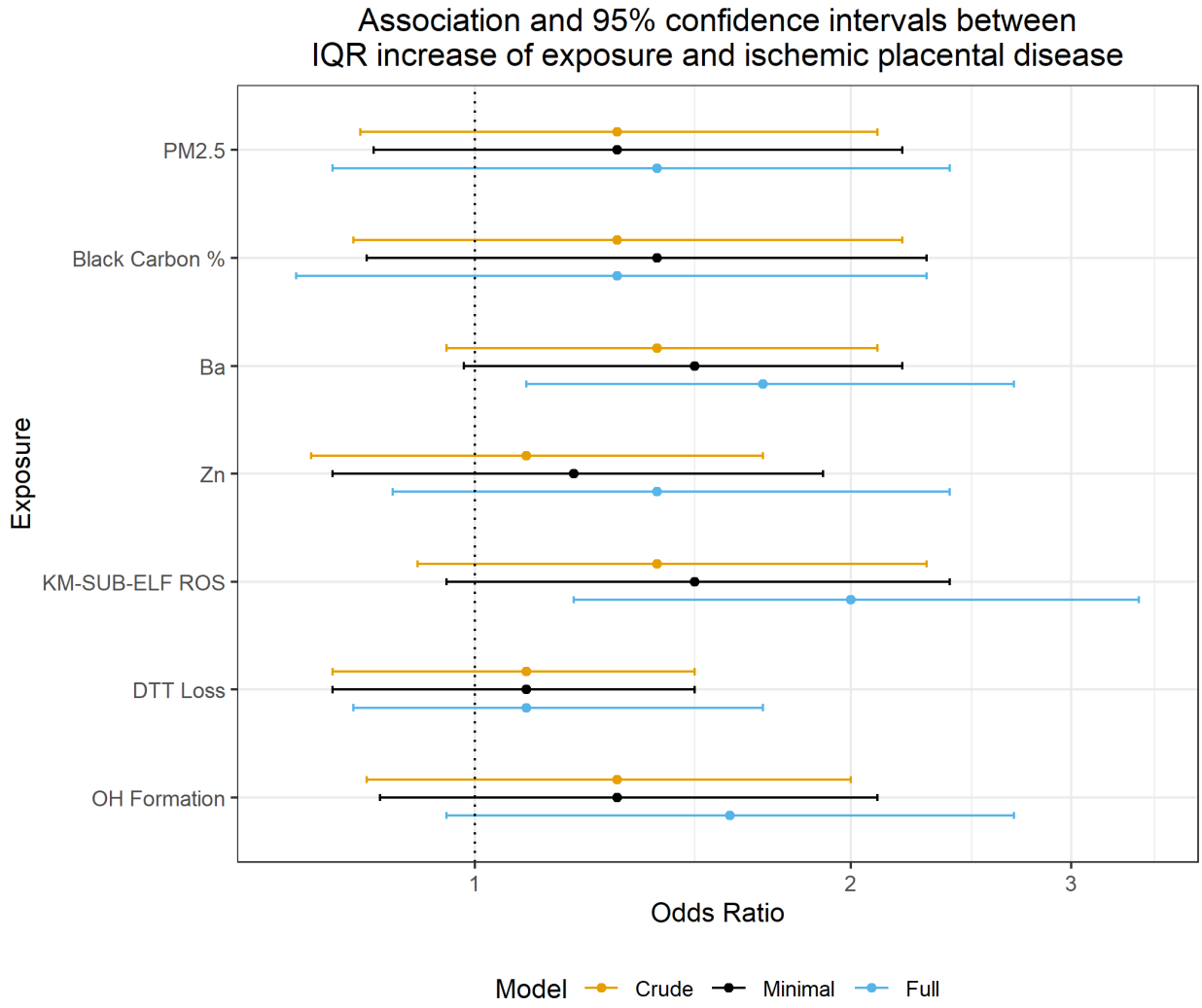

Exposure	Crude (N = 178)	Minimal (N = 178)	Full (N = 178)
PM2.5	1.3 (0.81, 2.1)	1.3 (0.83, 2.2)	1.4 (0.77, 2.4)
Black Carbon %	1.3 (0.8, 2.2)	1.4 (0.82, 2.3)	1.3 (0.72, 2.3)
Ba	1.4 (0.95, 2.1)	1.5 (0.98, 2.2)	1.7 (1.1, 2.7)
Zn	1.1 (0.74, 1.7)	1.2 (0.77, 1.9)	1.4 (0.86, 2.4)
KM-SUB-ELF ROS	1.4 (0.9, 2.3)	1.5 (0.95, 2.4)	2 (1.2, 3.4)
DTT Loss	1.1 (0.77, 1.5)	1.1 (0.77, 1.5)	1.1 (0.8, 1.7)
OH Formation	1.3 (0.82, 2)	1.3 (0.84, 2.1)	1.6 (0.95, 2.7)

Figure 4.3: Associations between exposure to $PM_{2.5}$, speciated components, and oxidative potential during the first trimester and ischemic placental disease, forest plot (top) and table (bottom)

Table 4.1: Selected characteristics of study population, Los Angeles, California

	Cases (N=47)	**Non-cases** (N=131)	**Overall** (N=178)
Maternal Age			
Mean (SD)	34 (4.4)	33 (3.9)	33 (4.0)
Race			
Asian	14 (29.8%)	34 (26.0%)	48 (27.0%)
Black or African American	3 (6.4%)	7 (5.3%)	10 (5.6%)
Hispanic	7 (14.9%)	27 (20.6%)	34 (19.1%)
White, non-Hispanic	23 (48.9%)	62 (47.3%)	85 (47.8%)
American Indian or Alaskan Native	0 (0%)	1 (0.8%)	1 (0.6%)
Maternal Education			
High School Graduate or GED	0 (0%)	1 (0.8%)	1 (0.6%)
Vocational, Technical, Associates, or other 2 year degree	0 (0%)	8 (6.1%)	8 (4.5%)
Some College	2 (4.3%)	6 (4.6%)	8 (4.5%)
Bachelors Degree (4 Years)	14 (29.8%)	44 (33.6%)	58 (32.6%)
Masters Degree	19 (40.4%)	34 (26.0%)	53 (29.8%)
Professional Degree (MD, JD, etc)	5 (10.6%)	20 (15.3%)	25 (14.0%)
Doctoral Degree	7 (14.9%)	12 (9.2%)	19 (10.7%)
Missing	0 (0%)	6 (4.6%)	6 (3.4%)
Household Income			
Low	1 (2.1%)	8 (6.1%)	9 (5.1%)
Middle	4 (8.5%)	10 (7.6%)	14 (7.9%)
Upper-middle	10 (21.3%)	20 (15.3%)	30 (16.9%)
High	30 (63.8%)	87 (66.4%)	117 (65.7%)
Don't know	1 (2.1%)	1 (0.8%)	2 (1.1%)
Refused to answer	1 (2.1%)	0 (0%)	1 (0.6%)
Missing	0 (0%)	5 (3.8%)	5 (2.8%)
Fetal Sex			
Female	22 (46.8%)	60 (45.8%)	82 (46.1%)
Male	25 (53.2%)	71 (54.2%)	96 (53.9%)
Parity			
0	26 (55.3%)	60 (45.8%)	86 (48.3%)
1	19 (40.4%)	55 (42.0%)	74 (41.6%)
2	1 (2.1%)	13 (9.9%)	14 (7.9%)
3	0 (0%)	2 (1.5%)	2 (1.1%)
4	0 (0%)	1 (0.8%)	1 (0.6%)
6	1 (2.1%)	0 (0%)	1 (0.6%)
Maternal BMI			
Mean (SD)	25 (5.6)	24 (4.4)	25 (4.7)
Gestational Diabetes			
No	38 (80.9%)	117 (89.3%)	155 (87.1%)
Yes	9 (19.1%)	14 (10.7%)	23 (12.9%)
Smoking			
I don't smoke and I never have	28 (59.6%)	96 (73.3%)	124 (69.7%)
I don't smoke anymore but I have in the past	12 (25.5%)	23 (17.6%)	35 (19.7%)
Missing	7 (14.9%)	12 (9.2%)	19 (10.7%)

Table 4.2: Mean (IQR) values of first trimester exposure estimates among cases and non-cases

Exposure	**Unit**	**Cases (N = 47)**	**Non-Cases (N = 131)**	**Overall (N = 178)**
PM2.5	$\mu g/m^3$	9.83 (1)	9.68 (1)	9.72 (1)
Black Carbon %	%	4.85 (0)	4.74 (1)	4.77 (1)
Ba	ng/m^3	18.9 (6)	17.7 (4)	18.1 (4)
Zn	ng/m^3	9.91 (2)	9.76 (2)	9.8 (2)
KM-SUB-ELF ROS	nmol/L	119 (13.5)	116 (15.5)	117 (16)
DTT Loss	$pmol/min/m^3$	635 (108)	627 (119)	629 (119)
OH Formation	$pmol/min/m^3$	5.79 (1.5)	5.55 (1)	5.61 (1)

CHAPTER 5

Summary of Dissertation Findings

The research highlighted in this dissertation aimed to use novel combinations of data to model TRAP in light of recent acute and long-term changes. Automobile traffic and related pollution is a mainstay in urban areas worldwide. By studying large-scale disruptions in traffic as natural experiments in **Chapter 2**, we develop a stronger understanding of the relationships between traffic, human activity, and air quality at varying spatial and temporal scales. This study addresses one such disruption, namely the stay-at-home orders following the onset of the COVID-19 pandemic in California by fusing publicly available air quality, traffic, and meteorology data. Since the publication of the research featured in **Chapter 2** in *Environmental Science and Technology* [197], other researchers have explored further the nuances of traffic and air pollution decreases in the Southern California area, integrating social variables such as envrionmental justice [198].

Long-term changes include the increasing efficiency and electrification of automobile fleets. Recent regulations have altered the composition of TRAP, lowering tailpipe emissions but failing to regulate brake and tire emissions. Pollution trends reflect the decline in tailpipe emissions, with NO_2 levels in the US declining substantially in recent decades. Among other trends, ongoing reductions in tailpipe emissions has implications for TRAP exposure assessment. As tailpipe emissions continue to decline and the proportion of non-tailpipe emissions within TRAP consequently increases, studies that continue to on tracers such as NO_2 may lead to exposure misclassification of overall TRAP.

Briefly, the three studies in this dissertation address a short-term and long-term changes

in traffic with lasting implications for air quality. In **Chapter 2**, we report on changes in near-road air quality during stay-at-home orders following the COVID-19 pandemic in California. The earliest studies addressing the effect of stay-at-home orders on air quality operated on large spatial scales using remote sensing or other similar data. We corroborated these earlier studies on a near-road level, finding significantly reduced light and heavy duty traffic, which resulted in lower NO and NO_2 levels in both Northern and Southern California. This is the first study to our knowledge to integrate air quality data and real-time traffic data from the California Department of Transportation, and one of the first studies to evaluate the near-road air quality impacts of COVID-19 stay-at home order using both traffic data and ground-level measurements.

The research presented in **Chapter 3** was conducted in the context of two long-term trends: the expansion of connected low-cost sensors and the decline in tailpipe emissions. We integrated three main datasets in a co-kriging model: $PM_{2.5}$ chemical species and oxidative potential data from a fieldwork campaign; unspeciated $PM_{2.5}$ data from a spatially dense, crowdsourced low-cost sensor network; and land-use, traffic, and business data from a set of public and private databases. In modeling $PM_{2.5}$ species previously found associated with non-tailpipe emissions across the Los Angeles metropolitan area, we find substantial improvements in model precision and accuracy when adding in crowdsourced low-cost sensor network data. This is the first study to integrate low-cost sensor data and laboratory measurements to model speciated $PM_{2.5}$. We show that crowdsourced low-cost sensor networks – despite limitations surrounding reliability, sensor placement, and data quality – can provide spatially rich information in exposure models when combined with gold standard research tools. The research featured in **Chapter 3** has been published in *Environment International* [32]. At the time of writing, there are several to-be-published environmental epidemiology studies that derive exposure data from the surfaces presented in **Chapter 3**. Manuscripts in preparation address the effects of these exposures and outcomes such as term low birth weight in an Los Angeles-wide administrative birth cohort; the relationship between racial/ethnic

disparities and social and physical environments in the same administrative birth cohort; metabolomics outcomes in the PARENTs cohort; and the development of autism spectrum disorder in Los Angeles county.

In **Chapter 4**, we then assessed the relationship between exposures generated in the previous chapter and their associations with IPD in a prospectively-followed cohort of 178 then-pregnant women. In contrast to environmental epidemiology studies that rely on large administrative datasets, the PARENTs cohort collected clinically validated data on patient outcomes and detailed information on a large set of confounders. We evaluated our exposure-outcome associations under multiple conditions, including univariate, minimally-adjusted, and fully adjusted regression models. Temporally scaling exposure estimates originally calculated in **Chapter 3** to each subject's first trimester based on low-cost sensor network data, we find that in our prospectively followed cohort, air pollution exposures were consistently positively associated with IPD. Additionally, we found the strongest exposure-outcome associations for $PM_{2.5}$ chemical species and oxidative potential markers, underscoring the importance of specific exposure assessment in human health studies.

In summary, this dissertation explored the use of novel data combinations to investigate short- and long-term events in traffic and TRAP. From changes in fleet composition, to novel methods of measurement and modeling, the study of TRAP continues to evolve. Simultaneously, technology and the data landscape are constantly evolving. Growing interest in environment and health from the technology sector has led to the development and proliferation of low-cost sensors, for example. Further advancements in fields such as urban and environmental sensing may continue to change how scientists and lay audiences see, study, and interpret our built environments. Developing methods to combine different sources of data ranging from point pattern to medical records to satellite imagery, as this dissertation has done, will serve to guide researchers and policymakers as they continue to understand and shape the environment in service of public health.

Bibliography

(1) Fowler, D. et al. A Chronology of Global Air Quality. *Philosophical Transactions of the Royal Society A: Mathematical, Physical and Engineering Sciences* **2020**, *378*, 20190314.

(2) Meffert, P. *The Clean Air Act of 1963*; tech. rep.; US Bureau of Ocean Energy Management.

(3) CARB 2020 Mobile Source Strategy: A Vision for Clean Air, California Air Resources Board, 2020.

(4) US EPA, O. Why Do the Outdoor Air Monitoring Data Summaries Only Go Back to 1980? Isn't Older Data Available?, https://www.epa.gov/outdoor-air-quality-data/why-do-outdoor-air-monitoring-data-summaries-only-go-back-1980-isnt-older, Data and Tools, 2021.

(5) Snyder, E. G.; Watkins, T. H.; Solomon, P. A.; Thoma, E. D.; Williams, R. W.; Hagler, G. S. W.; Shelow, D.; Hindin, D. A.; Kilaru, V. J.; Preuss, P. W. The Changing Paradigm of Air Pollution Monitoring. *Environmental Science & Technology* **2013**, *47*, 11369–11377.

(6) Fussell, J. C.; Franklin, M.; Green, D. C.; Gustafsson, M.; Harrison, R. M.; Hicks, W.; Kelly, F. J.; Kishta, F.; Miller, M. R.; Mudway, I. S.; Oroumiyeh, F.; Selley, L.; Wang, M.; Zhu, Y. A Review of Road Traffic-Derived Non-Exhaust Particles: Emissions, Physicochemical Characteristics, Health Risks, and Mitigation Measures. *Environmental Science & Technology* **2022**, DOI: 10.1021/acs.est.2c01072.

(7) Boogaard, H. et al. Long-Term Exposure to Traffic-Related Air Pollution and Selected Health Outcomes: A Systematic Review and Meta-Analysis. *Environment International* **2022**, *164*, 107262.

(8) Habre, R.; Girguis, M.; Urman, R.; Fruin, S.; Lurmann, F.; Shafer, M.; Gorski, P.; Franklin, M.; McConnell, R.; Avol, E.; Gilliland, F. Contribution of Tailpipe and Non-tailpipe Traffic Sources to Quasi-Ultrafine, Fine and Coarse Particulate Matter in Southern California. *Journal of the Air & Waste Management Association* **2020**, *0*, null.

(9) Jarvis, D. J.; Adamkiewicz, G.; Heroux, M.-E.; Rapp, R.; Kelly, F. J., *Nitrogen Dioxide*; World Health Organization: 2010.

(10) Anenberg, S. C.; Mohegh, A.; Goldberg, D. L.; Kerr, G. H.; Brauer, M.; Burkart, K.; Hystad, P.; Larkin, A.; Wozniak, S.; Lamsal, L. Long-Term Trends in Urban NO2 Concentrations and Associated Paediatric Asthma Incidence: Estimates from Global Datasets. *The Lancet Planetary Health* **2022**, *6*, e49–e58.

(11) Fang, T.; Verma, V.; Bates, J. T.; Abrams, J.; Klein, M.; Strickland, M. J.; Sarnat, S. E.; Chang, H. H.; Mulholland, J. A.; Tolbert, P. E.; Russell, A. G.; Weber, R. J. Oxidative Potential of Ambient Water-Soluble $PM_{2.5}$ in the Southeastern United States: Contrasts in Sources and Health Associations between Ascorbic Acid (AA) and Dithiothreitol (DTT) Assays. *Atmospheric Chemistry and Physics* **2016**, *16*, 3865–3879.

(12) Rich, D. Q. Accountability studies of air pollution and health effects: lessons learned and recommendations for future natural experiment opportunities. *Environment International* **2017**, *100*, 62–78.

(13) Cai, H.; Xie, S. Traffic-Related Air Pollution Modeling during the 2008 Beijing Olympic Games: The Effects of an Odd-Even Day Traffic Restriction Scheme. *The Science of the Total Environment* **2011**, *409*, 1935–1948.

(14) He, G.; Fan, M.; Zhou, M. The Effect of Air Pollution on Mortality in China: Evidence from the 2008 Beijing Olympic Games. *Journal of Environmental Economics and Management* **2016**, *79*, 18–39.

(15) Friedman, M. S.; Powell, K. E.; Hutwagner, L.; Graham, L. M.; Teague, W. G. Impact of Changes in Transportation and Commuting Behaviors during the 1996 Summer Olympic Games in Atlanta on Air Quality and Childhood Asthma. *JAMA* **2001**, *285*, 897–905.

(16) Institute, H. E. Impact of Improved Air Quality During the 1996 Summer Olympic Games in Atlanta on Multiple Cardiovascular and Respiratory Outcomes Health Effects Institute, `https://www.healtheffects.org/publication/impact-improved-air-quality-during-1996-summer-olympic-games-atlanta-multiple` (accessed 11/10/2020).

(17) Peel, J. L.; Klein, M.; Flanders, W. D.; Mulholland, J. A.; Tolbert, P. E.; HEI Health Review Committee Impact of Improved Air Quality during the 1996 Summer Olympic Games in Atlanta on Multiple Cardiovascular and Respiratory Outcomes. *Research Report (Health Effects Institute)* **2010**, 3–23, discussion 25–33.

(18) Quiros, D. C.; Zhang, Q.; Choi, W.; He, M.; Paulson, S. E.; Winer, A. M.; Wang, R.; Zhu, Y. Air Quality Impacts of a Scheduled 36-h Closure of a Major Highway. *Atmospheric Environment* **2013**, *67*, 404–414.

(19) HEI *Systematic Review and Meta-analysis of Selected Health Effects of Long-Term Exposure to Traffic-Related Air Pollution*; 23; Boston MA: Health Effects Institute, 2022.

(20) Zeldovich, Y.; Sadonikov, P.; Frank-Kamenetskii, D. Oxidation of Nitrogen in Combustion, Translated by M. Shelef. *Academy of Sciences of the USSR, Moscow* **1947**.

(21) Board, C. A. R. *California Greenhouse Gas Emissions for 2000 to 2017*; California Air Resources Board, 2019.

(22) Khan, J.; Ketzel, M.; Kakosimos, K.; Sorensen, M.; Jensen, S. S. Road Traffic Air and Noise Pollution Exposure Assessment - A Review of Tools and Techniques. *Science of the Total Environment* **2018**, *634*, 661–676.

(23) Lowther, S. D.; Jones, K. C.; Wang, X.; Whyatt, J. D.; Wild, O.; Booker, D. Particulate Matter Measurement Indoors: A Review of Metrics, Sensors, Needs, and Applications. *Environmental science & technology* **2019**, *53*, 11644–11656.

(24) Baron, R.; Saffell, J. Amperometric Gas Sensors as a Low Cost Emerging Technology Platform for Air Quality Monitoring Applications: A Review. *ACS sensors* **2017**, *2*, 1553–1566.

(25) Daepp, M. et al. In 2022 International Conference on Information Processing in Sensor Networks (IPSN), 2022.

(26) Zhou, B.; Zhang, S.; Xue, R.; Li, J.; Wang, S. A Review of Space-Air-Ground Integrated Remote Sensing Techniques for Atmospheric Monitoring. *Journal of Environmental Sciences* **2023**, *123*, 3–14.

(27) Kang, Y.; Aye, L.; Ngo, T. D.; Zhou, J. Performance Evaluation of Low-Cost Air Quality Sensors: A Review. *SCIENCE OF THE TOTAL ENVIRONMENT* **2022**, *818*, DOI: 10.1016/j.scitotenv.2021.151769.

(28) Hoek, G.; Beelen, R.; de Hoogh, K.; Vienneau, D.; Gulliver, J.; Fischer, P.; Briggs, D. A Review of Land-Use Regression Models to Assess Spatial Variation of Outdoor Air Pollution. *Atmospheric Environment* **2008**, *42*, 7561–7578.

(29) Li, L.; Wu, J.; Wilhelm, M.; Ritz, B. Use of Generalized Additive Models and Cokriging of Spatial Residuals to Improve Land-Use Regression Estimates of Nitrogen Oxides in Southern California. *Atmospheric Environment (Oxford, England: 1994)* **2012**, *55*, 220–228.

(30) Brokamp, C.; Jandarov, R.; Rao, M. B.; LeMasters, G.; Ryan, P. Exposure Assessment Models for Elemental Components of Particulate Matter in an Urban Environment: A Comparison of Regression and Random Forest Approaches. *Atmospheric Environment (Oxford, England: 1994)* **2017**, *151*, 1–11.

(31) Tripathy, S.; Tunno, B. J.; Michanowicz, D. R.; Kinnee, E.; Shmool, J. L. C.; Gillooly, S.; Clougherty, J. E. Hybrid Land Use Regression Modeling for Estimating Spatio-Temporal Exposures to PM2.5, BC, and Metal Components across a Metropolitan Area of Complex Terrain and Industrial Sources. *The Science of the Total Environment* **2019**, *673*, 54–63.

(32) Liu, J.; Banerjee, S.; Oroumiyeh, F.; Shen, J.; Rosario, I. D.; Lipsitt, J.; Paulson, S.; Ritz, B.; Su, J.; Weichenthal, S.; Lakey, P.; Shiraiwa, M.; Zhu, Y.; Jerrett, M. Co-Kriging with a Low-Cost Sensor Network to Estimate Spatial Variation of Brake and Tire-Wear Metals and Oxidative Stress Potential in Southern California. *Environment International* **2022**, 107481.

(33) Nuckols, J. R.; Ward, M. H.; Jarup, L. Using Geographic Information Systems for Exposure Assessment in Environmental Epidemiology Studies. *Environmental Health Perspectives* **2004**, *112*, 1007–1015.

(34) Khreis, H.; Kelly, C.; Tate, J.; Parslow, R.; Lucas, K.; Nieuwenhuijsen, M. Exposure to Traffic-Related Air Pollution and Risk of Development of Childhood Asthma: A Systematic Review and Meta-Analysis. *Environment International* **2017**, *100*, 1–31.

(35) Mudway, I.; Kelly, F.; Holgate, S. Oxidative Stress in Air Pollution Research. *Free Radical Biology & Medicine* **2020**, *151*, 2–6.

(36) Sies, H. Oxidative Stress: A Concept in Redox Biology and Medicine. *Redox Biology* **2015**, *4*, 180–183.

(37) Saenen, N. D.; Martens, D. S.; Neven, K. Y.; Alfano, R.; Bové, H.; Janssen, B. G.; Roels, H. A.; Plusquin, M.; Vrijens, K.; Nawrot, T. S. Air Pollution-Induced Placental Alterations: An Interplay of Oxidative Stress, Epigenetics, and the Aging Phenotype? *Clinical Epigenetics* **2019**, *11*, 124.

(38) Sharma, S.; Chandra, M.; Kota, S. H. Health Effects Associated with PM2.5: A Systematic Review. *Current Pollution Reports* **2020**, *6*, 345–367.

(39) Newsom, G. *Executive Order N-33-20*; Executive Department, State of California, 2020.

(40) Bao, R.; Zhang, A. Does Lockdown Reduce Air Pollution? Evidence from 44 Cities in Northern China. *Science of the Total Environment* **2020**, *731*, 139052.

(41) Wang, Q.; Su, M. A Preliminary Assessment of the Impact of COVID-19 on Environment – A Case Study of China. *Science of The Total Environment* **2020**, *728*, 138915.

(42) Xu, H.; Yan, C.; Fu, Q.; Xiao, K.; Yu, Y.; Han, D.; Wang, W.; Cheng, J. Possible Environmental Effects on the Spread of COVID-19 in China. *Science of the Total Environment* **2020**, *731*, 139211.

(43) Zhang, R.; Zhang, Y.; Lin, H.; Feng, X.; Fu, T.-M.; Wang, Y. NOx Emission Reduction and Recovery during COVID-19 in East China. *Atmosphere* **2020**, *11*, 433.

(44) Zhang, J.; Cui, K.; Wang, Y.-F.; Wu, J.-L.; Huang, W.-S.; Wan, S.; Xu, K. Temporal Variations in the Air Quality Index and the Impact of the COVID-19 Event on Air Quality in Western China. *Aerosol and Air Quality Research* **2020**, *20*, 1552–1568.

(45) Zhao, Y.; Zhang, K.; Xu, X.; Shen, H.; Zhu, X.; Zhang, Y.; Hu, Y.; Shen, G. Substantial Changes in Nitrogen Dioxide and Ozone after Excluding Meteorological Impacts during the COVID-19 Outbreak in Mainland China. *Environmental Science & Technology Letters* **2020**, *7*, 402–408.

(46) Zheng, H. et al. Significant Changes in the Chemical Compositions and Sources of PM2.5 Wuhan since the City Lockdown as COVID-19. *Science of the Total Environment* **2020**, *739*, 140000.

(47) Chen, Q.-X.; Huang, C.-L.; Yuan, Y.; Tan, H.-P. Influence of COVID-19 Event on Air Quality and Their Association in Mainland China. *Aerosol and Air Quality Research* **2020**, *20*, 1541–1551.

(48) Fan, C.; Li, Y.; Guang, J.; Li, Z.; Elnashar, A.; Allam, M.; de Leeuw, G. The Impact of the Control Measures during the COVID-19 Outbreak on Air Pollution in China. *Remote Sensing* **2020**, *12*, 1613.

(49) Filonchyk, M.; Hurynovich, V.; Yan, H.; Gusev, A.; Shpilevskaya, N. Impact Assessment of COVID-19 on Variations of SO2, NO2, CO and AOD over East China. *Aerosol and Air Quality Research* **2020**, *20*, 1530–1540.

(50) Grif, S. M.; Huang, W.-S.; Lin, C.-C.; Chen, Y.-C.; Chang, K.-E.; Lin, T.-H.; Wang, S.-H.; Lin, N.-H. Long-Range Air Pollution Transport in East Asia during the First Week of the COVID-19 Lockdown in China. *Science of the Total Environment* **2020**, *741*, 140214.

(51) Marlier, M. E.; Xing, J.; Zhu, Y.; Wang, S. Impacts of COVID-19 Response Actions on Air Quality in China. *Environmental Research Communications* **2020**, *2*, 075003.

(52) Ming, W.; Zhou, Z.; Ai, H.; Bi, H.; Zhong, Y. COVID-19 and Air Quality: Evidence from China. *Emerging Markets Finance and Trade* **2020**, *56*, 2422–2442.

(53) Shakoor, A.; Chen, X.; Farooq, T. H.; Shahzad, U.; Ashraf, F.; Rehman, A.; Sahar, N. E.; Yan, W. Fluctuations in Environmental Pollutants and Air Quality during the Lockdown in the USA and China: Two Sides of COVID-19 Pandemic. *Air Quality Atmosphere and Health*, DOI: 10.1007/s11869-020-00888-6.

(54) Sui, X.; Zhang, J.; Zhang, Q.; Sun, S.; Lei, R.; Zhang, C.; Cheng, H.; Ding, L.; Ding, R.; Xiao, C.; Li, X.; Cao, J. The Short-Term Effect of PM2.5/O3 on Daily Mortality from 2013 to 2018 in Hefei, China. *Environmental Geochemistry and Health* **2020**, DOI: 10.1007/s10653-020-00689-x.

(55) Agarwal, A.; Kaushik, A.; Kumar, S.; Mishra, R. K. Comparative Study on Air Quality Status in Indian and Chinese Cities before and during the COVID-19 Lockdown Period. *Air Quality Atmosphere and Health* **2020**, DOI: 10.1007/s11869-020-00881-z.

(56) Bera, B.; Bhattacharjee, S.; Shit, P. K.; Sengupta, N.; Saha, S. Significant Impacts of COVID-19 Lockdown on Urban Air Pollution in Kolkata (India) and Amelioration of Environmental Health. *Environment Development and Sustainability* **2020**, DOI: 10.1007/s10668-020-00898-5.

(57) Gautam, S. COVID-19: Air Pollution Remains Low as People Stay at Home. *Air Quality Atmosphere and Health* **2020**, *13*, 853–857.

(58) Ghosh, S.; Ghosh, S. Air Quality during COVID-19 Lockdown: Blessing in Disguise. *Indian Journal of Biochemistry & Biophysics* **2020**, *57*, 420–430.

(59) Mahato, S.; Pal, S.; Ghosh, K. G. Effect of Lockdown amid COVID-19 Pandemic on Air Quality of the Megacity Delhi, India. *The Science of the Total Environment* **2020**, *730*, 139086.

(60) Sharma, S.; Zhang, M.; Anshika; Gao, J.; Zhang, H.; Kota, S. H. Effect of Restricted Emissions during COVID-19 on Air Quality in India. *Science of the Total Environment* **2020**, *728*, 138878.

(61) Shehzad, K.; Sarfraz, M.; Shah, S. G. M. The Impact of COVID-19 as a Necessary Evil on Air Pollution in India during the Lockdown. *Environmental Pollution* **2020**, *266*, 115080.

(62) Siddiqui, A.; Halder, S.; Chauhan, P.; Kumar, P. COVID-19 Pandemic and City-Level Nitrogen Dioxide (NO2) Reduction for Urban Centres of India. *Journal of the Indian Society of Remote Sensing* **2020**, DOI: 10.1007/s12524-020-01130-7.

(63) Baldasano, J. M. COVID-19 Lockdown Effects on Air Quality by NO2 in the Cities of Barcelona and Madrid (Spain). *Science of the Total Environment* **2020**, *741*, 140353.

(64) Menut, L.; Bessagnet, B.; Siour, G.; Mailler, S.; Pennel, R.; Cholakian, A. Impact of Lockdown Measures to Combat Covid-19 on Air Quality over Western Europe. *Science of the Total Environment* **2020**, *741*, 140426.

(65) Zoran, M. A.; Savastru, R. S.; Savastru, D. M.; Tautan, M. N. Assessing the Relationship between Surface Levels of PM2.5 and PM10 Particulate Matter Impact on COVID-19 in Milan, Italy. *Science of the Total Environment* **2020**, *738*, 139825.

(66) Kondo Nakada, L. Y.; Urban, R. C. COVID-19 Pandemic: Impacts on the Air Quality during the Partial Lockdown in Sao Paulo State, Brazil. *Science of the Total Environment* **2020**, *730*, 139087.

(67) Roman-Gonzalez, A.; Vargas-Cuentas, N. Variation of Aerosol Pollution in Peru during the Quarantine Due to COVID-19. *International Journal of Advanced Computer Science and Applications* **2020**, *11*, 47–50.

(68) Siciliano, B.; Dantas, G.; da Silva, C. M.; Arbilla, G. Increased Ozone Levels during the COVID-19 Lockdown: Analysis for the City of Rio de Janeiro, Brazil. *Science of the Total Environment* **2020**, *737*, 139765.

(69) Kerimray, A.; Baimatova, N.; Ibragimova, O. P.; Bukenov, B.; Kenessov, B.; Plotitsyn, P.; Karaca, F. Assessing Air Quality Changes in Large Cities during COVID-19 Lockdowns: The Impacts of Traffic-Free Urban Conditions in Almaty, Kazakhstan. *Science of the Total Environment* **2020**, *730*, 139179.

(70) Berman, J. D.; Ebisu, K. Changes in US Air Pollution during the COVID-19 Pandemic. *Science of the Total Environment* **2020**, *739*, 139864.

(71) Hudda, N.; Simon, M. C.; Patton, A. P.; Durant, J. L. Reductions in Traffic-Related Black Carbon and Ultrafine Particle Number Concentrations in an Urban Neighborhood during the COVID-19 Pandemic. *Science of the Total Environment* **2020**, *742*, 140931.

(72) Son, J.-Y.; Fong, K. C.; Heo, S.; Kim, H.; Lim, C. C.; Bell, M. L. Reductions in Mortality Resulting from Reduced Air Pollution Levels Due to COVID-19 Mitigation Measures. *Science of the Total Environment* **2020**, *744*, 141012.

(73) Zhang, H.; Wang, Q.; He, S.; Wu, K.; Ren, M.; Dong, H.; Di, J.; Yu, Z.; Huang, C. Ambient Air Pollution and Gestational Diabetes Mellitus: A Review of Evidence from Biological Mechanisms to Population Epidemiology. *The Science of the Total Environment* **2020**, *719*, 137349.

(74) US EPA, O. Integrated Science Assessment (ISA) for Nitrogen Dioxide - Health Criteria US EPA, `https://www.epa.gov/isa/integrated-science-assessment-isa-nitrogen-dioxide-health-criteria` (accessed 10/08/2020).

(75) Almaraz, M.; Bai, E.; Wang, C.; Trousdell, J.; Conley, S.; Faloona, I.; Houlton, B. Z. Agriculture Is a Major Source of NOx Pollution in California. *Science Advances* **2018**, *4*, eaao3477.

(76) McDonald, B. C.; McBride, Z. C.; Martin, E. W.; Harley, R. A. High-Resolution Mapping of Motor Vehicle Carbon Dioxide Emissions. *Journal of Geophysical Research: Atmospheres* **2014**, *119*, 5283–5298.

(77) Chen, K.; Wang, M.; Huang, C.; Kinney, P. L.; Anastas, P. T. Air Pollution Reduction and Mortality Benefit during the COVID-19 Outbreak in China. *Lancet Planetary Health* **2020**, *4*, E210–E212.

(78) Goldberg, D. L.; Goldberg, D. L.; Anenberg, S. C.; Griffin, D.; Mclinden, C. A.; Lu, Z.; Streets, D. G. Disentangling the Impact of the COVID-19 Lockdowns on Urban NO2 from Natural Variability Earth and Space Science Open Archive, `http://www.essoar.org/doi/10.1002/essoar.10503396.1` (accessed 07/28/2020).

(79) Tyagi, P.; Braun, D.; Sabath, B.; Henneman, L.; Dominici, F. Short-Term Change in Air Pollution Following the COVID-19 State of Emergency: A National Analysis for the United States. *medRxiv* **2020**, 2020.08.04.20168237.

(80) About AirNow — AirNow.Gov `https://www.airnow.gov/about-airnow` (accessed 07/27/2020).

(81) Caltrans PeMS `http://pems.dot.ca.gov/?logout=1` (accessed 07/27/2020).

(82) MesoWest MesoWest Data `https://mesowest.utah.edu/` (accessed 07/27/2020).

(83) Choi, W.; Paulson, S. E.; Casmassi, J.; Winer, A. M. Evaluating Meteorological Comparability in Air Quality Studies: Classification and Regression Trees for Primary Pollutants in California's South Coast Air Basin. *Atmospheric Environment* **2013**, *64*, 150–159.

(84) Ravindra, K.; Rattan, P.; Mor, S.; Aggarwal, A. N. Generalized Additive Models: Building Evidence of Air Pollution, Climate Change and Human Health. *Environment International* **2019**, *132*, 104987.

(85) Sarizadeh, R.; Dastoorpoor, M.; Goudarzi, G.; Simbar, M. The Association Between Air Pollution and Low Birth Weight and Preterm Labor in Ahvaz, Iran. *International Journal of Women's Health* **2020**, *12*, 313–325.

(86) *California Auto Outlook Covering Fourth Quarter 2019: State New Vehicle Market Predicted to Remain Strong in 2020*; California New Car Dealers Association (CNCDA), 2020.

(87) Climate-Data.org Climate California: Temperature, Climate Graph, Climate Table for California - Climate-Data.Org California Climate, `https://en.climate-data.org/north-america/united-states-of-america/california-917/` (accessed 07/28/2020).

(88) R Core Team R: A Language and Environment for Statistical Computing, manual; R Foundation for Statistical Computing, Vienna, Austria, 2021.

(89) Chen, L.-W. A.; Chien, L.-C.; Li, Y.; Lin, G. Nonuniform Impacts of COVID-19 Lockdown on Air Quality over the United States. *The Science of the Total Environment* **2020**, *745*, 141105.

(90) Cai, H.; Xie, S. Traffic-Related Air Pollution Modeling during the 2008 Beijing Olympic Games: The Effects of an Odd-Even Day Traffic Restriction Scheme. *The Science of the Total Environment* **2011**, *409*, 1935–1948.

(91) Friedman, M. S.; Powell, K. E.; Hutwagner, L.; Graham, L. M.; Teague, W. G. Impact of Changes in Transportation and Commuting Behaviors during the 1996 Summer Olympic Games in Atlanta on Air Quality and Childhood Asthma. *JAMA* **2001**, *285*, 897–905.

(92) Yao, Z.; Zhang, Y.; Shen, X.; Wang, X.; Wu, Y.; He, K. Impacts of Temporary Traffic Control Measures on Vehicular Emissions during the Asian Games in Guangzhou, China. *Journal of the Air & Waste Management Association (1995)* **2013**, *63*, 11–19.

(93) Kumar, P.; Gulia, S.; Harrison, R. M.; Khare, M. The Influence of Odd-Even Car Trial on Fine and Coarse Particles in Delhi. *Environmental Pollution (Barking, Essex: 1987)* **2017**, *225*, 20–30.

(94) De Jesus, A. L. et al. Ultrafine Particles and PM2.5 in the Air of Cities around the World: Are They Representative of Each Other? *Environment International* **2019**, *129*, 118–135.

(95) Wang, Q.; Li, J.; Yang, J.; Chen, Y.; Li, Y.; Li, S.; Xie, C.; Chen, C.; Wang, L.; Wang, L.; Wang, W.; Tong, S.; Sun, Y. Seasonal Characterization of Aerosol Composition and Sources in a Polluted City in Central China. *Chemosphere* **2020**, *258*, 127310.

(96) Wang, Y.; Wang, Q.; Ye, J.; Yan, M.; Qin, Q.; Prevot, A. S. H.; Cao, J. A Review of Aerosol Chemical Composition and Sources in Representative Regions of China during Wintertime. *Atmosphere* **2019**, *10*, 277.

(97) Grieshop, A. P.; Lipsky, E. M.; Pekney, N. J.; Takahama, S.; Robinson, A. L. Fine Particle Emission Factors from Vehicles in a Highway Tunnel: Effects of Fleet Composition and Season. *Atmospheric Environment* **2006**, *40*, 287–298.

(98) Jeong, C.-H.; Traub, A.; Huang, A.; Hilker, N.; Wang, J. M.; Herod, D.; Dabek-Zlotorzynska, E.; Celo, V.; Evans, G. J. Long-Term Analysis of PM2.5 from 2004 to 2017 in Toronto: Composition, Sources, and Oxidative Potential. *Environmental Pollution* **2020**, *263*, 114652.

(99) Pant, P.; Harrison, R. M. Estimation of the Contribution of Road Traffic Emissions to Particulate Matter Concentrations from Field Measurements: A Review. *Atmospheric Environment* **2013**, *77*, 78–97.

(100) Amato, F.; Pandolfi, M.; Moreno, T.; Furger, M.; Pey, J.; Alastuey, A.; Bukowiecki, N.; Prevot, A. S. H.; Baltensperger, U.; Querol, X. Sources and Variability of Inhalable Road Dust Particles in Three European Cities. *Atmospheric Environment* **2011**, *45*, 6777–6787.

(101) Grigoratos, T.; Martini, G. Brake Wear Particle Emissions: A Review. *Environmental Science and Pollution Research International* **2015**, *22*, 2491–2504.

(102) Milani, M.; Pucillo, F. P.; Ballerini, M.; Camatini, M.; Gualtieri, M.; Martino, S. First Evidence of Tyre Debris Characterization at the Nanoscale by Focused Ion Beam. *Materials Characterization* **2004**, *52*, 283–288.

(103) Oroumiyeh, F.; Jerrett, M.; Del Rosario, I.; Lipsitt, J.; Liu, J.; Paulson, S. E.; Ritz, B.; Schauer, J. J.; Shafer, M. M.; Shen, J.; Weichenthal, S.; Banerjee, S.; Zhu, Y. Elemental Composition of Fine and Coarse Particles across the Greater Los Angeles Area: Spatial Variation and Contributing Sources. *Environmental Pollution* **2022**, *292*, 118356.

(104) Wang, J. M.; Jeong, C.-H.; Hilker, N.; Healy, R. M.; Sofowote, U.; Debosz, J.; Su, Y.; Munoz, A.; Evans, G. J. Quantifying Metal Emissions from Vehicular Traffic Using Real World Emission Factors. *Environmental Pollution* **2021**, *268*, 115805.

(105) Valko, M.; Morris, H.; Cronin, M. T. D. Metals, Toxicity and Oxidative Stress. *Current Medicinal Chemistry* **2005**, *12*, 1161–1208.

(106) Briggs, D. The Role of Gis: Coping With Space (And Time) in Air Pollution Exposure Assessment. *Journal of Toxicology and Environmental Health, Part A* **2005**, *68*, 1243–1261.

(107) Jerrett, M.; Burnett, R. T.; Ma, R.; Pope, C. A.; Krewski, D.; Newbold, K. B.; Thurston, G.; Shi, Y.; Finkelstein, N.; Calle, E. E.; Thun, M. J. Spatial Analysis of Air Pollution and Mortality in Los Angeles. *Epidemiology* **2005**, *16*, 727–736.

(108) De Hoogh, K. et al. Development of Land Use Regression Models for Particle Composition in Twenty Study Areas in Europe. *Environmental Science & Technology* **2013**, *47*, 5778–5786.

(109) Zhang, J. J. Y.; Sun, L.; Barrett, O.; Bertazzon, S.; Underwood, F. E.; Johnson, M. Development of Land-Use Regression Models for Metals Associated with Airborne Particulate Matter in a North American City. *Atmospheric Environment* **2015**, *106*, 165–177.

(110) Ito, K.; Johnson, S.; Kheirbek, I.; Clougherty, J.; Pezeshki, G.; Ross, Z.; Eisl, H.; Matte, T. D. Intraurban Variation of Fine Particle Elemental Concentrations in New York City. *Environmental Science & Technology* **2016**, *50*, 7517–7526.

(111) Weichenthal, S.; Shekarrizfard, M.; Kulka, R.; Lakey, P. S. J.; Al-Rijleh, K.; Anowar, S.; Shiraiwa, M.; Hatzopoulou, M. Spatial Variations in the Estimated Production of Reactive Oxygen Species in the Epithelial Lung Lining Fluid by Iron and Copper in Fine Particulate Air Pollution. *Environmental Epidemiology* **2018**, *2*, e020.

(112) PurpleAir Our Technology - PurpleAir Laser Particle Counters & Arduinos PurpleAir, Inc., `https://www2.purpleair.com/pages/technology` (accessed 08/05/2021).

(113) Johnson, K.; Gantt, B.; VonWald, I.; Clemements, A. L. PurpleAir PM2.5 Performance across the U.S. US EPA, 2019.

(114) Kosmopoulos, G.; Salamalikis, V.; Pandis, S. N.; Yannopoulos, P.; Bloutsos, A. A.; Kazantzidis, A. Low-Cost Sensors for Measuring Airborne Particulate Matter: Field Evaluation and Calibration at a South-Eastern European Site. *The Science of the Total Environment* **2020**, *748*, 141396.

(115) Li, J.-Q.; Gupta, S. D.; Zhang, L.; Zhou, K.; Zhang, W.-B. Evaluate Bus Emissions Generated near Far-Side and near-Side Stops and Potential Reductions by ITS: An Empirical Study. *Transportation Research Part D-Transport and Environment* **2012**, *17*, 73–77.

(116) Jerrett, M. *Air Monitoring Site Selection Methodology for Particulate Matter from Brake and Tire Wear*; California Air Resources Board, 2021.

(117) Gonzalez, D. H.; Cala, C. K.; Peng, Q.; Paulson, S. E. HULIS Enhancement of Hydroxyl Radical Formation from Fe(II): Kinetics of Fulvic Acid-Fe(II) Complexes in the Presence of Lung Antioxidants. *Environmental Science & Technology* **2017**, *51*, 7676–7685.

(118) Cho, A. K.; Sioutas, C.; Miguel, A. H.; Kumagai, Y.; Schmitz, D. A.; Singh, M.; Eiguren-Fernandez, A.; Froines, J. R. Redox Activity of Airborne Particulate Matter at Different Sites in the Los Angeles Basin. *Environmental Research* **2005**, *99*, 40–47.

(119) Lakey, P. S. J.; Berkemeier, T.; Tong, H.; Arangio, A. M.; Lucas, K.; Pöschl, U.; Shiraiwa, M. Chemical Exposure-Response Relationship between Air Pollutants and Reactive Oxygen Species in the Human Respiratory Tract. *Scientific Reports* **2016**, *6*, 32916.

(120) MRLC National Land Cover Database 2019 (NLCD2019) Legend — Multi-Resolution Land Characteristics (MRLC) Consortium Multi-Resolution Land Characteristics Consortium, `https://www.mrlc.gov/data/nlcd-2019-land-cover-conus` (accessed 12/08/2020).

(121) Roff, T. HPMS Public Release of Geospatial Data in Shapefile Format - Policy — Federal Highway Administration US Department of Transportation Federal HIghway Administration, `https://www.fhwa.dot.gov/policyinformation/hpms/shapefiles.cfm` (accessed 04/16/2021).

(122) Bureau, U. C. TIGER/Line Shapefiles The United States Census Bureau, https://www.census.gov/geographies/mapping-files/time-series/geo/tiger-line-file.html (accessed 05/16/2021).

(123) ESRI Business Analyst Data https://www.esri.com/en-us/arcgis/products/arcgis-business-analyst/data-infographics (accessed 04/16/2021).

(124) Akpinar, A.; Barbosa-Leiker, C.; Brooks, K. R. Does Green Space Matter? Exploring Relationships between Green Space Type and Health Indicators. *Urban Forestry & Urban Greening* **2016**, *20*, 407–418.

(125) Henderson, S. B.; Beckerman, B.; Jerrett, M.; Brauer, M. Application of Land Use Regression to Estimate Long-Term Concentrations of Traffic-Related Nitrogen Oxides and Fine Particulate Matter. *Environmental Science & Technology* **2007**, *41*, 2422–2428.

(126) Klot, S. Equivalence of Using Nested Buffers and Concentric Adjacent Rings as Predictors in Land Use Regression Models. *Atmospheric Environment - ATMOS ENVIRON* **2011**, *45*, 4108–4110.

(127) Beckerman, B. S.; Jerrett, M.; Serre, M.; Martin, R. V.; Lee, S.-J.; van Donkelaar, A.; Ross, Z.; Su, J.; Burnett, R. T. A Hybrid Approach to Estimating National Scale Spatiotemporal Variability of PM2.5 in the Contiguous United States. *Environmental Science & Technology* **2013**, *47*, 7233–7241.

(128) Sinisi, S. E.; van der Laan, M. J. Deletion/Substitution/Addition Algorithm in Learning with Applications in Genomics. *Statistical Applications in Genetics and Molecular Biology* **2004**, *3*, Article18.

(129) AQMD, S. PurpleAir PA-II South Coast Air Quality Management District, https://www.aqmd.gov/aq-spec/product/purpleair-pa-ii (accessed 09/16/2019).

(130) Journel, A. G.; Huijbregts, C. J., *Mining Geostatistics*; Academic Press: London ; New York, 1978; 600 pp.

(131) Matheron, G. Recherche de Simplification Dans Un Problème de Cokrigeage. *Publication N-628, Centre de Géostatistique, Ecole des Mines de Paris, Fontainebleau* **1979**.

(132) Pebesma, E. J.; Wesseling, C. G. Gstat: A Program for Geostatistical Modelling, Prediction and Simulation. *Computers & Geosciences* **1998**, *24*, 17–31.

(133) Kuang, X. M.; Gonzalez, D. H.; Scott, J. A.; Vu, K.; Hasson, A.; Charbouillot, T.; Hawkins, L.; Paulson, S. E. Cloud Water Chemistry Associated with Urban Aerosols: Rapid Hydroxyl Radical Formation, Soluble Metals, Fe(II), Fe(III), and Quinones. *ACS Earth and Space Chemistry* **2020**, *4*, 67–76.

(134) Jones, R. R.; Hoek, G.; Fisher, J. A.; Hasheminassab, S.; Wang, D.; Ward, M. H.; Sioutas, C.; Vermeulen, R.; Silverman, D. T. Land Use Regression Models for Ultrafine Particles, Fine Particles, and Black Carbon in Southern California. *Science of The Total Environment* **2020**, *699*, 134234.

(135) Charrier, J. G.; Anastasio, C. On Dithiothreitol (DTT) as a Measure of Oxidative Potential for Ambient Particles: Evidence for the Importance of Soluble Transition Metals. *Atmospheric chemistry and physics (Print)* **2012**, *12*, 11317–11350.

(136) Yang, A.; Wang, M.; Eeftens, M.; Beelen, R.; Dons, E.; Leseman, D. L. A. C.; Brunekreef, B.; Cassee, F. R.; Janssen, N. A. H.; Hoek, G. Spatial Variation and Land Use Regression Modeling of the Oxidative Potential of Fine Particles. *Environmental Health Perspectives* **2015**, *123*, 1187–1192.

(137) Kuang, X. M.; Scott, J. A.; da Rocha, G. O.; Betha, R.; Price, D. J.; Russell, L. M.; Cocker, D. R.; Paulson, S. E. Hydroxyl Radical Formation and Soluble Trace Metal Content in Particulate Matter from Renewable Diesel and Ultra Low Sulfur Diesel in At-Sea Operations of a Research Vessel. *Aerosol Science and Technology* **2017**, *51*, 147–158.

(138) Li, X.; Kuang, X. M.; Yan, C.; Ma, S.; Paulson, S. E.; Zhu, T.; Zhang, Y.; Zheng, M. Oxidative Potential by PM2.5 in the North China Plain: Generation of Hydroxyl Radical. *Environmental Science & Technology* **2019**, *53*, 512–520.

(139) Davies, M. M.; van der Laan, M. J. Optimal Spatial Prediction Using Ensemble Machine Learning. *The International Journal of Biostatistics* **2016**, *12*, 179–201.

(140) Liang, Y.; Sengupta, D.; Campmier, M. J.; Apte, J.; Lunderberg, D. M.; Goldstein, A. Wildfire Smoke Impacts on Indoor Air Quality Assessed Using Crowdsourced Data in California. **2021**, DOI: 10.26434/chemrxiv.14739219.v1.

(141) Carvlin, G. Purple Air Calibration: Effect of Space, Time and Environment, Air Sensors International Conference, 2019.

(142) Cohen, A. J. et al. Estimates and 25-Year Trends of the Global Burden of Disease Attributable to Ambient Air Pollution: An Analysis of Data from the Global Burden of Diseases Study 2015. *Lancet (London, England)* **2017**, *389*, 1907–1918.

(143) Jeong, C.-H.; Traub, A.; Huang, A.; Hilker, N.; Wang, J. M.; Herod, D.; Dabek-Zlotorzynska, E.; Celo, V.; Evans, G. J. Long-Term Analysis of PM2.5 from 2004 to 2017 in Toronto: Composition, Sources, and Oxidative Potential. *Environmental Pollution* **2020**, *263*, 114652.

(144) Sternbeck, J.; Sjödin, Å.; Andréasson, K. Metal Emissions from Road Traffic and the Influence of Resuspension—Results from Two Tunnel Studies. *Atmospheric Environment* **2002**, *36*, 4735–4744.

(145) Joo, E. H.; Kim, Y. R.; Kim, N.; Jung, J. E.; Han, S. H.; Cho, H. Y. Effect of Endogenic and Exogenic Oxidative Stress Triggers on Adverse Pregnancy Outcomes: Preeclampsia, Fetal Growth Restriction, Gestational Diabetes Mellitus and Preterm Birth. *International Journal of Molecular Sciences* **2021**, *22*, 10122.

(146) Roberts, J. M.; Escudero, C. The placenta in preeclampsia. *Pregnancy Hypertension: An International Journal of Women's Cardiovascular Health* **2012**, *2*, 72–83.

(147) Ananth, C. V.; Vintzileos, A. M. Ischemic Placental Disease: Epidemiology and Risk Factors. *European Journal of Obstetrics, Gynecology, and Reproductive Biology* **2011**, *159*, 77–82.

(148) Saenen, N. D.; Martens, D. S.; Neven, K. Y.; Alfano, R.; Bové, H.; Janssen, B. G.; Roels, H. A.; Plusquin, M.; Vrijens, K.; Nawrot, T. S. Air Pollution-Induced Placental Alterations: An Interplay of Oxidative Stress, Epigenetics, and the Aging Phenotype? *Clinical Epigenetics* **2019**, *11*, 124.

(149) Nachman, R. M.; Mao, G.; Zhang, X.; Hong, X.; Chen, Z.; Soria, C. S.; He, H.; Wang, G.; Caruso, D.; Pearson, C.; Biswal, S.; Zuckerman, B.; Wills-Karp, M.; Wang, X. Intrauterine Inflammation and Maternal Exposure to Ambient PM2.5 during Preconception and Specific Periods of Pregnancy: The Boston Birth Cohort. *Environmental Health Perspectives* **2016**, *124*, 1608–1615.

(150) Yu, H.; Yin, Y.; Zhang, J.; Zhou, R. The impact of particulate matter 2.5 on the risk of preeclampsia: an updated systematic review and meta-analysis. *Environmental Science and Pollution Research International* **2020**, *27*, 37527–37539.

(151) Kaur, K.; Lesseur, C.; Deyssenroth, M. A.; Kloog, I.; Schwartz, J. D.; Marsit, C. J.; Chen, J. PM2.5 Exposure during Pregnancy Is Associated with Altered Placental Expression of Lipid Metabolic Genes in a US Birth Cohort. *Environmental Research* **2022**, *211*, 113066.

(152) Ghazi, T.; Naidoo, P.; Naidoo, R. N.; Chuturgoon, A. A. Prenatal Air Pollution Exposure and Placental DNA Methylation Changes: Implications on Fetal Development and Future Disease Susceptibility. *Cells* **2021**, *10*, 3025.

(153) Wesselink, A. K.; Carwile, J. L.; Fabian, M. P.; Winter, M. R.; Butler, L. J.; Mahalingaiah, S.; Aschengrau, A. Residential Proximity to Roadways and Ischemic Placental Disease in a Cape Cod Family Health Study. *International Journal of Environmental Research and Public Health* **2017**, *14*, 682.

(154) Pan, S.; Qiu, Y.; Li, M.; Yang, Z.; Liang, D. Recent Developments in the Determination of PM2.5 Chemical Composition. *Bulletin of Environmental Contamination and Toxicology* **2022**, DOI: 10.1007/s00128-022-03510-w.

(155) Shen, J.; Taghvaee, S.; La, C.; Oroumiyeh, F.; Liu, J.; Jerrett, M.; Weichenthal, S.; Del Rosario, I.; Shafer, M. M.; Ritz, B.; Zhu, Y.; Paulson, S. E. Aerosol Oxidative Potential in the Greater Los Angeles Area: Source Apportionment and Associations with Socioeconomic Position. *Environmental Science & Technology* **2022**, *56*, 17795–17804.

(156) Franklin, M.; Koutrakis, P.; Schwartz, J. The Role of Particle Composition on the Association Between PM2.5 and Mortality. *Epidemiology (Cambridge, Mass.)* **2008**, *19*, 680–689.

(157) Schauer, J. J.; Lough, G. C.; Shafer, M. M.; Christensen, W. F.; Arndt, M. F.; DeMinter, J. T.; Park, J.-S. Characterization of Metals Emitted from Motor Vehicles. *Research Report (Health Effects Institute)* **2006**, 1–76, discussion 77–88.

(158) Sun, Q.; Li, Y.; Shi, L.; Hussain, R.; Mehmood, K.; Tang, Z.; Zhang, H. Heavy Metals Induced Mitochondrial Dysfunction in Animals: Molecular Mechanism of Toxicity. *Toxicology* **2022**, *469*, 153136.

(159) Xu, Z.; Xu, X.; Zhong, M.; Hotchkiss, I. P.; Lewandowski, R. P.; Wagner, J. G.; Bramble, L. A.; Yang, Y.; Wang, A.; Harkema, J. R.; Lippmann, M.; Rajagopalan, S.; Chen, L.-C.; Sun, Q. Ambient Particulate Air Pollution Induces Oxidative Stress and Alterations of Mitochondria and Gene Expression in Brown and White Adipose Tissues. *Particle and Fibre Toxicology* **2011**, *8*, 20.

(160) Punshon, T.; Li, Z.; Marsit, C. J.; Jackson, B. P.; Baker, E. R.; Karagas, M. R. Placental Metal Concentrations in Relation to Maternal and Infant Toenails in a US Cohort. *Environmental science & technology* **2016**, *50*, 1587–1594.

(161) Janzen, C. et al. A Description of the Imaging Innovations for Placental Assessment in Response to Environmental Pollution study (PARENTs). *American Journal of Perinatology* **2022**, *0*, Publisher: Thieme Medical Publishers, Inc., DOI: 10.1055/a-1961-2059.

(162) Devaskar, S. *Imaging Innovations for Placental Assessment in Response to Environmental Pollution (NCT02786420)*; Clinical trial registration NCT02786420; clinicaltrials.gov, 2021.

(163) ACOG ACOG Practice Bulletin No. 202: Gestational Hypertension and Preeclampsia. *Obstetrics and Gynecology* **2019**, *133*, 1.

(164) Osuchukwu, O. O.; Reed, D. J. In *StatPearls*; StatPearls Publishing: Treasure Island (FL), 2022.

(165) Liu, J.; Banerjee, S.; Oroumiyeh, F.; Shen, J.; del Rosario, I.; Lipsitt, J.; Paulson, S.; Ritz, B.; Su, J.; Weichenthal, S.; Lakey, P.; Shiraiwa, M.; Zhu, Y.; Jerrett, M. Cokriging with a Low-Cost Sensor Network to Estimate Spatial Variation of Brake and Tire-Wear Metals and Oxidative Stress Potential in Southern California. *Environment International* **2022**, *168*, 107481.

(166) Dillner, A. M.; Shafer, M. M.; Schauer, J. J. A Novel Method Using Polyurethane Foam (PUF) Substrates to Determine Trace Element Concentrations in Size-Segregated Atmospheric Particulate Matter on Short Time Scales. *Aerosol Science and Technology* **2007**, *41*, 75–85.

(167) Herner, J. D.; Green, P. G.; Kleeman, M. J. Measuring the Trace Elemental Composition of Size-Resolved Airborne Particles. *Environmental Science & Technology* **2006**, *40*, 1925–1933.

(168) Verma, V.; Pakbin, P.; Cheung, K. L.; Cho, A. K.; Schauer, J. J.; Shafer, M. M.; Kleinman, M. T.; Sioutas, C. Physicochemical and Oxidative Characteristics of Semi-

Volatile Components of Quasi-Ultrafine Particles in an Urban Atmosphere. *Atmospheric Environment* **2011**, *45*, 1025–1033.

(169) Biswas, S.; Verma, V.; Schauer, J. J.; Cassee, F. R.; Cho, A. K.; Sioutas, C. Oxidative Potential of Semi-Volatile and Non Volatile Particulate Matter (PM) from Heavy-Duty Vehicles Retrofitted with Emission Control Technologies. *Environmental Science & Technology* **2009**, *43*, 3905–3912.

(170) Lakey, P. S. J.; Berkemeier, T.; Tong, H.; Arangio, A. M.; Lucas, K.; Pöschl, U.; Shiraiwa, M. Chemical Exposure-Response Relationship between Air Pollutants and Reactive Oxygen Species in the Human Respiratory Tract. *Scientific Reports* **2016**, *6*, 32916.

(171) Cassee, F. R.; Héroux, M.-E.; Gerlofs-Nijland, M. E.; Kelly, F. J. Particulate Matter beyond Mass: Recent Health Evidence on the Role of Fractions, Chemical Constituents and Sources of Emission. *Inhalation Toxicology* **2013**, *25*, 802–812.

(172) County, L. CAMS Geocoder `https://cams-lacounty.hub.arcgis.com/pages/cams-geocoder` (accessed 01/06/2022).

(173) Kahle, D.; Wickham, H. Ggmap: Spatial Visualization with Ggplot2. *The R Journal* **2013**, *5*, 144.

(174) Parker, S. E.; Werler, M. M. Epidemiology of Ischemic Placental Disease: A Focus on Preterm Gestations. *Seminars in perinatology* **2014**, *38*, 133–138.

(175) Allison, P. D. Multiple Imputation for Missing Data: A Cautionary Tale. *Sociological Methods & Research* **2000**, *28*, 301–309.

(176) Li, X. et al. Association between Ambient Fine Particulate Matter and Preterm Birth or Term Low Birth Weight: An Updated Systematic Review and Meta-Analysis. *Environmental Pollution* **2017**, *227*, 596–605.

(177) Dadvand, P. et al. Maternal Exposure to Particulate Air Pollution and Term Birth Weight: A Multi-Country Evaluation of Effect and Heterogeneity. *Environmental Health Perspectives* **2013**, *121*, 267–373.

(178) Lavigne, É.; Burnett, R. T.; Stieb, D. M.; Evans, G. J.; Godri Pollitt, K. J.; Chen, H.; van Rijswijk, D.; Weichenthal, S. Fine Particulate Air Pollution and Adverse Birth Outcomes: Effect Modification by Regional Nonvolatile Oxidative Potential. *Environmental Health Perspectives* **2018**, *126*, 077012.

(179) Jiang, S.; Liu, H.; Li, C. Dietary Regulation of Oxidative Stress in Chronic Metabolic Diseases. *Foods* **2021**, *10*, 1854.

(180) NCI Diet History Questionnaire II (DHQ II) for U.S. and Canada — EGRP/DCCPS/NCI/NIH National Cancer Institute Divison of Cancer Control and Population Sciences, `https://epi.grants.cancer.gov/dhq2/` (accessed 09/29/2022).

(181) Jauniaux, E.; Bhide, A.; Burton, G. J. In *Oxford Textbook of Obstetrics and Gynaecology*, 1st; Oxford University Press: 2020, pp 120–133.

(182) Myllynen, P.; Pasanen, M.; Pelkonen, O. Human Placenta: A Human Organ for Developmental Toxicology Research and Biomonitoring. *Placenta* **2005**, *26*, 361–371.

(183) Johnson, N. M.; Hoffmann, A. R.; Behlen, J. C.; Lau, C.; Pendleton, D.; Harvey, N.; Shore, R.; Li, Y.; Chen, J.; Tian, Y.; Zhang, R. Air Pollution and Children's Health-a Review of Adverse Effects Associated with Prenatal Exposure from Fine to Ultrafine Particulate Matter. *Environmental Health and Preventive Medicine* **2021**, *26*, 72.

(184) Riddell, C. A.; Goin, D. E.; Morello-Frosch, R.; Apte, J. S.; Glymour, M. M.; Torres, J. M.; Casey, J. A. Hyper-Localized Measures of Air Pollution and Risk of Preterm Birth in Oakland and San Jose, California. *International Journal of Epidemiology* **2022**, *50*, 1875–1885.

(185) Brauer, M.; Lencar, C.; Tamburic, L.; Koehoorn, M.; Demers, P.; Karr, C. A Cohort Study of Traffic-Related Air Pollution Impacts on Birth Outcomes. *Environmental Health Perspectives* **2008**, *116*, 680–686.

(186) Kingsley, S. L.; Eliot, M. N.; Glazer, K.; Awad, Y. A.; Schwartz, J. D.; Savitz, D. A.; Kelsey, K. T.; Marsit, C. J.; Wellenius, G. A. Maternal Ambient Air Pollution, Preterm Birth and Markers of Fetal Growth in Rhode Island: Results of a Hospital-Based Linkage Study. *Journal of Epidemiology and Community Health* **2017**, *71*, 1131–1136.

(187) Gehring, U.; Wijga, A. H.; Fischer, P.; de Jongste, J. C.; Kerkhof, M.; Koppelman, G. H.; Smit, H. A.; Brunekreef, B. Traffic-Related Air Pollution, Preterm Birth and Term Birth Weight in the PIAMA Birth Cohort Study. *Environmental Research* **2011**, *111*, 125–135.

(188) Chen, B.; Hong, W.; Yang, P.; Tang, Y.; Zhao, Y.; Aguilar, Z. P.; Xu, H. Nano Zinc Oxide Induced Fetal Mice Growth Restriction, Based on Oxide Stress and Endoplasmic Reticulum Stress. *Nanomaterials (Basel, Switzerland)* **2020**, *10*, E259.

(189) Zhai, Q.-Y.; Ge, W.; Wang, J.-J.; Sun, X.-F.; Ma, J.-M.; Liu, J.-C.; Zhao, Y.; Feng, Y.-Z.; Dyce, P. W.; Felici, M. D.; Shen, W. Exposure to Zinc Oxide Nanoparticles during Pregnancy Induces Oocyte DNA Damage and Affects Ovarian Reserve of Mouse Offspring. *Aging (Albany NY)* **2018**, *10*, 2170.

(190) Kravchenko, J.; Darrah, T. H.; Miller, R. K.; Lyerly, H. K.; Vengosh, A. A Review of the Health Impacts of Barium from Natural and Anthropogenic Exposure. *Environmental Geochemistry and Health* **2014**, *36*, 797–814.

(191) Elwej, A.; Ghorbel, I.; Chaabane, M.; Soudani, N.; Mnif, H.; Boudawara, T.; Zeghal, N.; Sefi, M. Zinc and Selenium Modulate Barium-Induced Oxidative Stress, Cellular Injury and Membrane-Bound ATPase in the Cerebellum of Adult Rats and Their

Offspring during Late Pregnancy and Early Postnatal Periods. *Archives of Physiology and Biochemistry* **2018**, *124*, 237–246.

(192) Bates, J. T.; Fang, T.; Verma, V.; Zeng, L.; Weber, R. J.; Tolbert, P. E.; Abrams, J. Y.; Sarnat, S. E.; Klein, M.; Mulholland, J. A.; Russell, A. G. Review of Acellular Assays of Ambient Particulate Matter Oxidative Potential: Methods and Relationships with Composition, Sources, and Health Effects. *Environmental Science & Technology* **2019**, *53*, 4003–4019.

(193) Zhao, Z. Iron and Oxidizing Species in Oxidative Stress and Alzheimer's Disease. *Aging Medicine* **2019**, *2*, 82–87.

(194) Bové, H.; Bongaerts, E.; Slenders, E.; Bijnens, E. M.; Saenen, N. D.; Gyselaers, W.; Van Eyken, P.; Plusquin, M.; Roeffaers, M. B. J.; Ameloot, M.; Nawrot, T. S. Ambient Black Carbon Particles Reach the Fetal Side of Human Placenta. *Nature Communications* **2019**, *10*, 3866.

(195) Beddows, D. C. S.; Harrison, R. M. PM10 and PM2.5 Emission Factors for Non-Exhaust Particles from Road Vehicles: Dependence upon Vehicle Mass and Implications for Battery Electric Vehicles. *Atmospheric Environment* **2021**, *244*, 117886.

(196) Keenan-Devlin, L. S.; Smart, B. P.; Grobman, W.; Adam, E. K.; Freedman, A.; Buss, C.; Entringer, S.; Miller, G. E.; Borders, A. E. B. The Intersection of Race and Socioeconomic Status Is Associated with Inflammation Patterns during Pregnancy and Adverse Pregnancy Outcomes. *American Journal of Reproductive Immunology (New York, N.Y.: 1989)* **2022**, *87*, e13489.

(197) Liu, J.; Lipsitt, J.; Jerrett, M.; Zhu, Y. Decreases in Near-Road NO and NO2 Concentrations during the COVID-19 Pandemic in California. *Environmental Science & Technology Letters* **2020**, DOI: 10.1021/acs.estlett.0c00815.

(198) Tanvir, S.; Ravichandran, D.; Ivey, C.; Barth, M.; Boriboonsomsin, K. In 2023, pp 131–148.